Theoretical Analysis of High Spin States of Transitional Nuclei Around the Mass Number 120

A

THESIS

SUBMITTED TO

THE UNIVERSITY OF JAMMU

FOR THE AWARD OF DEGREE OF

DOCTOR OF PHILOSOPHY (Ph.D.)

IN

PHYSICS

BY

Dhanvir Singh

UNDER THE SUPERVISION OF

Prof. Arun Bharti

POST-GRADUATE DEPARTMENT OF PHYSICS

UNIVERSITY OF JAMMU,

JAMMU-TAWI, 180006

(NOVEMBER-2017)

DECLARATION

I, **Dhanvir Singh**, S/O Late Sh. Sehdev Singh, hereby declares that my Ph.D. thesis work entitled **"Theoretical Analysis of High Spin States of Transitional Nuclei Around the Mass Number 120"** is original and not copied from other sources without due acknowledgement and having 3% degree of plagiarism as per Urkund analysis report.

Dhanvir Singh

Prof. P.V.K .S Baba
(Head of the Department)

Prof. Arun Bharti
(Research Supervisor)

POST-GRADUATE DEPARTMENT OF PHYSICS,

UNIVERSITY OF JAMMU, JAMMU-180006

CERTIFICATE

It is hereby certified that **Mr. Dhanvir Singh**, a registered research scholar of the Department of Physics, University of Jammu, Jammu, has completed his research work entitled **"Theoretical Analysis of High Spin States of Transitional Nuclei Around the Mass Number 120"** for the degree **of Doctor of Philosophy (Ph.D.) in Physics** under my supervision and guidance. It is further certified that,

1. The thesis embodies the work of **Mr. Dhanvir Singh** and is worthy of consideration for the award of Ph.D. degree.
2. The candidate has worked under me for the period required under statutes.
3. The candidate has put in required attendance in Post-Graduate Department of Physics, University of Jammu, Jammu during that period.
4. The candidate has fulfilled the statutory conditions as laid down in **Section 18** of statutes governing degree of Doctor of Philosophy issued vide notification no. 4 dated 04.03.2013.
5. The Candidate has fulfilled all the requisite conditions for Award of Ph.D Degree in accordance with UGC (Minimum Standards and Procedure for award of M.Phil/Ph.D. degree), Regulations, 2009/2016 including course work.

Prof. P.V.K .S Baba
(Head of the Department)

Prof. Arun Bharti
(Research Supervisor)

ACKNOWLEDGEMENT

"Important are those who give importance to God and Love."

Tu hi Nirankar Main Teri Sharan Haan Mainu Baksh lo

All admire goes to Almighty Nirankar the supreme power of the universe without whom I would not have been able to complete my Research work.

Firstly, I would like to express my sincere gratitude to my supervisor ***Prof. Arun Bharti, Professor, Department of Physics*** *for the continuous support of my Ph.D study and related research, for his patience, motivation, and immense knowledge. His guidance helped me in all the time of research and writing of this thesis. I could not have imagined having a better advisor and mentor for my Ph.D study. Without his assistance and dedicated involvement in every step throughout the research, this research work would have never been accomplished. I would like to thank you very much sir for your support and understanding me over these past four years. I also feel grateful to* ***Mrs. Monika Gupta*** *(wife of Prof. Arun Bharti) for her helpful attitude and goodwill. I cannot forget her passion towards providing hospitality whenever I visited my supervisor at his home for research related activities.*

Besides my advisor, I would like to thank ***Prof. S. K. Khosa, Department of Physics, Central University, Jammu,*** *for his insightful comments and encouragement, but also for the hard question which incented me to widen my research from various perspectives. I would also like to thank* ***Dr. Rani Devi****, Assistant Professor, Department of Physics and member of Nuclear Theory Group, University of Jammu, for her best wishes.*

I express my thanks to ***Prof. P.V.K .S Baba,*** *Head of the Department, who took over this administrative position of Headship during the last stage of my Ph.D work, for helping me and giving encouragement in submitting my Ph.D thesis. I am thankful to* ***Prof. Vivek Gupta,*** *Ex-Head of the Department, who gave access to the laboratory and research facilities. Without his precious support it would have not been possible to conduct this research.*

My sincere thanks also go to my friend ***Dr. Suram Singh*** *whose doors of heart were always open whenever I ran into a trouble spot or had a question about my research work. I thank my other lab-mates cum friends* ***Mr. Amit Kumar, Dr. Chetan Sharma, Mr. Aman Priya and Dr. Arun Sharma*** *for the stimulating discussions, for the sleepless nights we were working together before deadlines, and for all the fun we had during my stay as a scholar for the last*

more than four years. Also I thank my friends ***Mr. Ranjit Singh, Mr. Manik Jasrotia, Mr. Puneet Thkural and Dr. Naresh Sharma*** *for their loving company and all the care and affection showered on me during the course of my research work. I feel highly grateful to my other research co-workers* ***Dr. Deepti Sharma and Ms. Anuradha Gupta*** *for their fruitful discussions and the joint study of some common topics. I am also thankful to my junior research mates* ***Ms. Surbhi Gupta*** *and* ***Mr. Rajat Gupta*** *for their kind cooperation.*

It's my pleasure to express my insightful and heartfelt appreciation to the Department of Physics, University of Jammu, Jammu, which have endeavored me the brilliant implements to complete this research work. It gives me huge pleasure to place on record my sincere thanks to all those who helped me in one way or the other in the accomplishment of this piece of research work with reflective sense of gratitude. I extend my thanks to all the members of the teaching and non-teaching staff as well as research scholars of the Department for their kind support and helpful attitude.

Any milestone we achieve in our life for ourselves and for the society is never possible without the support of family. It was the blessings of my parents, my father ***Late Ris/Maj. Sehdev Singh Chib and my mother Smt. Raj Chib*** *whose eternal inspiration, unending blessings and spirit of sacrifice has been the driving force behind the accomplishment of this small but a significant achievement of mine. I acknowledge the care, affection, support and goodwill of my sisters* ***Mrs. Darshana Manhas, Mrs. Asha Manhas, Mrs. Tripta Manhas, Mrs. Vijay Chanotra, Mrs. Anju Jamwal, Mrs. Rajni Jamwal and Mrs. Kiran Manhas*** *and my brothers-in- law* ***Capt. Karan Singh, Sub. Surinder Singh, Col. Karan Singh, Mr. Vishav Dev Singh, Mr. Gulshan Singh, Mr Ragubir Singh and Mr. Kulbushan Singh****.*

I also thank my loving daughter ***Sharanya Singh*** *for the patience which was beyond her age and her unconditional love for me.*

Last but not the least; I feel pleasure in acknowledging the sincere cooperation and the sweet company provided by my wife ***Mrs. Bhavana Jamwal Chib****. Thanks for always being there and bearing with me the good and bad times during my wonderful days of Ph.D.*

DHANVIR SINGH

Ek Tu Hi Nirankar

Dedicated to Almighty Nirankar

And

My loving Parents

Contents

ABSTRACT

The research work presented in the thesis is based on theoretical study of nuclear structure of some nuclei lying in the mass region A ≈ 120. The basic nuclear properties help us to explain the structure of a nucleus and in the present work, the properties of nuclei have been obtained by using a quantum-mechanical theoretical approach. It is well known that nuclear physics deals with the study of properties of nuclei. Measuring nuclear properties is of great importance to understand the interactions which bind the protons and neutrons together in the nucleus. The basic properties of nuclei allow one to extract directly or indirectly information on the nuclear structure, as well as, on the strong nuclear force. A new variety of sophisticated techniques have been developed for studying the properties of nuclei. Unlike the atom, which has a spherically symmetric Coulomb field generated by the nucleus, the nuclear field is composed of a complicated superposition of short range interactions between nucleons, and the most stable nuclear shape is the one that minimizes the energy of the system. In general, nucleus is not spherical, and the nuclear shape is most simply described by a multipole power series, the most important term of which is the nuclear quadrupole moment. A positive quadrupole moment reflects the elongation of nuclei into a prolate shape, while a negative value reflects an oblate shape. The amount of quadrupole moment present in a nucleus gives rise to its deformation. Nuclei undergo collective vibrations about both spherical and deformed shapes. The degree of softness of these vibrations is characterized by the excitation energy required to populate states. Over the last three decades, one of the main tasks of the nuclear research is the study of nuclei in the nuclear deformation region. In nuclear physics, nuclear deformation region is that region where nuclei are deformed showing departure from spherecity and hence, one can study the transition of nuclear shape from spherical to well-deformed within an isotopic mass chain. It has been a goal of nuclear structure studies to develop models that incorporate all of the features described above in order to produce a unified nuclear picture. So, various models, like Liquid Drop Model, Shell Model and Deformed Shell Model - Nilsson Model, etc, have been developed to study the various nuclear structure properties. But the modified version of Shell Model known as Projected Shell Model (PSM), has become quite successful in explaining a broad range of properties of deformed nuclei in different mass regions. The most striking aspect of this quantum mechanical model is its ability to describe the finer details of high-spin spectroscopy data with simple physical interpretations for medium to

heavy nuclei. Among the known medium to heavy nuclei, one region of large deformation has been observed around the mass number A ≈ 120.

Since the discovery of this region of large deformation, a lot of experimental effort has gone into understanding the properties of nuclei falling in this region of deformation.

The nuclei have been grouped into various categories like even-even, odd-mass, and odd-odd nuclei and the present work has been carried out on odd-mass nuclei. The study of the high-spin states of odd-A nuclei above the Z=50 closed shell have provided a wealth of experimental information regarding the nature of collectivity in this region. The coexistence of states with different degrees of collectivity in these transitional nuclei has great importance. The Antimony (Z=51) and iodine (Z = 53) nuclei lie between the spherical (Z =50) and the well-deformed (Z = 58) region and are of considerable interest because of competing shape driving tendencies of the orbitals occupied by the neutrons and the protons. Spectroscopic investigations carried out in the odd- mass A ≈ 120 Iodine nuclei have revealed several bands based upon $\pi g_{7/2}(d_{5/2})$ and $\pi h_{11/2}$ orbitals. These bands are associated with moderately deformed prolate and oblate shapes. In addition, bands based upon particle-hole excitations involving $\pi g_{9/2}$ extruder orbitals, which play a decisive role in the development of collective bands in Sn and Sb nuclei, also persist in the iodine nuclei. High-spin structures of Iodine nuclei in this region are described by abrupt appearance of energetically favored non-collective oblate states and coexistence of weakly collective and non-collective quasiparticle aligned configurations. Recent studies of odd mass Iodine nuclei around mass number A ≈ 120 revealed maximally aligned states involving all the particles outside the Sn core. In addition to these states, non-collective states with the angular momentum of one and two particles anti-aligned with respect to the rotation axis were also identified in these nuclei. It has also been reported that, since a maximally aligned state is formed by exhausting all the spin available within the valence space, further angular momentum can only be generated by particle-hole excitations from the core.

Moreover, the odd mass Sb nuclei around mass number A ≈ 120 display a variety of excitations at low to very high spins. At low spins, proton shell closure effects at Z~50 manifest themselves in the form of vibrational and near spherical excitations, whereas the high spin structure is dominated by intruder rotational bands. The intruder bands in Sb isotopes arise due to the coupling of the odd proton to the deformed states of the Sn core. The deformed states in Sn nuclei are due to the proton two-particle-two-hole

($2p$-$2h$) excitation across the Z=50 shell gap. These states have prolate deformation and occur at low excitation energy of ≈ 2 MeV. Structures involving a valence proton coupled to both spherical and deformed core states have been observed in the odd mass A ≈ 120 Sb isotopes, in which spherical and deformed states built on the proton configurations $d_{5/2,}$ $g_{7/2}$, and $h_{11/2}$ were observed. Bands with enhanced deformation due to the odd proton in $h_{11/2}$ orbital have been mapped out in a number of odd mass Sb and iodine isotopes. The recent development in experimental techniques has witnessed many interesting nuclear structure properties like yrast spectra, band crossing and reduced transition probability [B(E2) and B(M1)] in these nuclei. Thus, in order to meet the quality of measurements of experimental nuclear structure properties, a quantum mechanical microscopic theory is applied which could explain quantitatively and qualitatively the finest features of observed data and provides us with a systematic and unified understanding of ever accumulating experimental data. Recently, the Projected Shell Model (PSM) has become quite popular to study the structure of deformed nuclei. The advantage in this method is that the numerical requirements are minimal and therefore, it is possible to perform a systematic study for a group of nuclei in a reasonable time frame. The PSM is based on the spherical shell model and in PSM, the angular momentum projected states are used as the basis for the diagonalization of shell model Hamiltonian.

Looking at the success of the PSM framework, I was tempted to determine its applicability and reliability in the neutron deficient Iodine and Antimony nuclei in the A ≈ 120 mass region. Thus, to have a deeper insight in the understanding of Yrast bands and other nuclear structure properties, a PSM study of $^{119\text{-}127}$I and $^{115\text{-}125}$Sb isotopes has been undertaken in the present work.

The purpose of the present work is to perform a systematic PSM study of the high spin properties for the odd mass Iodine and Antimony isotopes. The physical quantities that have been described are energy spectrum, transition energies, B(E2) and B(M1) values, band diagrams and back-bending. In the present study, an attempt has been made to study odd-mass ($^{119\text{-}127}$I) and Antimony ($^{115\text{-}125}$Sb) isotopes in the framework of PSM by employing quadrupole-quadrupole interactions plus monopole and quadrupole paring force in the Hamiltonian. The research work is presented in different chapters in the thesis and the thesis is outlined as below:

CHAPTER 1

Preface to the thesis

Chapter 1 contains a brief introduction of the work documented in the present thesis. It starts with the general introduction of the nucleus, followed by beginning of nuclear physics, its applicability and importance. Introduction with special emphasis on the nuclei belonging to mass region A~120, is given in this section. A brief account of various studies- theoretical as well as experimental, made in the past on these nuclei using different approaches/techniques, is included in this section. A review of various interesting nuclear structure properties like rotational bands, back-bending in moment of inertia, shape coexistence, transitional probabilities, etc., of these nuclei, obtained by various other research groups in the past, have also been highlighted in this chapter. The presence of these features in the nuclei belonging to this region, especially in odd mass $^{119\text{-}127}$I and $^{115\text{-}125}$Sb nuclei, is the motivation behind carrying out the present work. Since the present thesis is based on application of theoretical nuclear model, so a brief account of various theoretical models is also presented in this chapter. The success of PSM in studying the nuclear structure properties of nuclei belonging to other mass regions further motivated me to employ PSM for carrying out calculations in A ~120 mass region. The chapter is ended with the incorporation of plan of the whole work.

CHAPTER 2

Theory of applied Projected Shell Model

The chapter 2 carries the details of the applied calculational framework, Projected Shell Model (PSM). It is, in the pure phenomenological form, probably the most widely applied model for analysis and extrapolation of low energy nuclear structure data. The PSM, although rigorous but still is capable of describing all types of nuclear structure mechanisms. The Hamiltonian used in the PSM calculations is composed of single-particle energies, quadrupole-quadrupole interactions, monopole pairing between like particles, and quadrupole pairing interactions, which result in a modification of the generally used shell-model approach, and have been discussed in detail in this chapter.

CHAPTER 3

Structure evolution of odd-mass $^{119–127}$I nuclei within Projected Shell Model

This chapter deals with the study of deformed odd mass isotopic chains of Iodine nuclei with mass number varying from 119-127 (i.e. $^{119-127}$I) using Projected Shell Model approach. Iodine nuclei have only three protons outside the Z=50 shell gap, and thus belong to a transitional region between vibrational and well deformed nuclei. These nuclei are known to exhibit multiplicity of shapes and richness of nuclear structure phenomenon and thus, have been of great experimental as well as theoretical interest. In the present chapter, PSM calculations are performed on positive and negative parity bands of deformed odd mass $^{119-127}$I nuclei, to analyse the band structure of low lying states with quasiparticle excitations. Some nuclear structure properties like yrast spectra, band diagrams, back-bending in moment of inertia and reduced transition probabilities have been obtained using this approach. From these calculations, it has been found that the band head spins of all these isotopes are successfully reproduced which come out to be $5/2^+$ for positive parity and $11/2^-$ for negative parity. Yrast spectra for $^{119-127}$I isotopes have been calculated for prolate and oblate deformations and compared with the available experimental data. An interesting feature of shape coexistence for $^{119-127}$I nuclei has also been hinted through these calculations by the satisfactory reproduction of experimental data corresponding to both prolate and oblate kind of deformations. An occurrence of back-bendings have been found in $^{119-127}$I isotopes which can be thought to be due to change of shape from prolate to oblate as we move towards high spin states. These back-bendings are found to be taking place at around the same spins at which band crossings occur for all these Iodine isotopes. Besides this, an attempt has also been made to understand the structure of these isotopes with the help of band diagrams. These band diagrams predict that the yrast spectra for all these Iodine isotopes arise because of 1-qp states at low spins, whereas for higher spins, 3-qp bands are dominant and contribute to the occurance of yrast band, thereby showing the composite structure of these nuclei. Further, the reduced transition probabilities, B(E2) and B(M1) values have also been calculated for all these Iodine isotopes for which no experimental data was available, which provide an opportunity for the experimentalists to look for this data in future.

The research data presented in this chapter has been published in an international journal Nuclear physics A [Nuclear Physics A 952 (2016) 41–61].

CHAPTER 4:

Projected Shell Model study of odd-mass $^{115-125}$Sb isotopes

In the 4th chapter of this thesis, the nuclear structure properties of neutron-deficient $^{115-125}$Sb isotopic chain by using the projected shell model (PSM) have been explained. The projected shell model approach has been applied to study these odd-mass isotopic chains of Antimony nuclei using the same set of interaction parameters for all the Antimony isotopes. It has been found that the experimental yrast states are very well reproduced by the calculated results and the calculated side bands, when plotted in the form of band diagrams, predict that the yrast states at lower spins have been dominated by the 1-qp band while, at the higher spin values, these states have multi-quasiparticle configurations. The PSM calculations have produced the back-bending in moment of inertia in these nuclei ($^{115-125}$Sb) at those values of rotational frequencies which are close to the experimental ones. Nevertheless, the PSM results on back-bending have been able to reproduce this phenomenon at the same values of spins at which the phenomenon of back-crossing in band diagrams occurs. Moreover, the band-head spins of all the $^{115-125}$Sb nuclei have been reproduced successfully by PSM calculations, which turn out to be $11/2^-$. The reduced transition probabilities, B(M1) and B(E2), have also been calculated for these nuclei for which no experimental data was available, which provide an opportunity for the experimentalists to look for this data in future.

The research data presented in this chapter has been published in an International Journal [International Journal of Modern Physics E Vol. 26, No. 6 (2017) 175004].

CHAPTER 5:

Summary of the thesis and its future perspectives

Finally, in the 5th chapter of this thesis, the conclusions drawn from the present research work on the nuclear structure of odd mass nuclei like Iodine and Antimony lying in the mass region A ≈ 120 have been framed. The successes of the projected shell model in explaining the nuclear structure of these odd mass nuclei and the degree by which these calculations have reproduced the experimental data have been emphasized in this chapter. The research work presented in this thesis is based on the PSM calculations within 1-qp and 3-qp excitations but using higher qp excitations may provide some improvement to the results and this exercise can be taken up as a future perspectives of the present work.

LIST OF TABLES

LIST OF FIGURES

List of Publications

A. Journal Publications

1. Study of nuclear structure of odd mass $^{119-127}$I nuclei in a phenomenological approach
   Dhanvir Singh, Anuradha Gupta, Amit Kumar, Chetan Sharma, Suram Singh, Arun Bharti, S.K.Khosa, G.H.Bhat and J.A.Sheikh
   Nuclear Physics A, Vol. **952** (2016) 41–61 [North Holland]
2. Study of odd mass $^{115-125}$Sb isotopes with the projected shell model calculations
   Dhanvir Singh, Arun Bharti, Amit Kumar, Suram Singh, G. H. Bhat and J.A.Sheikh
   International Journal of Modern Physics E**,** Vol. **26** (2017) 175004 [Singapore]
3. Rotational Structure of odd-proton ^{103,105,107,109,111}Tc isotopes.
   Amit Kumar, **Dhanvir Singh**, Suram Singh, Arun Bharti, G. H. Bhat and J.A.Sheikh.
   European Physical Journal A, Vol. **53** (2017) 200 [Italy]
4. Theoretical Study of Band Structure of odd-Mass $^{115-117}$I Isotopes
   Dhanvir Singh, Amit Kuma, Chetan Sharma, Suram Singh and Arun Bharti
   AIP Conf. Proc., Vol. **1728** (2016) 020303 [USA]
5. Projected Shell Model Study of Band Structure of ^{90}Nb
   Amit Kumar, **Dhanvir Singh**, Anuradha Gupta, Suram Singh and Arun Bharti
   AIP Conf. Proc., Vol. 1728 (2016) 020337 [USA]
6. Theoretical analysis of ^{111,113}I by a Microscopic framework of calculation
   Dhanvir Singh, Chetan Sharma, Amit Kumar, Suram Singh, and Arun Bharti
   Journal of Biosphere, Vol. **5** (2016) 20-24 [India]
7. Study of High Spin States in $^{77-83}$Sr Isotopes.
   Chetan Sharma, **Dhanvir Singh**, Neha Gupta and Arun Bharti
   Journal of Biosphere,Vol. **5** (2016) 10-15 [India]
8. Projected Shell Model Description of Positive-Parity Band of ^{130}Pr Nucleus
   Suram Singh, Amit Kumar, **Dhanvir Singh**, Chetan Sharma, Arun Bharti, G.H.Bhat and J.A.Sheikh
   (Accepted for publication in Brazilian Journal of Physics) [In press]

B. Conference Papers Abstracts

1. Non Axial study of some even-even Tellurium isotopes

Suram Singh, **Dhanvir Singh** and Arun Bharti

9th JK Science Congress-2013, University of Kashmir, Kashmir

2. Structure of ^{121,123}I in the Projected Shell Model

   Dhanvir Singh, Suram Singh, Chetan Sharma, and Arun Bharti

   DAE Symposium on Nuclear Physics-2013, BARC, Mumbai

3. Projected Shell Model Study of ^{129}Ba

   Suram Singh, **Dhanvir Singh**, Chetan Sharma, Amit Kumar, Deepti Sharma, Anuradha Gupta, Preeti Verma and Arun Bharti

   101st Indian Science Congress-2014, University of Jammu, Jammu

4. Projected Shell Model Study of Some Odd Mass Iodine Isotopes.

   Dhanvir Singh, Suram Singh, Chetan Sharma and Arun Bharti

   National Conference on Emerging challenges in Nuclear and Many-body Physics-2014, University of Jammu, Jammu

5. Theoretical Investigation of Nuclear Structure Properties of Some N=80 Isotopes

   Chetan Sharma, Amit Kumar, **Dhanvir Singh** and Arun Bharti

   National Conference on Emerging challenges in Nuclear and Many-body Physics-2014, University of Jammu, Jammu

6. Microscopic Study of ^{115,117}Sb in the Projected Shell Model

   Dhanvir Singh, Amit Kumar, Chetan Sharma, Suram Singh and Arun Bharti

   DAE Symposium on Nuclear Physics-2016, SINP, Kolkata

7. Study of A=79 Isobars in a microscopic framework of calculations

   Chetan Sharma, **Dhanvir Singh** and Arun Bharti

   DAE Symposium on Nuclear Physics-2016, SINP, Kolkata

8. Band Structure of Odd-Mass ^{115,117}I Nuclei

   Dhanvir Singh, Amit Kumar, Chetan Sharma, Suram Singh and Arun Bharti

   ICNP-2017, PU, Chandigarh

9. Microscopic study of positive parity yrast states in neutron-deficient ^{119,121}Ba isotopes.

   Suram Singh, **Dhanvir Singh**, Amit Kumar, Anuradha Gupta and Arun Bharti

   ICNP-2017, PU, Chandigarh

10. Quasi-particle Structure of Doubly-odd ^{92,94}Nb Isotopes

    Amit Kumar, **Dhanvir Singh**, Suram Singh, Arun Bharti and G.H. Bhat

    ICNP-2017, PU, Chandigarh

1. Preface to the thesis

1.1 Introduction

At the center of every atom lies a small and dense nucleus. The nucleus of an atom consists of positively charged protons and electrically neutral neutrons which are held together by strong nuclear forces that are not normally perceptible in nature because of their extremely short range. It carries more than 99.97% of the atomic mass in less than 10^{-12} of the volume of an atom. Due to the small size, strong forces, and many particles in the nucleus result in a highly complex and unique quantum system. The study of the nucleus and the forces that hold it together constitute the field of nuclear structure physics. The protons of the nucleus, being positively charged, generate a spherically symmetric electric field in which the atomic electrons orbit. The cloud of negatively charged atomic electrons normally balances the positive nuclear charge, making the atom electrically neutral. The mass of the nucleus is less than the sum of the constituents, the missing mass ΔM being accounted for by the binding energy ΔMc^2 (where c is the speed of light), which holds the nuclear system together. The nuclear forces generate an attractive potential field which holds the nucleus together and in which the nucleons orbit in highly correlated patterns. The volume of nuclei increases approximately linearly with mass number A, and the radius is roughly $R = 1.2 \times 10^{-15} \cdot A^{1/3}$ m. The radius of the nucleus is very small but this small nucleus is very massive. The whole mass of the atom is concentrated in this tiny nucleus and because of this mass it has a very high density. It is of the order of 10^{17} Kg/m^3. Various techniques have been developed to estimate of nuclear charge distribution, including electron scattering, the study of muonic atoms, and the laser spectroscopy of hyperfine atomic structure. An overall picture of the nuclear charge distributions emerges. The nuclear charge density saturates in the interior and has a roughly constant value in all but the lightest nuclei. The nucleus has a diffuse skin which is of nearly constant thickness. Many nuclei are found to have non spherical shapes. Unlike the atom, which has a spherically symmetric Coulomb field generated by the nucleus, the nuclear field is composed of a complicated superposition of short range interactions between nucleons, and the most stable nuclear shape is the one that minimizes the energy of the system. In general, it is not spherical, and the nuclear shape is most simply described by a multipole power series, the most important term of which is the nuclear quadrupole moment.

A positive quadrupole moment means the elongation of nuclei into a prolate or football like shape, while a negative value reflects an oblate shape like that of Earth. An accurate determination of nuclear matter distributions, that is, the distribution of both protons and neutrons in nuclei, is harder to precisely ascertain. The small nuclear size and tightly bound nature impose very restrictive constraints on the orbits that protons and neutrons can undergo inside the system. Thus, each nucleus has a series of quantum states that particles can occupy. The Pauli principle requires that each particle have a unique set of quantum labels. Each nuclear state can then be filled with four particles: two protons with internal angular momentum "up" and "down," and likewise two neutrons. A nucleus is most stable when all of its nucleons occupy the lowest possible states without violating this occupancy rule. This is called the nuclear ground state. During nuclear collisions the protons and neutrons can be excited from their most bound states and promoted to higher lying unoccupied states. The process is usually very short lived and the particles de excites to their most stable configuration on a time scale of the order of 10^{-12} s. The energy is usually released in the form of gamma rays of well defined energy corresponding to the difference in energy of the initial and final nuclear states. Occasionally, gamma decay is not favored because of angular momentum selection rules.

The nucleus as a unique many-body system possesses a rich variety of quantum-mechanical excitations. The competition and resulting balance between the single particle and collective degrees of freedom are important factors in the determination of the nuclear structure. The single-particle structure that exists for spherical nuclei near closed shells gives way to more collective rotational structure for deformed nuclei that have a large number of valence nucleons outside closed shells. A challenge of contemporary nuclear structure physics is to measure the properties of nuclei far from beta stability in order to unearth the unusual changes expected to be there and to test the predictive power of nuclear models.

The neutron-deficient odd-mass nuclei in the $Z > 50$ transition region show collective features which have generated considerable theoretical and experimental interest in the past. The traditional theoretical approaches used for the interpretation of the collective properties of these nuclei are based on models of deformed rotors [1] or anharmonic vibrators [2]. Some microscopic theories like perturbation expansion [3] and the interacting boson-fermion model [4] had been applied for a more detailed understanding of the collectivity of transitional

nuclei with 49<Z<61. The transition nuclei with Z =52,53,54,55,56 form an important link in the systematics of the transitional region between the primarily spherical Sn nuclei and the well-deformed La and Ce nuclei. In early 80s, the experimental studies of very proton-rich, medium- to heavy-mass nuclei were difficult. When using fusion-evaporation reactions with stable beams and targets to populate these nuclei, the production cross sections are often very small (less than 100 μb) and other reaction channels account for more than 99% of the reaction products. The physics importance of such studies, however, has been made clear by theoretical predictions. For example, the self consistent mean field calculations [5] show that established nuclear structure properties found in nuclei near the line of stability may be significantly modified in those near or beyond particle-drip lines. Knowledge about the structure of nuclei beyond the proton drip line, therefore, can provide an important basis for the understanding of fundamental nuclear interactions.

The development of modern electromagnetic devices, such as the Argonne Fragment Mass Analyzer (FMA) [6], as well as the use of a new generation of highly efficient γ –ray detector arrays, such as Gammasphere [7], makes it possible to study some nuclei at or beyond the proton-drip line. Experimental studies [8–13] made in the last more than a decade have taken advantage of such instruments and successfully obtained information on excited states in a number of proton-unbound nuclei.

The neutron deficient nuclei in the mass A ~120 lie in a transitional region between the primarily spherical Sn (Z =50) nuclei and the well-deformed La (Z =57) and Ce (Z =58) nuclei. Transitional nuclei with $Z > 50$ and A~120 have been a subject of much interest as they exhibit significant variations of shapes and deformations with the configuration of the valence quasi-particles. As it is observed from the literature [14] that the nuclei in this mass region, with a limited number of valence nucleons outside the ^{114}Sn core, undergo a transition from weakly prolate deformation at low spin to an oblate shape at medium spin. This shape change is induced by the successive alignment of nucleons along the rotation axis and, finally, the level sequences terminate in maximally aligned oblate states [15-20]. The shape coexistence in this region is confirmed by various experimental and theoretical techniques, as for example, the low-energy states of the odd-mass I isotopes (Z = 53) are formed by a coupling of the odd proton to the levels of neighboring even-even Te nuclei. Bands of low collectivity are observed up to the medium-spin region. At higher energies, however, these

nuclei exhibit a more complex structure with coexisting weakly collective and noncollective quasiparticle aligned configurations [16]. Moreover yrast-line spectroscopy in this region has identified rotational bands, most commonly representing collective motion of a rapidly rotating prolate spheroid. Additionally, however, detailed analysis has revealed the existence of new structures with less commonly observed oblate shapes [21,22].

Nuclei near the Z = 50 closed proton shell have revealed exotic collective structures, which coexist with the expected single-particle properties. In early 90s, rotational "intruder bands," extending to both high spin and excitation energy, have been observed. These bands have been found in several odd-A antimony (Z = 51) isotopes ranging from ^{109}Sb to ^{117}Sb [23-27], in addition to several even tin nuclei, e.g., ^{108}Sn [28]. These systematics have been extended to Z = 52, 53 nuclei with data from the Eurogam array [29].

Beside these properties, some more interesting experimental results like high spin states of the nuclei like Sb, Te, I, and Xe falling in this mass region have also been recently [14] studied experimentally using in-beam γ-ray spectroscopy technique. The half-life times and excited bands are also observed experimentally in these nuclei.

Apart from this, the experimental evidence, so far accumulated in this mass region, also indicates that many nuclei are characterized by strong oblate and prolate deformation.

The above mentioned nuclear structure phenomena indicate that there is a good number of nuclear structure properties known experimentally for nuclei lying in the mass region A~120 and there may be some more nuclear structure properties of interest which are still to be known in these nuclei.

Thus, in order to meet the quality of measurements of experimental nuclear structure properties, a quantum mechanical microscopic theory is applied which could explain quantitatively and qualitatively the finest features of observed data and provide us with a systematic and unified understanding of ever accumulating experimental data.

It is with this motivation, I have planned to study these nuclear structure properties in the nuclei falling in the mass region A~120 in a microscopic framework of calculations known as Projected Shell Model (PSM). The PSM has been developed and designed by Hara and his co-workers [30]. Among the theoretical models proposed to describe the high spin states of the nucleus, the PSM is one of the most successful one. So, in my present research work, PSM has been used to explain and interpret, qualitatively and quantitatively, the

available experimental data of some odd-mass isotopic chains of iodine and Antimony nuclei. Since the topic of my Ph.D. work is based on the study of nuclei in the mass region A~120, I am therefore, presenting below a brief review of research work made by various research groups in past, revealing this region to be of interest for study.

1.2 Review of Literature

In-beam γ- spectroscopy of the most neutron-deficient nuclei around the Z = 50 shell closure has provided further insight into the structural evolution of nuclei at high angular momentum. Several nuclei in this mass region exhibit novel structures, well-deformed intruder bands, which extend to the highest rotational frequencies observed in heavy nuclei. A gradual decline of the dynamic moments of inertia with increasing spin -a common feature to these intruder bands - has been attributed to a mode of "soft" band termination involving the alignment of the valence nucleons [31]. In this process, an initially prolate collective band progresses gradually, rather than abruptly, towards a noncollective oblate band, as the aligned valence spin is exhausted at termination. An underlying softness of the nuclear potential withrespect to the triaxiality parameter γ in the A ~120 region has been extensively examined, both experimentally and theoretically, at lower spin [21]. This γ softness permits the strong prolate and oblate driving forces, exerted by high-j (proton) orbitals, to stabilize the nucleus at prolate and, less frequently, oblate collective deformations, respectively. Indeed, the existence of this oblate shape stability may influence a behavior as observed in experimental investigations of spin(I) up to 30ħ, where the abrupt occurrence (in one γ-ray transition) of termination of the yrast band into a non collective oblate state has been reported [22,32]. This has to be contrasted with the behavior at higher spins of the bands discovered at that time, where the soft band terminating process appears to be stretched out over a number of transitions in a very wide frequency interval (Δω> 1.0 MeV/ħ).

The novel intruder bands, which have emerged from recent studies in this mass region, have been discovered in (Z=51) $^{109\text{-}117}$Sb [24,26,27, 33,34] and in (Z=50) ^{106,108}Sn [35, 28] and (Z=52) ^{112,114}Te nuclei [33,36]. These decoupled bands characteristically extend to high spins (I =50ħ) and the highest rotational frequencies observed (ħω~1.4 MeV in ^{109}Sb [24]). At the lowest spins, they represent collective nuclear rotation built on prolate deformed particle-hole proton excitations (intruder states) coupled to single-particle valence orbitals.

The 2plh intruder states were first defined in (Z=51) Sb [37], and 2p2h states were isolated in (Z=50) Sn nuclei [38]. At increased rotational frequency, the Coriolis force causes the valence nucleons to align their spins along the axis of rotation. Concurrent with the increasing rotational frequency ω, the slow decline of the dynamic moment of inertia $j^{(2)}$ to 1/2 to 1/3 of the rigid body value is observed. This remarkable effect may be attributed [31] to the process of soft band termination, in which the rotational alignment of the valence neutrons occurs in a gradual fashion, driving the nuclear shape from collective prolate (γ = 0°) toward the non-collective oblate (γ = +60º) shape.

The odd-mass iodine nuclei with A=117–125 are characterized by the presence of a large number of bands, with the odd proton occupying the different Nilsson orbitals available near the Fermi level [39-44]. Both oblate and prolate deformed bands have been reported with a moderate quadrupole deformation, characteristics of transitional nuclei. With the availability of new experimental data, interpretations have been provided for several of these bands in the light of theoretical calculations. The ground-state yrast bands in the odd-A $^{121-125}$I arise from the oblate high-K $\pi g_{7/2}$ and $\pi d_{5/2}$ orbitals [41-44]. Excited $\pi g_{9/2}$ and $\pi h_{11/2}$ bands have also been observed in these as well as the lighter ^{117,119}I isotopes [39,40]. Three quasiparticle bands at an excitation energy of about 2 MeV are also reported in ^{119,121,125}I [40,41,44]. Liang *et al* [45] have performed potential-energy-surface [PES] calculations in order to study the kind of nuclear shapes that are likely for the low-lying one quasiparticle configurations in the odd-A iodine nuclei. These calculations predict competing prolate and oblate shapes for the $d_{5/2}$ and $g_{7/2}$ configurations. Although the oblate states are predicted to be lower in energy for the iodine nuclei with A >121 and the prolate states are favored for the lighter ^{119}I, the energy difference between the oblate and the prolate states are predicted to be small. This suggests that while the oblate high-K $\pi g_{7/2}$ and $\pi d_{5/2}$ orbitals are associated with the ground-state bands in ^{121,123,125}I [41-44], consistent with the predictions of the PES calculations, prolate deformed states based on the low-K proton $d_{5/2}$ and $g_{7/2}$ configurations are not ruled out in these nuclei. Liang *et al* [41] have indeed pointed out subsequently that the states built on the second $7/2^+_2$ state in ^{121}I may be associated with the low-K $\pi g_{7/2}$ prolate configuration.

Interestingly, sequences of similar ΔI=2 states built on the excited $7/2^+$ state have been reported in the three odd-A iodine nuclei with A=121–125 [41-44]. The bandheads lie at

excitation energy of about 500 keV and decay to the $5/2^+$ ground state. Interband transitions, to and from these states, are either very weak or not observed at all. However, the literature, which confirms the ground-state bands to be associated with the oblate $d_{5/2}$ and $g_{7/2}$ orbitals, does not provide a clear interpretation of the structure of the states belonging to the above mentioned ΔI=2 sequences in these nuclei. Considering the results of the PES calculations of Liang *et al* [45] that predict competing oblate and prolate shapes associated with the $d_{5/2}$ and $g_{7/2}$ orbitals, the main aim in this work was to study if the bands built on the second $7/2^+$ states in ^{121,123,125}I indeed have a prolate deformation and are associated with low-K $\pi d_{5/2}$ and $\pi g_{7/2}$ configurations.

In xenon nuclei, there are four protons outside the Z=50 shell closure and isotopes are known with neutron numbers spanning almost the full range of the $50 \leq N \leq 82$ major shell. Xe (Z = 54) nuclei lie in a transitional region between the spherical Sn (Z = 50) and the deformed rotator Ce (Z = 58), and thus the transitional characters in Xe are found to be enhanced leading to a very fragile coexistence of excitation modes based on different deformations. The shapes of nuclei in this region are soft to the polarizing effects of rotation and quasiparticle alignment, and the intruder $h_{11/2}$ orbital plays a dominant role in such a polarizing phenomenon at high angular momentum for both neutron and proton quasiparticles. In other words, the deformation depends strongly on the occupation of neutron and proton intruder $h_{11/2}$ subshells. Calculations of the total Routhian surface (TRS) [46,47] and the cranked shell model (CSM) [48,49] suggest that these high j valence particles exert a strong and specific driving force on the γ -soft core. In odd mass Xe, the $h_{11/2}$ neutron orbital with the unique-negative parity forms the yrast rotational bands and their signature splitting features can be nicely described by the CSM calculations. In addition, the second negative-parity rotational bands based on the $h_{11/2}$ neutron orbital (called the yrare bands) have been observed in ^{119}Xe [50,51], ^{121}Xe [52], ^{123}Xe [53,54], and ^{125}Xe [55,56]. In contrast to the behaviour of the yrast band where the favored states are lower lying in energy, the yrare favored states are found to lie above the unfavored states, which mean the signature splitting is inverted. Although several investigations for the high-spin structures of ^{125}Xe have been done in previous works [55,56], experimental information on the yrare states has been very limited because of insufficient statistics. Recently Moon *et al* [57] have firmly established the favored and the unfavored yrare states and reported a new band based on the three-

quasiparticle $\nu[h_{11/2}]\pi[(h_{11/2})^2]$ configuration in ^{125}Xe. They have extended the energy spectrum upto the spin state $43/2^-$. The high spin states have been studied in neutron deficient ^{113}Xe[58] through complementary backed- and thin-target ^{58}Ni + ^{58}Ni experiments. Several band structures have been observed to high spin and rotational frequencies. The first identification of ^{109}Xe and ^{105}Te[59] has been made through the detection of the α-decay chain ^{109}Xe→ ^{105}Te →^{101}Sn and marks the closest approach to the $N= Z$ line above ^{100}Sn. Fine structure was observed in the α- decay of ^{109}Xe → ^{105}Te placing the energy difference between the tentatively assigned $5/2^+$ ground state and $7/2^+$ excited state at 150 ± 13 keV.

Thus, it is observed from the analysis of the literature for mass region A~120 that the nuclei in this mass region have both oblate and prolate deformed bands with a moderate quadrupole deformation i.e., shape coexistence is found to occur in this mass region.

The nucleus possess an internal structure leads naturally to a desire to understand and predict its structure. The nuclei are composed of quantum mechanical particles, their behavior can be predicted by solving the Schrodinger given below.

$$H\psi = E\psi \qquad (1)$$

With H=T+U, where T is the Kinetic energy and U is the nuclear potential. Unfortunately, while various properties of the nuclear force are known, the exact form or the nuclear potential U is not known. For this reason, a great deal of effort has gone and continues to go into discovering ways to model the nucleus despite not knowing the nuclear potential.

As the results of the studies presented within this work are primarily applicable to the study of nuclear structure, a few comments about nuclear structure models are discussed below.

1.3 Liquid Drop Model

This model was first proposed by N.Bohr and Kalcker [60] and later on applied by Von Weizsacker and Bathe [61,62]. The Liquid drop model assumed that the nuclei of all elements are considered to be behave like a liquid drop of incompressible liquid of very high density. In an equilibrium state, the nuclei of atoms remain spherically symmetric under the strong action of strong attractive nuclear force just like a drop of a liquid which is spherical due to surface tension. The density of a nucleus is independent of its size. The nucleons of the nucleus move about within a spherical enclosure called the nuclear potential barrier just

like the movement of molecules of a liquid within a spherical drop of liquid. The picture of a nucleus as a drop of liquid accounts for the observed variation of binding energy per nucleon with mass number. The expression for binding energy (Weizsaecker formula) obtained from this model takes the form:

$$B.E = a_1 A - a_2 A^{2/3} - a_3 \frac{Z^2}{A^{1/3}} - a_4 \frac{(A-2Z)^2}{A} + a_5 A^{4/3}$$

1st, 2nd ,3rd, 4th and 5th terms corresponds to volume, surface, coulomb, asymmetry and pairing energies respectively.

Though liquid drop model explains some of the features of the nuclei, but said nothing about the single nucleon. This model predicts very closely spaced energy levels in nuclei which is contrary to the observation that the low lying excited states in the nuclei are quite widely spaced. It also fails to explain the magnetic moment and spin of the nuclei. It is also not successful in explaining the excited states in most of the nuclei. These limitations were removed by Shell model, whose brief introduction is given below.

1.4 Shell Model

This model has been very successful in explaining a number of nuclear properties such as magnetic moment, parity, nuclear angular momentum etc. according to shell model the protons and neutrons are arranged around the nucleus in various shells like electrons in outer nuclear part. The protons and neutrons shells appear to be independent to each other that is why it is also called as independent particle model. When the shell closure occurs, the resulting configuration is found to be quite stable. It has been found that the shell closure occurs when either the number of protons or neutrons are equal to 2,8,20,28,50,82,126. These numbers are referred to as magic numbers. In this model, a nucleon is assumed to move in a common potential, determined by the average motion of all nucleons. By considering the potentials (square well and harmonic oscillator) one is able to reproduce magic numbers only upto 20. In order to obtain a better agreement with experiment, Mayer, Haxel, Jensen and Sues in 1949 introduced a non central component in the force acting on the nucleon in the nucleus [63]. It corresponds to the interaction between the orbital (l) and intrinsic spin (s) angular momentum. Here we assume strong coupling between spin and orbital angular momenta of the individual angular momenta giving rise to total angular momentum j, which

can take two possible values for s = +1/2 and s = -1/2 respectively. The splitting of these levels is given by the empirical formula

$$\Delta\varepsilon_{l,s} = 10(2l+1)A^{-2/3} \text{ MeV}$$

The level with j value (j = 1-1/2) lies higher than the one with larger j value (j = 1+1/2). Thus shell model able to explain experimentally observed magic numbers. In addition to this, it also explains many other properties of spherical nuclei like the ground state spins and parities and energy spectra. But its biggest disadvantage was that it could not explain the properties of deformed nuclei. To overcome this problem, Nilsson model came into existence, which is briefly explained in the following section.

1.5 Deformed Shell Model - Nilsson Model

According to Shell model, many nuclei particularly those in the middle of the shell region have large quadrupole moments implying large deformations. This means that nucleons do not move in a spherical potential given for shell model, but this potential needs to be generalised. S.N.Nilsson did this and after his name the model is known as Nilsson Model. The Nilsson model describes motion of nucleons in a deformed potential well. It treats a deformed nucleus as consisting of independent particles moving in a deformed potential well. This model describes the states of motion of the particles in the potential field of a core. This model has been successful in describing the properties of the heavier deformed nuclei. Nilsson introduced a term proportional to l^2 and a spin-orbit term proportional to l.s in the Hamiltonian of an isotropic oscillator. The interaction of nucleon with the nuclear field is represented by a single-particle Hamiltonian of the form:

$$\hat{H} = -\frac{\hbar^2}{2m}\nabla^2 + \frac{m}{2}(\omega_x^2 x^2 + \omega_y^2 y^2 + \omega_z^2 z^2) + C\vec{l}.\vec{s} + D(\vec{l}^2 - <\vec{l}^2>)$$

where, ω_i (i = x,y.z) are oscillator frequencies corresponding to the three axes and is given by

$$\omega_x = \omega_o(\varepsilon, \gamma)[1 - \frac{2}{3}\varepsilon\cos(\gamma + \frac{2\pi}{3})],$$

$$\omega_y = \omega_o(\varepsilon, \gamma)[1 - \frac{2}{3}\varepsilon\cos(\gamma - \frac{2\pi}{3})],$$

$$\omega_z = \omega_o(\varepsilon, \gamma)[1 - \frac{2}{3}\varepsilon\cos\gamma]$$

Here, the frequencies are chosen to be proportional to the half axes a_x, a_y, a_z of the ellipsoid. The spin orbit term is conventionally parameterized with a constant κ, and there is also a new $\hat{l}^2$ term parameterized by μ, which is introduced to lower the energy of the single particle states closer to the nuclear surface in order to correct for the steep rise in the harmonic oscillator potential there. Both κ and μ may be different for protons and neutrons and also depend on the nucleon number. The Hamiltonian may be diagonalised in the basis of the harmonic oscillator using either spherical or cylindrical coordinates. In a Nilsson diagram, for a single j and $\varepsilon > 0$, there is a drop in energy for low K values while for higher K values, the energy rises. The separation of adjacent K values increases sharply with K. The positive value of Nilsson parameter ε corresponds to prolate shape, while the negative value of ε represents an oblate shape. Due to very short range forces of the nuclei, a particle in low K orbital has large interaction with the rest of the nuclear matter which makes low Ω values of a particular j-multiplet, energetically favored as compared to the higher one for a prolate shape. For oblate shapes, the situation is reversed. In addition to spherical magic numbers for a Nilsson diagram, which appear at 2,8,20,28,50,82,126, there also occur deformed magic numbers, which appear at different deformations. For example, in rare-earth region, for prolate deformed nuclei, shell gaps occur at nucleon number 66, 70, 76, while for oblate deformation shell gap appears at nucleon number 80. As Nilsson model helps in the understanding of many of the properties of deformed nuclei, but its main disadvantage is that it gives only part of the total energy. In the following section, a brief introduction of yet another model which can successfully describe deformed nuclei is given.

1.6 Projected Shell Model

The PSM is based on the spherical shell model concept but differs from the conventional shell model. The PSM uses the angular momentum projected states as the basis for the diagonalization of the shell model Hamiltonian. The diagonalization gives rise to the energy spectra, and the transition strengths are subsequently calculated using the resulting wave functions. These energies can be plotted as a function of spin for various bands and important physics can be drawn from these plots. PSM not only describes the high spin states but also provides information on the electromagnetic properties of these nuclei. It can also be

successfully applied to study the long isotopic chains. Yet another advantage of PSM is that the important nuclear correlations can easily be taken into account and configuration space is manageable. One can perform a systematic study of nuclei in a limited time frame and numerical requirement is also minimal. In recent years, the PSM has become quite successful in explaining a broad range of properties of deformed nuclei in different mass regions [64-82]. The most striking aspect of this quantum mechanical model is its ability to describe the finer details of high-spin spectroscopy data with simple physical interpretations. Owing to these observations, I have decided to carry out the research work on odd mass $^{119-127}$I and $^{115-125}$Sb nuclei in a framework of calculations known as Projected Shell Model (PSM). The detail of PSM is given in chapter 2. I have also compared the results of the calculations with the experimentally available data.

This research work is organized in the form of a thesis comprising of five chapters as follows:

(1) In Chapter 1, the general introduction of nucleus as well as introduction of the present thesis along with review of literature is given.

(2) In chapter 2, the basic philosophy of the applied model, Projected Shell Model, is given, in detail.

(3) Chapter 3 deals with the detailed microscopic study of positive as well as negative parity yrast states of odd mass isotopic chains of $^{119-127}$I nuclei within PSM formalism. Various results obtained in this study along with its physical interpretation have been given in this chapter. These results are also compared with the available experimental data.

(4) In chapter 4, different nuclear structure properties like yrast spectra, back-bending, band diagrams and transition probabilities have been discussed for negative parity yrast states of $^{115-125}$Sb isotopes by using PSM technique and have also been compared with the experimental counterparts.

(5) Finally, chapter 5 summarizes the whole work of this thesis and final conclusions are drawn with regard to the nuclear structure of nuclei lying in the mass region A~120.

Bibliography

[1] F. S. Stephens, Rev. Mod. Phys. **47** (1975) 43.

[2] U. Hagemann and F. Donau, Phys. Lett. **B59** (1975) 321.

[3] M. Gai, A. Arima, and D. Strottman, Phys. Lett. **B106** (1981) 6.

[4] F. Iachello aud D. Scholteu, Phys. Rev. Lett. **43** (1979) 679.

[5] J. Dobaczewski *et al.*, Phys. Rev. Lett. **72** (1994) 981.

[6] C. N. Davids *et al.*, Nucl. Instrum. Methods Phys. Res. **B70** (1992) 358.

[7] I. Y. Lee, Nucl. Phys. **A520** (1990) 361.

[8] E. S. Paul *et al.*, Phys. Rev. **C51** (1995) 78.

[9] D. Seweryniak *et al.*, Phys. Rev. **C55** (1997) R2137.

[10] C. H. Yu *et al.*, Phys. Rev. **C58** (1998) R3042.

[11] C. J. Gross *et al.*, in Proceedings of the International Conference on Exotic Nuclei and Atomic Masses, edited by B.M. Sherrill, D.J. Morrissey and C.N. Davids, AIP Conf. Proc. No.**455** (AIP, New York, 1998), 444.

[12] M. P. Carpenter, *et al.*, in Proceedings of the Conference on Nuclear Structure 98, Gatlinburg, Tennessee, Vol. **1** (1998) 13.

[13] J. Uusitalo *et al.*, Bull. Am. Phys. Soc. **43** (1998) 1572.

[14] Purnima Singh *et al.*, Phys. Rev. **C86** (2012) 067305.

[15] E. S. Paul *et al.*, J. Phys. **G19** (1993) 913.

[16] P. Singh *et al.*, Phys. Rev. **C85** (2012) 034319.

[17] P. Singh *et al.*, Phys. Rev. **C82** (2010) 034301.

[18] A. Al-Khatib *et al.*, Eur. Phys. J. **A36** (2008) 21.

[19] A. K. Singh *et al.*, Phys. Rev. **C70** (2004) 034315.

[20] A. Al-Khatib *et al.*, Phys. Rev. **C74** (2006) 014305.

[21] D. B. Fossan, J. R. Hughes, Y. Liang, R. Ma, E. S. Paul, and N. Xu, Nucl. Phys. **A520** (1990) 241c.

[22] Y. Liang, D. B. Fossan, J. R. Hughes, D. R. LaFosse, T. Lauritsen, R. Ma, E. S. Paul, P. Vaska, M. P. Waring, and N. Xu, Phys. Rev. **C44** (1991) R578.

[23] V. P. Janzen *et al.* , in Proceedings of the International Conference on Nuclear Structure at High Angular Momentum, Ottawa, 1992, edited by J.C. Waddington and D. Ward (AECL Report No. AECL-10613) **Vol. 2** (1992) 333.

[24] V.P. Jsnzen, *et al.*, Phys. Rev. Lett. **72** (1994) 1160.

[25] D.R. LaFosse, *et al.,* Phys. Rev. **C56** (1997) 760.

[26] V.P. Janzen, *et al.*, Phys. Rev. Lett. **70** (1993) 1065.

[27] D. R. LaFosse, D. B. Fossan, J. R. Hughes, Y. Liang, P. Vaska, M.P. Waring, and J. -Y. Zhang, Phys. Rev. Lett. **69** (1992) 1332.

[28] R. Wadsworth *et al.*, Nucl. Phys. **A559** (1993) 461.

[29] E. S. Paul, *et al.*, Phys. Rev. **C48** (1993) R490.

[30] K. Hara and Y. Sun, Int. J. Mod. Phys. **E4** (1995) 637.

[31] I. Ragnarsson, V. P. Janzen, D.B. Fossan, N. C. Schmeing, and R. Wadsworth, Phys. Rev. Lett. **74** (1995) 3935.

[32] E. S. Paul, J. Simpson, H. Timmers, M. A. Bentley, A. M. Bruce, D. M. Cullen, P. Fallon, and F. Hanna, J.Phys. **G18** (1992) 971.

[33] D.B. Fossan, *et al.*, Proceedings of the Conference on Physics for Large γ-Ray Detector Arrays [1], 194.

[34] D. R. LaFosse, *et al.,* Phys. Rev. **C50** (1994) 1819.

[35] R. Wadsworth, *et al.*, Phys. Rev. **C50** (1994) 104.

[36] E. S. Paul, *et al.*, Phys. Rev. **C50** (1994) 698.

[37] A. K. Gaigalas, R. E. Shroy, G. Schatz, and D. B. Fossan, Phys. Rev, Lett. **35** (1975) 555; Phys. Rev. **C19** (1979) 1324.

[38] J. Bron, W. H. A. Hesselink, A. van Poelgeest, J. J. A. Zalmstra, M. J. Uitzinger, H. Verheul, K. Heyde, M. Waroquier, H. Vincx, and P. Van Isacker, Nucl. Phys. **A318** (1979) 335.

[39] E. S. Paul, *et al.*, Phys. Rev. **C59** (1999) 1984.

[40] S. Tormanen, *et al.*, Nucl. Phys. **A613** (1997) 282.

[41] Y. Liang, D. B. Fossan, J. R. Hughes, D. R. LaFosse, T. Lauritsen, R. Ma, E. S. Paul, P. Vaska, M. P. Waring, and N. Xu, Phys. Rev. **C45** (1992) 1041.

[42] Ranjana Goswami, B. Sethi, P. Banerjee, and R.K. Chattopadhyay, Phys. Rev. **C47** (1993) 1013.

[43] Hariprakash Sharma, B. Sethi, Ranjana Goswami, P. Banerjee, R.K. Bhandari, and Jahan Singh, Phys. Rev. **C59** (1999) 2446.

[44] Hariprakash Sharma, B. Sethi, P. Banerjee, Ranjana Goswami, R.K. Bhandari, and Jahan Singh, Phys. Rev. **C63** (2001) 014313.

[45] Y. Liang, *et al.*, in Proceedings of the International Conference on High Spin Physics and Gamma-Soft Nuclei, Pittsburgh, 1990, edited by J.X. Saladin, R.A. Sorensen, and C.M. Vincent (World Scientific, Singapore) (1991) 308.

[46] R. Wyss, J. Nyberg, A. Johnson, R. Bengtsson, andW. Nazarewicz, Phys. Lett. **B215** (1988) 211.

[47] W. Nazarewicz, R. Wyss, and A. Johnson, Nucl. Phys. **A503** (1989) 285.

[48] R. Bengtsson and S. Frauendorf, Nucl. Phys. **A327** (1979) 139.

[49] R. Bengtsson, S. Frauendorf, and F.-R. May, At. Data Nucl. Data Tables **35** (1986) 15.

[50] C.B. Moon, T. Komatsubara, Y. Sasaki, T. Jumatsu, K. Yamada, K. Satou, and K.Furuno, Eur. Phys. J. **A14** (2002) 13.

[51] C.B. Moon, S. J. Chae, J. H. Ha, T. Komatsubara, Y. Sasaki, T. Jumatsu, K. Yamada, K. Satou, and K. Furuno, J. Korean Phys. Soc. **41** (2002) 188.

[52] C.B. Moon, T. Komatsubara, T. Shizuma, K. Uchiyama, T. Sasaki, and K. Furuno, Eur. Phys. J. A **4** (1999) 107.

[53] A. Schmidt, *et al.*, Eur. Phys. J. **A2** (1998) 21.

[54] A. Gade, H. Meise, I. Wiedenh¨over, A. Schmidt, A. Gelberg, and P. von Brentano, Nucl. Phys. **A686** (2001) 3.

[55] A. Granderath, D. Lieberz, A. Gelberg, S. Freund, W. Lieberz, R. Wirowski, P. von Brentano and R. Wyss, Nucl. Phys. **A524** (1991) 153.

[56] I. Wiedenh¨over, J. Yan, U. Neuneyer, R. Wirowski, P. von Brentano, A. Gelberg, N. Yoshida, and T. Otsuka, Nucl. Phys. **A582** (1995) 77.

[57] C. B. Moon, C. S Lee T. Komatsubara, Y. Sasaki, and K. Furuno, Phys. Rev. **C76** (2007) 067301.

[58] H. C. Scraggs *et al.,* Phys. Rev. **C61** (2000) 064316.

[59] S. N. Liddick *et al.,* Phys. Rev. Lett. **97** (2006) 082501.

[60] N.Bohr and F.Kalcker, Kgl. Danske Videnskab. Selskab. Mat-Fys. Medd **14,** 10 (1937).

[61] C.F.Von Weizsacker, Z.Physik **96**, (1935) 431.

[62] H.A.Bethe and R.F.Bacher, Rev. Mod. Phys. **8**, (1936) 82.

[63] K.Heyde, The Nuclear Shell Model (Springer-Verlag, Berlin, Heidelberg, New York, (1994).

[64] Y.Sun and M.Guidry; Phys. Rev. **C52**, (1995) R2844.

[65] Y.Sun, J.-Y.Zhang and M.Guidry; Phys. Rev. Lett.**78**, (1997) 2321.

[66] Y.Sun, J.-Y.Zhang, M.Guidry and C.-L Wu; Phys. Rev. Lett.**83**, (1999) 686.

[67] R.Palit, J.A.Sheikh, Y.Sun and H.C.Jain; Phys. Rev. **C67**, (2003) 014321.

[68] N.Marginean et al., Phys. Rev. **C69**, (2004) 054301.

[69] R.A.Kaye et al., Phys. Rev. **C75**, (2007) 034311.

[70] V.Velazquez, J.Hirsch, Y.Sun and M.Guidry; Nucl. Phys. **A653**, (1999) 355.

[71] V.Velazquez, J.Hirsch and Y.Sun; Nucl. Phys. **A686**, (2001) 129.

[72] A.Bhat, A.Bharti and S.K.Khosa; Eur. Phys. J. **A48**, (2012) 39.

[73] A.Bharti, S.Singh and S.K.Khosa; Int. J. Mod. Phys. **E20**, (2011) 1183.

[74] S.Verma, P.A.Dar and R.Devi; Phys. Rev. **C77**, (2008) 024308.

[75] F.Al-Khudair, G.-L. Long and Y.Sun; Phys. Rev. **C79**, (2009) 034320.

[76] Y.Sun, Y.-C Yang, H.-L.Liu, K.Kaneko, M.Hasegawa and T.Mizusaki; Phys. Rev. **C80**, (2009) 053306.

[77] Y.X. Liu, Y.Sun, X. -H.Zhou,Y.-H Zhang, S.-Y.Yu, Y.-C. Yang and H.Jin; Nucl. Phys. **A658**, (2011) 11.

[78] R.Palit, J.A.Sheikh, Y.Sun and H.C.Jain; Nucl. Phys. **A686**, (2001) 141.

[79] Y.Sun; Eur. Phys. J. **A20**, (2004) 133.

[80] D. Bucurescu, et al., Phys. Rev. **C69**, (2004) 064319.

[81] A. Ibannez-Sandoval, M.E.Ortiz, V.Velazquez, A.Galindo-Uribarri, P.O.Hess and Y.Sun; Phys. Rev. **C83**, (2011) 034308.

[82] R.S.Guo and L.M.Chen, Chin. J Phys.**41**, (2003) 1.

2. Theory of the applied Projected Shell Model

2.1 Introduction

In order to understand the different properties of the nucleus of an atom, it is necessary to have a sufficient knowledge about the nature of the inter-nucleon interaction. Nuclear force is a very short range force that acts between the nucleons. Yukawa theory gives us some idea about it, which is based on the exchange of a pion between two nucleons, when they are at a distance less than the range of the interaction. It may be noted that even if the exact nature of the inter-nucleon interaction were known, it would have been extremely difficult to develop a satisfactory theory of the structure of the nucleus made up of a large number of neutrons and protons, since it is impossible to solve the Schrödinger equation exactly for such a many-body system. Various methods have been developed for tackling the problem with different degrees of approximation. However, the problem is still far from being solved completely. The situation is quite different if we consider the theory of the atomic structure. The nature of the forces acting on the electrons in the atom is electromagnetic which is well understood. The quantum mechanical theory of atomic structure is extensively developed and agrees well with experimental data. Because of the above difficulties in developing a satisfactory theory of nuclear structure, different models have been proposed for the nucleus, each of which can explain some of the different characteristics of the nucleus. The usefulness of a model depends on the extent to which its predictions are confirmed by experiments. Every model is not suitable to solve a particular problem. Different models have got different limitations like particle rotor model, when applied to nuclei with coexisting shapes, can explain only a limiting number of states as long as the shape parameters are kept constant right through the calculations in this model. High spin states can't be studied by simple boson model. Further, cranking model doesn't yield proper quantum mechanical wave functions and hence can't be used to obtain quantitative information about electromagnetic transitions or form factors. Similarly, spherical shell model can't reproduce the characteristics of very high spin states due to the presence of a large number of quasi-particles, which make the prescription of residual interaction between them much more complex. It is also possible that a large deformation, which tends to appear at such high spin states, may deform the single particle orbits used with the spherical core. To overcome these

limitations, Kenji Hara and Yang Sun used an intrinsic basis which spontaneously violates the symmetry of the system and restore it by the Projection method. It led to the development of Projected Shell Model (PSM) [1].

2.2 Logical structure of PSM theory

Elliott [2] was the first to point out the advantage of deformed (intrinsic) many-body basis and developed the *SU(3)* shell model for *sd*-shell nuclei. In this method, the classification of basis states and their projection onto good angular-momenta can be carried out using the group theoretical method. The *SU(3)* scheme works satisfactorily for lighter nuclei, where the *ls*- coupling is very weak. Though, in the heavier nuclei, where the presence of a strong spin-orbit force is essential for reproducing the shell closures (magic numbers) [3], it is no longer valid. Such systems can be better understood by Nilsson model [4]. In PSM, the Nilsson+BCS scheme is used for the basis selection and the projection of this deformed basis onto good angular-momentum is done numerically. These deformed basis help in interpreting the results in a simpler way. Past few decades have seen a rise in experimental techniques with the introduction of large γ-ray spectrometers and versatile heavy ion accelerators which led to successful accumulation of large experimental data on many nuclear species. This has further enabled the experimentalists to extend the inter-band transitions to high spins as well as an incredibly sharp energy resolution. A unified understanding of this ever accumulating high spin data needs a proper quantum mechanical theory which can explain quantitatively the best features of observed data. PSM [1,5,6,7] has been designed and developed to gather the quality of measurements made possible by the modern experimental techniques. Before providing a detail theory of PSM, I have discussed the important properties of projection operator in brief in the following sub-section.

2.3 Projection Operator

The significant properties of the projection operator associated with a compact Lie group are attempted in this section. The explicit form of the rotational operator is

$$\hat{R}(\Omega) = e^{-i\alpha \hat{J}_y} e^{-i\beta \hat{J}_y} e^{-i\hat{J}_z}, \tag{2.1}$$

where Ω is the group parameter which represents a set of Euler angles ($\alpha,\gamma = [0, 2\pi]$ and $\beta = [0, \pi]$). Further, $\hat{J}$'s are the angular momentum operators. Its (unitary) representation is

$$\left\langle \mu IM \left| \hat{R}(\Omega) \right| \nu JK \right\rangle = \delta_{\mu\nu}\delta_{IJ} D^{I*}_{MK}(\Omega), \tag{2.2}$$

where $\hat{R}(\Omega)$ is the rotational operator and $D^{I*}_{MK}(\Omega)$ is the D-function [8] and the symbol * means the complex conjugation. The D-functions from a complete set of functions in the parameter space of Ω. For a state $\left|\mu IM\right\rangle$ belonging to the angular momentum IM, μ represents a set of quantum numbers that specify the quantum state uniquely, so that the following closure holds:

$$\sum_{\mu IM} \left| \mu IM \right\rangle \left\langle \mu IM \right| = 1 \tag{2.3}$$

On Comparing eqs. (2.2) and (2.3), one gets the following equation given below

$$\hat{R}(\Omega)\left|\nu IK\right\rangle = \sum_{M} \left|\nu IM\right\rangle D^{I*}_{MK}(\Omega), \tag{2.4}$$

which is the multiplet relation between the states belonging to a representation (angular momentum) I. Combining equation (2.4) with the orthogonality of the D-functions

$$\int d\Omega D^{I*}_{M'K'}(\Omega) D^{I'}_{M'K'}(\Omega) = \frac{8\pi^2}{2I+1}\delta_{II'}\delta_{MM'}\delta_{KK'} \tag{2.5}$$

one finds that,

$$\hat{P}^{I}_{MK}\left|\nu I'K'\right\rangle = \delta_{II'}\delta_{KK'}\left|\nu IM\right\rangle, \tag{2.6}$$

the operator $\left\{\hat{P}^{I}_{MK}\right\}$ appearing in above equation is known as angular momentum projection operator and is defined as

$$\hat{P}^{I}_{MK} = \frac{I+\frac{1}{2}}{4\pi^2}\int d\Omega \hat{R}(\Omega) D^{I*}_{MK}(\Omega), \tag{2.7}$$

Equations (2.3) and (2.6), gives the spectral representation of $\left\{\hat{P}^{I}_{MK}\right\}$ and the "sum rule"

$$\hat{P}^{I}_{MK} = \sum_{\nu} \left|\nu IM\right\rangle \left\langle \nu IK\right|, \quad \sum_{iM} \hat{P}^{I}_{MM} = 1 \tag{2.8}$$

By using the spectral representation, one can easily obtain the properties

$$\hat{P}^{I\dagger}_{MK} = \hat{P}^{I}_{KM} \quad \text{and} \quad \hat{P}^{I}_{KM}\hat{P}^{I'}_{M'K'} = \delta_{II'}\delta_{MM'}\hat{P}^{I}_{KK'} \tag{2.9}$$

The projection operators must satisfy the relations $P_i^{\dagger} = P_i$, $P_iP_j = \delta_{ij}P_i$ and $\sum_i P_i = 1$ so that $\hat{P}^{I}_{MK}$ is a projection operator only if $K \equiv M$.

The Particle Number Projection Operator (in terms of a Gauge group [element = exp $(-i\phi\hat{N})$ and representation = exp $(i\phi N)$]) can also be introduced in a similar way as

$$\hat{P}^{N} = \frac{1}{2\pi}\int_0^{2\pi} d\phi e^{-i\phi(\hat{N}-N)} \tag{2.10}$$

where $\hat{N} \rightarrow$ particle number operator.

$\phi \rightarrow$ gauge angle.

$\hat{P}^{N} \rightarrow$projection operator

On combining eqns. (2.7) and (2.10), one gets

$$\hat{P}^{IN}_{MK} \equiv \hat{P}^{I}_{MK}\hat{P}^{N} = \frac{2I+1}{16\pi^2}\int d\Omega D^{I*}_{M'K'}(\Omega)D^{I'}_{M'K'}(\Omega) = \frac{8\pi^2}{2I+1}\delta_{II'}\delta_{MM'}\delta_{KK'} \tag{2.11}$$

Here, $\hat{P}^{I}_{MK}$ and $\hat{P}^{N}$ commute with each other. In the following paragraph we have demonstrated how such an operator comes into play in a physical problem taking the angular momentum projection operator as an example.

Let $|\phi\rangle$ is a "deformed" state, i.e. it is not an eigen-state of the angular momentum. Rotational invariance of the Hamiltonian then gives

$$\hat{R}^{\dagger}(\Omega)\hat{H}\hat{R}(\Omega) = \hat{H} \ , \tag{2.12}$$

The energy expectation value will remain invariant even if $|\phi\rangle$ is rotated, i.e. all states $\hat{R}(\Omega)|\phi\rangle$ having different orientation Ω are mutually degenerate. Here $\hat{R}(\Omega)|\phi\rangle$ can be linearly independent of $|\phi\rangle$. Using the following superposition, one can construct a wider class of states

$$|\psi\rangle = \int d\Omega F(\Omega)\hat{R}(\Omega)|\phi\rangle, \tag{2.13}$$

where the function $F(\Omega)$ can be determined by minimizing the energy expectation value

$$E = \frac{\langle\psi|\hat{H}|\psi\rangle}{\langle\psi|\psi\rangle}, \tag{2.14}$$

This procedure gives an energy lower than that discussed earlier because the space spanned by $\hat{R}(\Omega)|\phi\rangle$ is larger than that consisting of just a single state $|\phi\rangle$ which corresponds to Ω =0. Using completeness of the *D*-functions, one can simplify this procedure. The trail function $F(\Omega)$ can be expanded as

$$F(\Omega) = \sum_{IMK} \frac{2I+1}{8\pi^2} F^I_{MK} D^I_{MK}(\Omega), \tag{2.15}$$

putting eq.(2.15) in eq.(2.13), one gets,

$$|\psi\rangle = \sum F^I_{MK} \hat{P}^I_{MK} |\phi\rangle, \tag{2.16}$$

Where, $\hat{P}^I_{MK}$ → the angular momentum projection operator defined by eq. (2.7).

F^I_{MK}→ variational parameters in place of the variational function $F(\Omega)$.

If the variational procedure is carried out with eq.(2.16), the summation over *I* and *M* drops away (i.e., a sharp *I* and *M*) due to eqs. (2.9) and (2.12). Here, (2.12) implies that the Hamiltonian commutes with the projection operator. Thus, the variational calculation can be carried out with

$$|\psi\rangle = \sum_K F^I_K \hat{P}^I_{MK} |\phi\rangle, \tag{2.17}$$

by omitting the summation over *I* and *M*. So, $|\psi\rangle$ becomes an eigen state of the angular momentum. The rotational symmetry violated in the original state $|\phi\rangle$ is thus recovered in the new state $|\psi\rangle$. The resulting variational equation takes the form of an eigen value equation (and a normalization condition) independent of *M*.

$$\sum_{K'} (H^I_{KK'} - EN^I_{KK'}) F^I_{K'} = 0, \qquad \sum_{KK'} F^I_K N^I_{KK'} F^I_{K'} = 1, \tag{2.18}$$

where the Hamiltonian and norm matrix take the form,

$$H^I_{KK'} = \langle\phi|\hat{H}\hat{P}^I_{KK'}|\phi\rangle \quad \text{and} \quad N^I_{KK'} = \langle\phi|\hat{P}^I_{KK'}|\phi\rangle, \tag{2.19}$$

A given spin I appears more than once in the whole spectrum, if the state $|\phi\rangle$ is triaxial, I=0 being a trivial exception. On the other hand, if it is axially symmetric i.e. if, $\hat{J}|\phi\rangle = K_0|\phi\rangle$ holds where K_0 is the conserved K-quantum number, the problem is simple. The solution of eq.(2.18) then becomes

$$E = \frac{H^I_{K_0K_0}}{N^I_{K_0K_0}} \quad \text{with} \quad F^I_{K_0} = \frac{1}{\sqrt{N^I_{K_0K_0}}}, \tag{2.20}$$

Only term with $K = K_0$ remains in the summation over K. This represents the most primitive form of the angular momentum projection theory, which can describe one "rotational band" whose "rotational energy" is obtained by evaluating E as a function of spin I, i.e. it does not allow admixture of excited bands. Here, spin I appears only once in the spectrum, which is contrary to the triaxial case. For an axially symmetric case, the projection operator $\hat{P}^I_{MK}$ becomes,

$$\left(I + \frac{1}{2}\right)\int_0^\pi d\beta \sin\beta d^I_{MK}(\beta) e^{-i\beta\hat{J}_y}, \tag{2.21}$$

since α and γ can be integrated explicitly when evaluating the matrix elements. The state $|\phi\rangle$ is an intrinsic state and as such is highly degenerate and symmetry breaking state, so a better state $|\psi\rangle$ can be constructed by using this degeneracy, where the violated symmetry can be recovered. So, one can accept $|\psi\rangle$ as a possible approximate solution of the Hamiltonian. Here $|\psi\rangle$ ($|\phi\rangle$) is referred to as a state in the "space-fixed" ("body-fixed") system. There exists two sets of (mutually commuting) differential operators, the space-fixed and body–fixed type, both representing the angular momentum, the latter being characterized by "wrong" signs in the angular momentum commutation relations. Here, the former (latter) originates the quantum number $M(K)$ of $D^I_{MK}(\Omega)$. Here, M and K of the operators $\hat{P}^I_{MK}$ can be associated with same physical interpretation as those of $D^I_{MK}(\Omega)$ and, as eq. (2.17) shows, the quantum number M belongs to $|\psi\rangle$ and K to $|\phi\rangle$.

Thus, the former (latter) is referred as the "space-fixed" ("body-fixed") state. So, the projection operator transforms a "body-fixed" state into a "space-fixed" state. One may find the contents of this projection theory as abstract, but many concepts developed in the semi-classical theory, such as the rotor model[9] can also be used in the projection theory as they can be translated using an analogy. For example, the structure of the wave functions should make it clear that the rotational motion of the "body" as a whole is described phenomenologically by the *D*-function $D^I_{MK}(\Omega)$ in the former and microscopically by the projection operator $\hat{P}^I_{MK}$ in the latter.

2.4 Semi-classical Limit

Previous subsection gives the projection of just one "configuration" $|\phi\rangle$ onto a good angular momentum. Initially, the formula (2.20) represented the whole contents of the angular momentum projection method [10]. Later, a pioneering calculation [11, 12] was carried out using the Nilsson + BCS quasiparticle vacuum state $|0\rangle$ for $|\phi\rangle$ (with $K_0 = 0$) which represents the ground state band or g-band of a doubly-even nucleus. The outcome of the theory is as follows:

After the α- and γ- integration, the matrix element $\langle 0|\hat{O}\,\hat{P}^I_{00}\,|0\rangle\left(\hat{O} = 1, \hat{H}\right)$ becomes

$$(2I+1)\int_0^{\frac{\pi}{2}} d\beta \sin\beta P_I(\cos\beta)\langle 0|\hat{O}e^{-i\beta\hat{J}_y}|0\rangle \text{ for } I = \text{even} \tag{2.22}$$

and 0 for I = odd. Here, $d^I_{00}(\beta) = (-)^I d^I_{00}(\pi-\beta) = P_I(\cos\beta)$ is used and the symmetry of the integrated with respect to $\beta = \dfrac{\pi}{2}$ due to $e^{-i\pi\hat{J}_y}|0\rangle = e^{-i\pi\hat{J}_z}|0\rangle = |0\rangle$ has been used.

The above integral is called the "semi-classical" limit. Since the fluctuation of the angular momentum is a good measure for the deformation, the result may be written as a power series in $1/\Delta J_y^2$.

The overlap of $\langle 0|e^{-i\beta\hat{J}_y}|0\rangle$ can be written in the form

$$\langle 0|e^{-i\beta\hat{J}_y}|0\rangle = \exp\left\{-i\int_0^{\beta} d\beta'\langle 0|\hat{J}_y[\beta']|0\rangle\right\},\ [\beta] \equiv \frac{e^{-i\beta\hat{J}_y}}{\langle 0|e^{-i\beta\hat{J}_y}|0\rangle}, \tag{2.23}$$

which, can be confirmed by differentiating both sides with respect to β. The left-hand side of eq. (2.23) corresponds to the characteristic function and the exponent of the right-hand side to the cumulant function known in statistical physics. The expansion in terms of moments is given by the cumulant expansion, which is a power series expansion of the cumulant function. In this case, it can be obtained from the power series expansion of the operator $[\beta]$ for small β,

$$[\beta] = 1 - i\beta\left(\hat{J}_y - J_y\right) - \frac{1}{2}\beta^2\left(\hat{J}_y^2 - \Delta J_y^2\right) + \ldots\ldots \tag{2.24}$$

Because of the time reversal symmetry of $|0\rangle$ the first order moment $J_y = \langle 0|\hat{J}_y|0\rangle$ is zero. It is better to stop at the second moment $\Delta J_y^2 = \langle 0|\hat{J}_y - J_y|0\rangle = \langle 0|\hat{J}_y^2|0\rangle$, which corresponds to the fluctuation of the angular momentum. The following approximate relations are thus obtained:

$$\langle 0|e^{-i\hat{J}_y}|0\rangle \approx e^{-\frac{1}{2}\Delta J_y^2\beta^2}; \qquad [\beta] \approx 1 - i\beta\hat{J}_y - \frac{1}{2}\beta^2 :\hat{J}_y^2: \tag{2.25}$$

where: $\hat{J}_y^2 :\equiv \hat{J}_y^2 - \Delta J_y^2$. The overlap is strongly peaked at $\beta = 0$ if ΔJ_y^2. is large. The integral in eq. (2.22) can be obtained in a closed form by using the approximation given by eq. (2.25) as well as an asymptotic form $P_I(\cos\beta) \approx J_0(\sqrt{I(I+1)}\beta)$ valid for small β, where $J_0(x)$ is the Bessel function of order zero, and by extending the integration range to infinity

$$\int_0^\infty d\beta\beta J_0(\sqrt{I(I+1)}\beta) e^{-\frac{1}{2}\Delta J_y^2\beta^2} \left\{ \langle 0|\hat{O}|0\rangle - \frac{1}{2}\langle 0|\hat{O}\hat{J}_y^2 :|0\rangle\beta^2 \right\} \tag{2.26}$$

Also one has,

$$\int_0^\infty dx x^{2n+1} J_0(bx) \exp\left\{-\frac{1}{2}a^2x^2\right\} = \frac{2^n n!}{a^{2n+2}} L_n\left(\frac{b^2}{2a^2}\right) \exp\left\{-\frac{b2}{2a^2}\right\}, \tag{2.27}$$

where $L_n(x)$ is the Laguerre Polynomial of the order n. The energy $E_I = {H_{00}^I}/{N_{00}^I}$ and the norm N_{00}^I (for I=even only) can thus be written as

$$E_I \approx E_0 + \frac{I(I+1)}{2\Im} \text{ and } N_{00}^I \approx Q_I \equiv \frac{2I+1}{\Delta J_y^2}\exp\left\{-\frac{I(I+1)}{2\Delta J_y^2}\right\}, \tag{2.28}$$

respectively, where,

$$\Im \approx \frac{(\Delta J_y^2)^2}{\langle 0|\hat{H} : \hat{J}_y^2 : |0\rangle} \text{ and } E_0 = \frac{H_{00}^0}{N_{00}^0} \approx \langle 0|\hat{H}|0\rangle - \frac{\Delta J_y^2}{\Im} \tag{2.29}$$

Where, $\Im$ is Peierls-Yoccoz moment of inertia, The projected ground state energy E_0 is lower that the unprojected one, $\langle 0|\hat{H}|0\rangle$, by an amount $\frac{\Delta J_y^2}{\Im}$. This energy gain is due to the fluctuation of the angular momentum, which causes a "zero-point rotation". Since $\Delta J_x^2 = \Delta J_y^2$, it may be written as $\frac{1}{2\Im}\left(\Delta J_x^2 + \Delta J_y^2\right)$, this corresponds to fluctuation of the rotational energy.

The norm N_{00}^I represents the probability distribution of the angular momentum in the ground state $|0\rangle$ as can be seen by using the spectral representation of eq.(2.8), $N_{00}^I = \langle 0|\hat{P}_{00}^I|0\rangle = \sum \langle 0|\nu I 0\rangle^2$. Its approximation Q_t is normalized to 1 under the replacement $\sum_{I=even} \to \int_0^\infty \frac{dI}{2}$. The metric $\frac{1}{2}$ corresponds to the summation only over *I = even*. From here one can see that the formulas depend only on two quantities, E_I . E_o on $\Im$ and N_{00}^I on ΔJ_y^2 , namely eq. (2.28) is the same for any Hamiltonian, which yields the same $\Im$ and ΔJ_y^2. So, the result does not depend on details of the Hamiltonian.

2.5 Choice of the Hamiltonian

Right through the text pertaining to the theory of PSM, we have talked about the Hamiltonian $\hat{H}$, but its nature is not yet described. The Hamiltonian which has been used throughout the present work consists of a sum of schematic (Quadrupole-Quadrupole + Monopole + Quadrupole pairing) forces which represent different kinds of characteristic correlations between active nucleons. The total Hamiltonian of the present model is represented by the equation

$$\hat{H} = \hat{H}_0 - \frac{\chi}{2}\sum_{\mu}\hat{Q}^{\dagger}_{\mu}\hat{Q}_{\mu} - G_M\hat{P}^{\dagger}\hat{P} - G_Q\sum_{\mu}\hat{P}^{\dagger}_{\mu}\hat{P}_{\mu} \tag{2.30}$$

where, $\hat{H}_0$, is the harmonic oscillator single particle Hamiltonian and is given by

$$\hat{H}_0 = \sum_{\alpha} c^{\dagger}_{\alpha} E_{\alpha} c_{\alpha} \quad , \qquad \text{with} \qquad E_{\alpha} = \hbar\omega[N - 2\kappa\hat{l}\cdot\hat{s} - \kappa\mu(\hat{l}^2 - \langle\hat{l}\rangle^2)] \tag{2.31}$$

Here, $E_\alpha \rightarrow$ single-particle energy and

$c^{\dagger}_{\alpha}$ (c_α)$\rightarrow$single-particle creation (annihilation) operators, spherical harmonic

$\alpha = \{N, j, m\}\rightarrow$ spherical harmonic oscillator quantum numbers

$\omega \rightarrow$ harmonic-oscillator parameter which incorporates the principle of volume conservation for nuclei deformed from spherical shapes, s and $l \rightarrow$ intrinsic nucleon spins and orbital angular momenta in the stretched co-ordinate basis.

κ and $\mu \rightarrow$ Nilsson parameters

The remaining terms in eq.(2.30) are residual quadrupole-quadrupole, monopole pairing and quadrupole pairing interactions, respectively. The operators appearing in eq.(2.30) are defined, as in ref.[13], as

$$\hat{Q}_{\mu} = \sum_{\alpha\beta} c^{\dagger}_{\alpha}(Q_{\mu})_{\alpha\beta}c_{\beta}, \qquad \hat{P}^{\dagger} = \frac{1}{2}\sum_{\alpha} c^{\dagger}_{\alpha}c^{\dagger}_{\bar{\alpha}} \quad , \qquad \hat{P}^{\dagger}_{\mu} = \frac{1}{2}\sum_{\alpha\beta} c^{\dagger}_{\alpha}(Q_{\mu})_{\alpha\beta}c^{\dagger}_{\bar{\beta}}, \tag{2.32}$$

$$\text{with } (Q_{\mu})_{\alpha\alpha'} = \sqrt{\frac{4\pi}{5}}\delta_{NN'}\langle N\ j\ m|\left(\frac{r}{b}\right)^2 Y_{2\mu}|N'\ j'\ m'\rangle, \tag{2.33}$$

where, $|\alpha\rangle = |N\ j\ m\rangle$, $|\alpha'\rangle = |N'\ j'\ m'\rangle$ and $b^2 = \hbar/m\omega$,

For the given deformation ε_2, the coupling constant (χ) of $Q.Q$ force *i.e* the (stretched) Nilsson potential $\frac{2}{3}\varepsilon_2\hbar\omega\,\hat{Q}_o$) which determines the strength of this force, is given by

$$\chi_{\tau\tau'} = \frac{\frac{2}{3}\varepsilon_2\hbar\omega_{\tau}\hbar\omega_{\tau'}}{\hbar\omega_{n}\langle\hat{Q}_0\rangle_{n} + \hbar\omega_{P}\langle\hat{Q}_0\rangle_{P}} \tag{2.34}$$

where, $\omega_\tau = \omega_o\left(1 \pm \frac{N-Z}{A}\right)^{\frac{1}{3}}$, with +(-) for τ = neutron(proton) and $\hbar\omega_o = 41.47A^{-1/3}$ fm^2

and its value is adjusted via self-consistent conditions with a given quadrupole deformation ε_2. The quadrupole moments of all active deformed Nilsson orbitals, weighed by their occupation numbers, are added to evaluate the expectation values $\langle Q_o \rangle_n$ and $\langle Q_o \rangle_p$. They depend on the assumed mean-field deformation ε_2 and vanish for spherical nuclei, leaving χ undetermined in that case.

It is assumed that all pairing interactions occur between the like nucleons (i.e., the isovector type). The monopole interaction, G_M, is given as

$$G_M = \left(G_1 \mp G_2 \frac{N-Z}{A}\right)\frac{1}{A}(MeV) \tag{2.35}$$

with - (+) for neutrons(protons). Here, G_1 and G_2 are the two adjustable constants. Adjusting the parameters ε_2, G_1 and G_2 will change the energy gap for each shell and, thus, will affect the selection of the quasiparticle basis. In the present case, the hexadecupole deformation, ε_4, has also been included. The values of the empirical deformation, ε_2, which we have used as an input in the PSM calculations for the nuclei lying in the mass region A~120, are given in Tables in the corresponding chapters.

The strength G_Q is assumed to be proportional to G_M, with an overall constant γ, *for* quadrupole pairing force, such that

$$G_Q = \gamma\, G_M \tag{2.36}$$

Here, γ can be carefully adjusted to get the best representations of the experimental observations.

The second step now is to diagonalize the Hamiltonian in the shell model space spanned by a selected set of projected multi-quasiparticle $\left\{\hat{P}^I_{MK}|\phi_\kappa\rangle\right\}$ state, where $\left\{\hat{P}^I_{MK}\right\}$ is the angular momentum projection operator which projects the quantum numbers *I, M* and is defined as

$$\hat{P}^{I}_{MK} = \frac{I+\frac{1}{2}}{4\pi^2}\int d\Omega \hat{R}(\Omega) D^{I*}_{MK}(\Omega), \tag{2.37}$$

Here, $\hat{R}(\Omega) \rightarrow$ rotational operator,

$D^{I*}_{MK}(\Omega) \rightarrow D$ function

$\Omega \rightarrow$Euler angle.

The D-functions form a complete set of functions in the parameter space of Ω.

In the PSM calculations presented in the thesis, I have used only angular momentum projection $\left\{\hat{P}^{I}_{MK}\right\}$ and not the particle number projection since the essential physics of the yrast spectroscopy can be described even without taking it into consideration. Further, violation of the particle number caused by the BCS (or HFB) approximation is not so dangerous for the projected shell model as usually believed in the sense that the essence of the physics obtained by the angular momentum projection alone is not altered even if the particle number projection is carried out in addition. It is, therefore, not considered to be of absolute necessity for understanding various phenomena related to nuclear rotational motion. Further, the spurious state(s) originating from the particle number violation will be removed automatically as a zero norm state when the Hamiltonian is diagonalized in the number projected basis.

The multi-quasiparticle configurations are listed below for different types of nuclei:

Doubly-even nucleus: $|0\rangle, a^{+}_{\nu 1}a^{+}_{\nu 2}|0\rangle, a^{+}_{\nu 1}a^{+}_{\nu 2}a^{+}_{\pi 1}a^{+}_{\pi 2}|0\rangle,$

Doubly-odd nucleus: $a^{+}_{\nu}a^{+}_{\pi}|0\rangle,$

Odd-Neutron Nucleus: $a^{+}_{\nu}|0\rangle, a^{+}_{\nu}a^{+}_{\pi 1}a^{+}_{\pi 2}|0\rangle,$

Odd-proton nucleus: $a^{+}_{\pi}|0\rangle, a^{+}_{\pi}a^{+}_{\nu 1}a^{+}_{\nu 2}|0\rangle,$

where $\nu's(\pi's)$ represent the neutron(proton) Nilsson quantum numbers which run over properly selected (low-lying) quasiparticle states. The configurations that contain three or

more like-nucleon quasiparticles been discarded because they have higher excitation energies due to mutual blocking of levels and thus are of little use in the present work.

In the present calculations, i.e. for odd proton Iodine and Antimony nuclei, the multi-quasiparticle configurations used is given as

$$|\phi_\kappa\rangle = \{\, a_\pi^\dagger|0\rangle, a_\pi^\dagger a_{\nu 1}^\dagger a_{\nu 2}^\dagger|0\rangle \,\} \tag{2.38}$$

where, $a_\pi^\dagger$ and $a_\pi^\dagger a_{\nu 1}^\dagger a_{\nu 2}^\dagger$ are the creation operators for 1-qp and 3-qp's and ν's(π's) are neutron (proton) nilsson quantum numbers which run over properly selected (low lying) quasiparticle states and |0> is the Nilsson + BCS vaccum (0-qp state). Configurations with three or more like particles are not included as they have higher excitation energies and as such are of little use in the present energy (and spin) ranges.

The PSM wave function can be written as

$$\left|\Psi_{IM}^{\sigma}\right\rangle = \sum_{K\kappa} f_K^\sigma \hat{P}_{MK}^I |\phi_\kappa\rangle \tag{2.39}$$

where, σ → states with same angular momentum

κ→ basis states

f_κ^σ →weights of the basis state, determined by diagonalization of shell model hamiltonian the space spanned by the projected basis states given above.

the eigen value equation (for a given spin I) is given as

$$\sum_{K'} (H_{KK'}^I - E_{\sigma,I} N_{KK'})_{K'}^I f_{\kappa'}^{\sigma,I} = 0 \tag{2.40}$$

With the following normalization condition

$$\sum_{\kappa\kappa'} f_\kappa^{\sigma,I} N_{\kappa\kappa'} f_{\kappa'}^{\sigma',I'} = \delta_{\sigma\sigma'}\delta_{II'} \tag{2.41}$$

Here, the Hamiltonian and norm matrix are given by

$$H_{\kappa\kappa'}^I = \langle\Phi_\kappa|\hat{H}\hat{P}_{K_\kappa K'_{\kappa'}}^I|\Phi_{\kappa'}\rangle \text{ and } N_{\kappa\kappa'} = \langle\Phi_\kappa|\hat{P}_{K_\kappa K'_{\kappa'}}^I|\Phi_{\kappa'}\rangle \tag{2.42}$$

The Projected Shell Model (PSM) works amazingly well despite its simplicity, though, it has obvious short comings. Firstly, the nuclear deformation is restricted to the quadrupole

type only. Secondly, the neutron-proton interaction is present only in the (particle-hole type) quadrupole-quadrupole force. Depending on the problem, all this might be too restrictive and one will have to introduce (schematic) forces of a more general type. However, for the nuclei under study in the present work, PSM works quite satisfactorily and further, as long as the physics under consideration is mainly of the quadrupole-and-pairing-type collectivities, I find no compelling reasons for not using these simple interactions.

Bibliography

[1] K. Hara and Y. Sun, *Int. J. Mod. Phys.* **E4** (1995) 637.

[2] J. P. Elliot, Proc. Roy. Soc. **245** (1968) 128.

[3] M. G. Mayer, Phys. Rev. **C75** (1949) 1968; O. J. Haxel, J. H. D. Jensen and H. E. Suess, Phys. Rev. **C75** (1949) 1766; M. G. Mayer and J. H. D. Jensen, *Elementary Theory of Nuclear Shell Structure* (John Wiley & Sons, New York, 1955).

[4] S. G. Nilsson, Dan. Mat. Fsy. Medd. **29** (1955) 16

[5] K. Hara, and Y. Sun, Nucl. Phys. **A529** (1991) 445.

[6] K. Hara, and Y. Sun, Nucl. Phys. **A531** (1991) 221

[7] K. Hara, and Y. Sun, Nucl. Phys. **A537** (1992) 77.

[8] A. Bohr and B. R. Mottelson, *Nuclear Structure Vol. **I**, Appendix 1A(Benjamin, Inc., London, 1969).*

[9] A. Bohr and B. R. Mottelson, *Nuclear Structure Vol. **II**, Chapter 4(Benjamin,Inc., London, 1975).*

[10] R. E. Pierls and I. Yoccoz, Proc. Phys. Soc. **A70** (1957) 381.

[11] N. Onishi and S. Yoshida, Nucl. Phys. **80** (1966) 367.

[12] N. Onishi , R. K. Sheline and S. Yoshida, Phys. Rev. **C3** (1970) 1304.

[13] T. Bengtsson , I. Ragnarsson, Nucl. Phys. **A436** (1985) 14.

3. Structure evolution of odd-mass $^{119-127}$I nuclei within Projected Shell Model

3.1 Introduction

The nuclei near the closed shell at $Z = 50$ with mass number $A\sim120$ have been the subject of extensive experimental and theoretical studies for the many years. These nuclei exhibit a variety of nuclear phenomena like co-existence of shapes, large ground state deformation, band crossing, rapid variation of structure with changing proton and neutron number, etc. The study of low- and high-spin phenomena in the neutron-rich mass-120 nuclei has also attracted considerable interest in recent years. This has been motivated by the increasing power of experimental facilities and improved theoretical descriptions in understanding the structure of these unstable nuclei. The Iodine isotopes ($Z = 53$), which lie in the transitional region between the near-spherical Sn ($Z = 50$) and the deformed Ce ($Z = 58$) nuclei, have well-developed rotational structures in the light odd-mass Iodine nuclei with $A < 121$ and these structures are built on proton $h_{11/2}$ states [1]. The negative-parity states in the heavier odd-mass Iodine isotopes with $A > 121$, associated with the neutron $h_{11/2}$ orbital, show a vibrational structure similar to the neighbouring even-mass Te isotopes [2]. The odd-mass Iodine nuclei with $A = 117–125$ are characterized by the presence of a large number of rotational bands, with the odd proton occupying the different Nilsson orbitals available near the Fermi level [3-9]. As a result of the availability of enormous experimental data in the odd mass Iodine nuclei near $A\sim120$, various theoretical approaches have been applied to explain the bands structure, for example, the ground-state yrast bands in the odd-A $^{121\text{-}125}$I arise from the high-K $\pi g_{7/2}$ and $\pi d_{5/2}$ proton orbitals [5-8]. Excited $\pi g_{9/2}$ and $\pi h_{11/2}$ bands have also been observed in these nuclei as well as the lighter ^{119}I isotope [4]. Three quasi-particle states with rotational bands at excitation energy of about 2 MeV are also reported [4,5,8,9] in ^{119,121,125}I. The configurations of these states involve the odd-proton coupled to the two quasi-particle states of the respective even-even Te core nuclei, where the protons occupy the $\pi d_{5/2}$ and $\pi g_{7/2}$ orbitals while the neutrons are distributed in the $\nu d_{5/2}$, $\nu g_{7/2}$ and $\nu h_{11/2}$ orbitals. The PES calculations by Liang et al. [10] have predicted competing prolate and oblate shapes for $d_{5/2}$ and $g_{7/2}$ configurations in ^{121,123,125}I isotopes. Although the oblate states are predicted to be lower in energy for the iodine nuclei with $A \geq 121$ and the prolate states are favoured for the lighter ^{119}I, the energy difference between the oblate and prolate

states is predicted to be very small. The experimental studies [4-6] in ^{119,121,123}I isotopes show evidence of oblate shape being associated with the bands based on $d_{5/2}$ and $g_{7/2}$ configurations. Low-spin states in ^{125}I were first established from β-decay studies of ^{125}Xe [11,12]. Later, high-spin states for positive-parity and negative-parity up to $25/2^+$ and $43/2^-$, respectively were identified through in-beam spectroscopy [7,8,13-16] using small detector arrays. The previously [16] known negative-parity states up to $43/2^-$ in ^{125}I were further extended up to the $63/2^-$ state by Singh et al. [17]. The γ -ray spectroscopic study [7] of the nuclear structure of ^{125}I has led to extensions and alterations of the previously reported [13,18,19] level scheme of this nucleus, in which several new intra-band and inter-band transitions are observed in the positive-parity bands based on $\pi d_{5/2}$ and $\pi g_{7/2}$ configurations, indicating mixing of the two configurations in these bands. Negative-parity high spin states in ^{123}I were measured experimentally [20] and rotational band, built on the $\pi h_{11/2}$ single particle state, was extended up to spin $I = 35/2^-$. Also, recently [21], the high-spin states of ^{123}I have been studied experimentally by using the ^{80}Se (^{48}Ca, $p4n$) ^{123}I reaction at 207 MeV in which the level scheme of ^{123}I has been extended up to spin $I = 63/2^-$, where the nucleus undergoes a shape transition from moderately deformed states with collective rotation at low spins to non-collective oblate configurations at higher spins. It has been reported [5,6] from the study of the structure of odd-mass iodine nuclei ^{121,123}I that the mixing of the $\pi d_{5/2}$ and $\pi g_{7/2}$ configurations of protons can significantly affect the structure of the positive-parity bands based on the $5/2^+$ and $7/2^+$ states, and that interconnecting dipole transitions occur between the members of these bands. A large number of bands with the odd proton occupying the different Nilsson orbitals near the Fermi level were observed [22,23] in the odd-mass $^{117-127}$I isotopes. Among these bands, $\Delta I = 2$ bands, built on the $11/2^-$, $7/2^+$ and $5/2^+$ states, have been identified and the level spacings of these bands follow those of the ground state (g.s.) bands of the corresponding even-even Te core nuclei. In-beam γ spectroscopy of the stable nucleus ^{127}I has been studied experimentally using the ^{124}Sn (^{7}Li,$4n\gamma$)^{127}I reaction at a beam energy of 32 MeV by Ding et al. [24]. They have significantly extended the level scheme of ^{127}I and the negative-parity levels, built on $11/2^-$, $\pi h_{11/2}$ particle state, are observed up to $35/2^-$ for this isotope. Thus, the literature, available on different research studies applied on the neutron-rich Iodine nuclei, reveals that the energy states in these nuclei have been extended up to high spins and this was also one of the motivating factors for carrying out the present work in the perspective of study of high spin structure of Iodine nuclei. The definite information on the spins, parities of the levels and the nature of the transitions,

both intra-band and inter-band, is necessary for the better understanding of the structures of the various bands in a nucleus. In this regard, different interpretations about the various bands have been given to understand the structure of these neutron rich Iodine isotopes. The projected shell model (PSM) [25-29] has become quite popular to study the structure of deformed nuclei in various mass regions. As PSM uses a truncated valence space, the numerical requirements here are minimal and, therefore, a systematic study for a group of nuclei in a reasonable time frame is being possible. In the present work, a systematic PSM study of some nuclear structure properties of the odd-mass $^{119-127}$I isotopes has been carried out. The physical quantities that have been described are the yrast line, band diagrams, backbending in moment of inertia and the reduced transition probabilities ($B(E2)$ and $B(M1)$ values). This chapter is planned in the following way. In this chapter, Section 3.2 deals with the formal aspects of the theory of applied approach, PSM. In Section 3.3, I have discussed various nuclear structure properties that have been obtained by using PSM wavefunctions, and have also compared these results with the corresponding available experimental ones. Section 3.4 of this chapter contains the concluding remarks of the present work.

3.2 Input parameters used in PSM calculations for $^{191-127}$I isotopes

The Projected Shell Model (PSM) [25] is a modified form of the shell model approach as it differs in a way that, unlike the conventional shell model, PSM begins with the deformed (Nilsson-type) single-particle basis for the diagonalization of the shell model Hamiltonian. Such a shell model basis violates the rotational symmetry, but it can be restored by the standard angular momentum projection technique. The advantage of using deformed basis is that it incorporates important nuclear correlations more readily, especially for a well deformed system. Detail of this model is given in chapter 2 of this thesis, where a general explanation of model is given and for the detailed theory of PSM, one may refer to the article given by Hara and Sun [25] and in this section, various input parameters used for carrying out calculations on these nuclei are discussed. The most striking aspect of this quantum mechanical model is its ability to describe the finer details of high-spin spectroscopy data with simple physical interpretations and this model has been proved to be quite successful in explaining a broad range of properties of deformed nuclei in various regions of nuclear periodic table.

Table 3.2.1 Parameters used in present calculations for positive-parity and negative-parity of $^{119-127}I$ nuclei.

	^{119}I	^{121}I	^{123}I	^{125}I	^{127}I
Positive-parity					
ε_2	-0.270	-0.215	-0.227	-0.245	-0.225
ε_4	0.000	0.000	0.000	0.000	0.00
Negative-parity					
ε_2	0.210	0.200	0.170	0.160	0.140
ε_4	0.000	0.000	0.000	0.000	0.000

Table 3.2.2 Set of Nilsson parameters used as input in the present calculations for $^{119-127}I$ nuclei.

Major Shell	**Protons**		**Neutrons**	
N	K	μ	κ	μ
3	0.090	0.300	0.090	0.250
4	0.070	0.480	0.070	0.390
5	0.560	0.540	0.062	0.430

The total Hamiltonian used in the present work is

$$\hat{H} = \hat{H}_o - \frac{\chi}{2}\sum_{\mu}\hat{Q}^{\dagger}_{\mu}\hat{Q}_{\mu} - G_M\hat{P}^{\dagger}\hat{P} - G_Q\sum_{\mu}\hat{P}^{\dagger}_{\mu}\hat{P}_{\mu} \qquad (3.2.1)$$

where $\hat{H}_o$ is the spherical single-particle Hamiltonian which contains a proper spin-orbit force. The second term in Eq. (3.2.1) is the quadrupole-quadrupole (QQ) interaction and χ represents its strength whose value is adjusted via self-consistent conditions with a given quadrupole deformation ε_2 , and the last two terms in Eq.(3.2.1) are the monopole and quadrupole pairing interactions, respectively. The hexadecapole deformation, ε_4 , has also been included in the mean-field Nilsson potential to reproduce experimental energies correctly, but in the present set of calculations, its value has been set as zero for all the $^{119-}$

^{127}I nuclei to reproduce the experimental data correctly. The deformation parameters, ε_2 and ε_4, used in the present calculations are given in Table 3.2.1. Spin-orbit force parameters (κ and μ) appearing in Nilsson potential are essential to reproduce the correct shell filling and are taken from Zhang et al. [30] for the present set of calculations, as given in the Table 3.2.2

The monopole pairing force constant G_M is adjusted to give the known energy gaps and in the present calculations, it is taken as

$$G_M = \left(G_1 \mp G_2 \frac{N-Z}{A} \right) \frac{1}{A} (\text{MeV}) \tag{3.2.2}$$

where "+ "("-") is for proton (neutron), while, in this work, the values of G_1 and G_2 are chosen as 20.70 and 12.12, respectively for both positive as well as negative parity calculations. In the present calculations, I have considered three major shells, N = 3, 4 and 5 for protons as well as neutrons for both positive-parity and negative-parity calculations.

In the present work, I have assumed that the deformed single-particle states have axial symmetry and thus, the basis states, $|\varphi_k\rangle$, have K as a good quantum number, i.e., the intrinsic states are the eigenstates of the K-quantum number.

Quasi-particles defined in the deformed Nilsson + BCS calculations are the starting point of the PSM and in the present case for odd-proton nuclei; the chosen *qp* subspace is spanned by the basis set

$$\{|\varphi_k\rangle\} = \{a_\pi^\dagger|0\rangle, a_\pi^\dagger a_{\upsilon_1}^\dagger a_{\upsilon_2}^\dagger|0\rangle\} \tag{3.2.3}$$

where $a^\dagger$'s are the quasi-particle (*qp*) creation operators, υ's (π's) denote the neutron (proton) Nilsson quantum numbers which run over low-lying orbitals and $|0\rangle$ is the Nilsson + BCS vacuum (0-*qp* state). In Eq. (3.2.3), the low-lying 3-*qp* states selected for the many-body basis are those consisting of 1-*qp* plus a pair of *qp*'s from nucleons of another kind. This selection is based on physical considerations. In general, 3-*qp* states made by three nucleons of the same kind are also allowed, but such states usually lie higher in energy and in the present case for odd-proton nuclei, I have taken 3-*qp* states consisting of one-quasi-proton and two quasi-neutrons. The inclusion of the 3-*qp* configurations is important for odd-mass nuclei for a description of the band-crossing phenomenon which is caused by a rotation alignment of a pair of quasi-neutrons.

In the PSM, the many-body wavefunction is a superposition of (angular momentum) projected multi-quasiparticle states. Angular momentum projection transforms the wavefunction from the intrinsic frame to the laboratory frame.
The total wavefunction is expressed as

$$\left|\Psi_{IM}^{\sigma}\right\rangle = \sum_{K\kappa} f_{\kappa}^{\sigma} \hat{P}_{MK}^{I} \left|\varphi_{\kappa}\right\rangle, \qquad (3.2.4)$$

$$\text{with} \quad \hat{P}_{MK}^{I} = \frac{2I+1}{8\pi^2} \int d\Omega D_{MK}^{I}(\Omega) \hat{R}(\Omega)$$

where, the index σ labels the states with same angular momentum and κ labels the basis states. $\hat{P}_{MK}^{I}$ is the angular momentum projection operator and f_{κ}^{σ} are the weights of the basis state κ.

3.2.1 Deformed single particle states

One of the most convenient ways to understand the shell structure of deformed nuclei is to plot single-particle energies versus axially symmetric quadrupole deformation parameter, ε_2, i.e., the Nilsson diagram. It is well known that single particle states in a deformed potential play an important role for the formation of low lying multi-quasi-particle excited configurations. Since the present work deals with the behavior of an isotopic chain, which is sensitive to the shell filling of nucleons, it is, therefore, important to discuss the deformed single particle states employed in the calculations. Further, due to the presence of significant pairing correlations present in the nuclear system, the low energy odd-A spectra for deformed nuclei can be completely described in terms of a single quasi-particle occupation of the Nilsson diagram orbits lying near the Fermi energy. By using Nilsson model, the deformed single particle states are calculated with a standard *N*- dependent Nilsson parameters, κ and μ, given in ref. [30]. In Figs. 3.2.1(a) and 3.2.1(b), Nilsson diagrams for protons as well as neutrons are plotted, respectively. I have taken only quadrupole deformation parameter, ε_2, as a variable. In these figures, solid curves denote positive parity single particle states while dashed curves indicate negative parity single particle states. In the same figure, the dotted rectangles are also shown that enclose the most important single particle states which are occupied by the active nucleons near the Fermi surface for formation of positive parity band spectra, whereas for negative parity band spectra, these single particle states are enclosed in solid rectangles (also shown in the figure) corresponding to deformation range -0.215 to -0.270 and 0.140 to 0.210, respectively.

On examining the Nilsson diagram (see Fig.3.2.1), it is clear that for positive parity band spectra, K = 7/2, 5/2, 3/2, 1/2 components from $g_{9/2}$ orbital, K = 7/2, 5/2 components from $g_{7/2}$ orbital for protons and K = 7/2, 5/2, 3/2, 1/2 components from $h_{11/2}$ for neutrons, lie in the neighbourhood of the Fermi surface, which are physically significant and play an important role to understand the evolution of positive parity band spectra in odd mass $^{119-127}$I nuclei. Similarly, in case of negative parity band spectra, the intruder levels, K= 1/2, 3/2 from $h_{11/2}$ orbital for protons and K= 1/2, 3/2, 5/2, 7/2, 9/2 components from $h_{11/2}$ orbital for neutrons lie near the Fermi surface of the iodine nuclei under study. Thus, I can conclude that the positive parity band spectra in $^{119-127}$I isotopes originate from the occupation of $g_{9/2}$ and $g_{7/2}$ sub-shells by protons and $h_{11/2}$ sub-shell by a pair of neutrons falling on the oblate side of the quadrupole deformation. The configurations of the Nilsson orbitals responsible for producing the positive parity band spectra are: $1\pi g_{9/2} \otimes 2\nu h_{11/2}$ and $1\pi g_{7/2} \otimes 2\nu h_{11/2}$. The negative parity band spectra in these nuclei arise from the configuration: $1\pi h_{11/2} \otimes 2\nu h_{11/2}$ for positive value of quadrupole deformation.

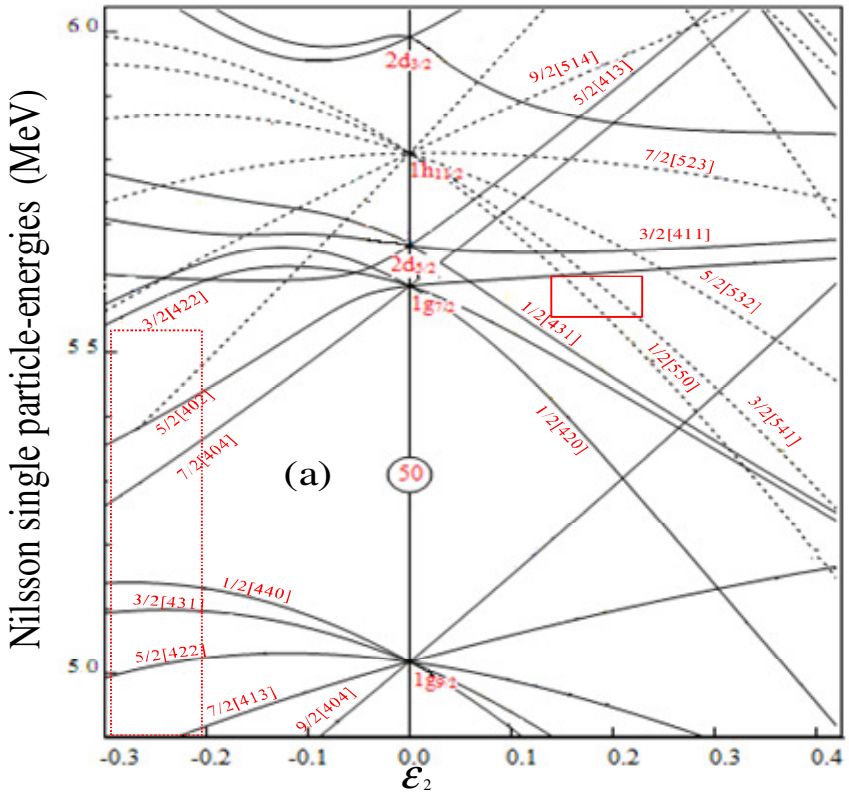

Fig. 3.2.1(a) Nilsson diagram for protons, where the Nilsson single particle energies are in MeV's.

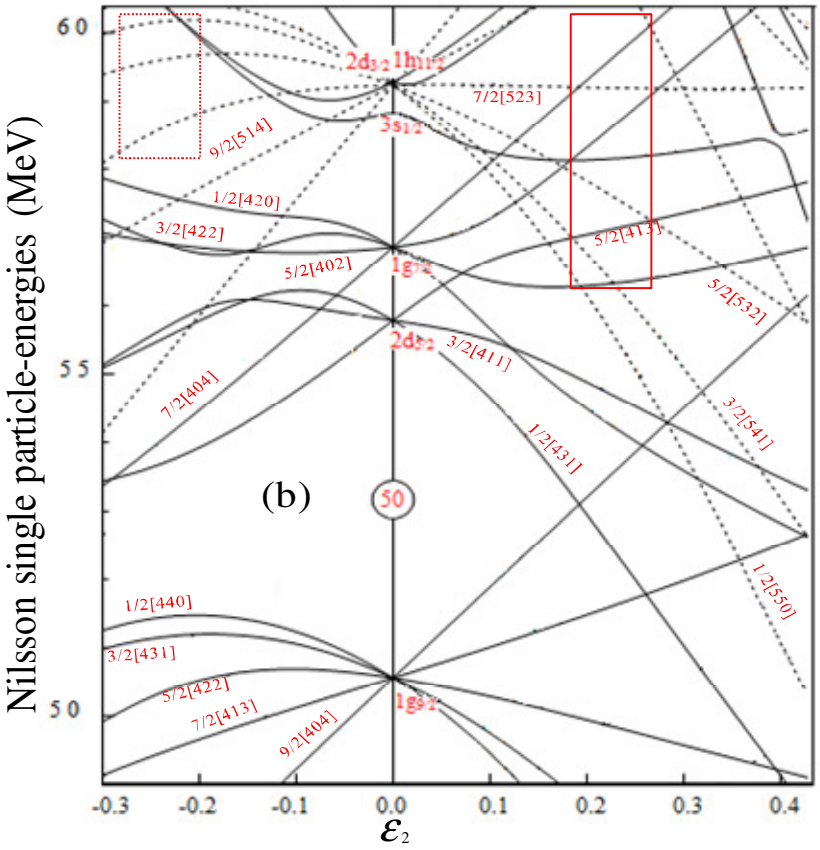

Fig. 3.2.1(b) Nilsson diagram for neutrons, where the Nilsson single particle energies are in MeV's.

3.3 Results and Discussions

Projection of good angular momentum onto each intrinsic state generates the rotational band associated with a certain intrinsic configuration$|\varphi_K\rangle$. The final results are obtained by, for each angular momentum I, solving the eigenvalue equation

$$\sum_{k'}(H_{kk'} - EN_{kk'})f_{k'} = 0 \tag{3.3.1}$$

where, $H_{\kappa\kappa'} = \left\langle \varphi_{\kappa} \middle| \hat{H}\ \hat{P}^{\mathrm{I}}_{K\kappa K'\kappa'} \middle| \varphi_{\kappa'} \right\rangle$ and $N_{\kappa\kappa'} = \left\langle \varphi_{\kappa} \middle| \hat{P}^{\mathrm{I}}_{K\kappa K'\kappa'} \middle| \varphi_{\kappa'} \right\rangle$ are the matrix elements of the Hamiltonian and the norm, respectively and $\hat{P}^{\mathrm{I}}$ is the angular momentum projection operator. The energies of each band, $E_{\mathrm{k}}(I)$, are given by the diagonal elements of H_{kk}/N_{kk} which can be plotted as a function of spin for various bands in the form of

band diagrams. Hence, the discussion about these band diagrams as well as some other nuclear structure properties is presented in the following subsections.

3.3.1 Quasi-particle structure of iodine isotopes

Band diagram plays an important role for the interpretation of the formation of yrast states. It is obtained by plotting different energy bands with respect to spin. The PSM results for band diagrams for $^{119-127}$I isotopes are discussed below isotope-wise for positive- as well as negative-parity states.

^{119}I

(a) Positive parity

Fig. 3.3.1(a) shows the band diagram calculated at the oblate minimum for ^{119}I isotope, where one can see that up to the spin of $17/2^+$, the yrast band i.e., the low lying band, is mainly formed by the combination of two 1-*qp* bands having Nilsson configurations: $\pi 7/2[404]$ and $\pi 5/2[402]$. At spin $17/2^+$, there occurs a band crossing of the above mentioned overlapped 1-*qp* bands by a 3-*qp* band with configuration: $\pi 1/2[440] \otimes \upsilon(7/2[523]$, $5/2[532])$, which then alternatively contributes to yrast band up to the spin $25/2^+$. At spin $25/2^+$, this 3-*qp* band gets superimposed with another 3-*qp* band having configuration: $\pi 7/2[404] \otimes \upsilon(7/2[523],5/2[532])$ and this combination is then responsible for the formation of yrast levels up to spin $29/2^+$. Beyond this spin, one more 3-*qp* band with configuration: $\pi 3/2[431] \otimes \upsilon(7/2[523], 5/2[532])$ joins the above mentioned set of overlapped 3-*qp* bands and forms the remaining part of the calculated yrast band.

(b) Negative parity

Fig. 3.3.1(b) presents the band diagram at the prolate minimum. From the figure, it is clear that up to the spin $27/2^-$, the yrast band is composed of two 1-*qp* bands, $\pi 1/2[550]$ and $\pi 3/2[541]$, which are then crossed by two 3-*qp* bands with configurations: $\pi 1/2[550] \otimes \upsilon(3/2[541], 5/2[532])$ and $\pi 1/2[550] \otimes \upsilon(5/2[532],7/2[523])$, and contribute to the yrast levels up to the spin $39/2^-$. At higher spins, one more 3-*qp* band with configuration: $\pi 3/2[541] \otimes \upsilon(5/2[532],7/2[523])$ superimpose on previously mentioned 3-*qp* bands and results in the formation of yrast band up to the maximun calculated spin.

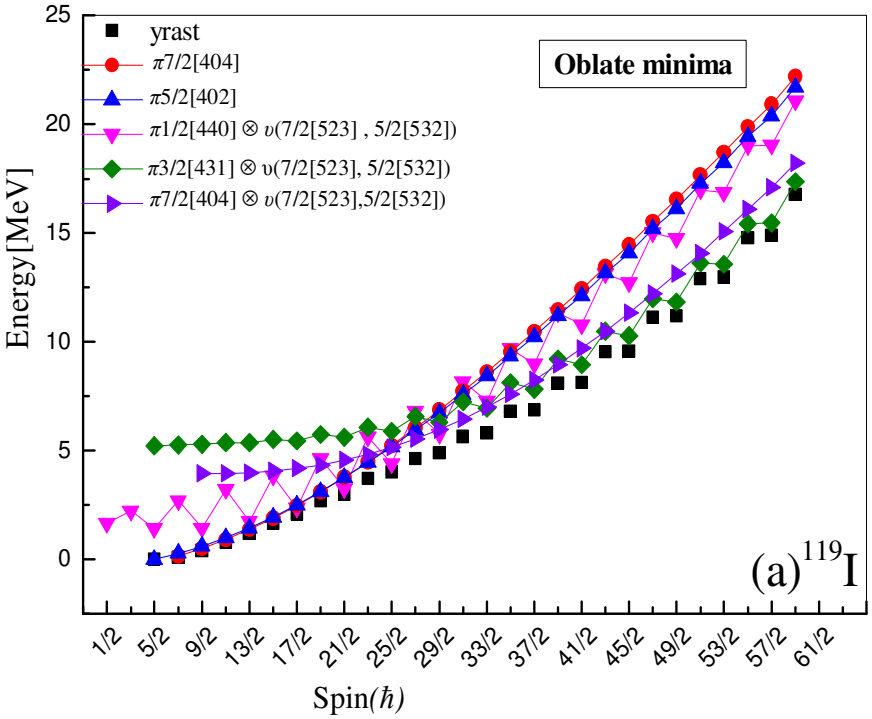

Fig. 3.3.1(a) Band diagram for positive parity for ^{119}I. Only the important lowest lying bands in each configuration are plotted.

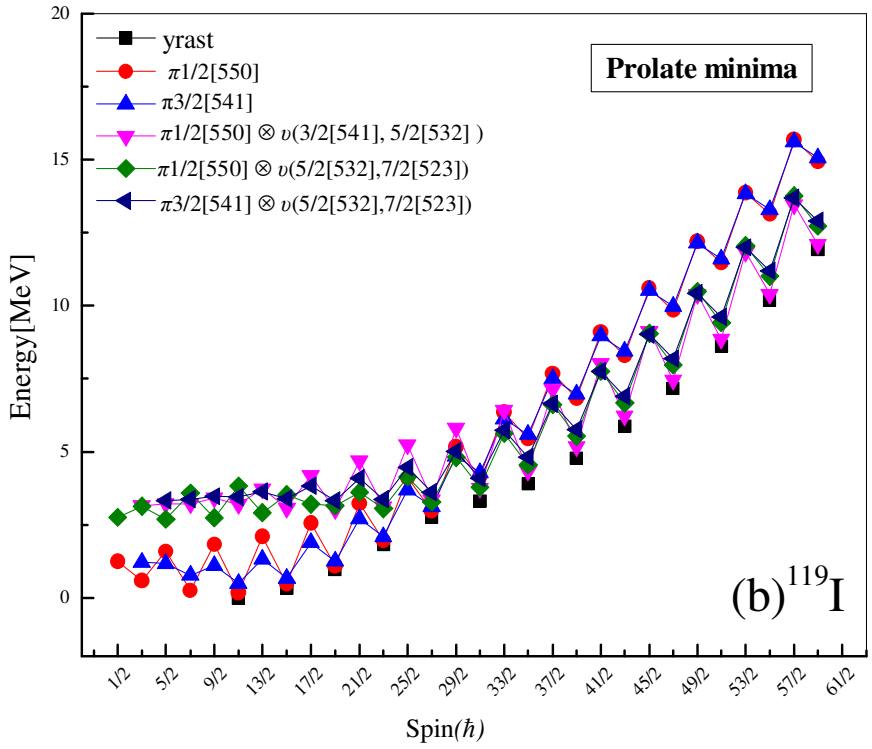

Fig. 3.3.1(b) Band diagram for negative parity for ^{119}I. Only the important lowest lying bands in each configuration are plotted.

^{121}I

(a) Positive parity

Similarly, for ^{121}I isotope (see Fig. 3.3.2(a)), the band diagram shows that the yrast band up to spin $19/2^{+}$consists of two superimposed 1-*qp* bands with configurations: $\pi 7/2[404]$ and $\pi 5/2[402]$. At the spin $19/2^{+}$, these overlapped 1-*qp* bands get crossed by one 3-*qp* band with configurations: $\pi 7/2[404] \otimes \upsilon(7/2[523], 5/2[532])$, which then contributes to the yrast states up to spin $35/2^{+}$. After this spin, three more 3-*qp* bands with configurations: $\pi 3/2[422] \otimes \upsilon(7/2[523], 5/2[532])$, $\pi 1/2[440] \otimes \upsilon(7/2[523], 5/2[532])$ and $\pi 3/2[431] \otimes \upsilon(7/2[523], 5/2[532])$, join the above mentioned 3-*qp* band and this combination of bands then gives rise to the formation of yrast levels for rest of the calculated spins.

(b) Negative parity

In case of ^{121}I, it is clear from the Fig. 3.3.2(b) that yrast band up to spin of $27/2^{-}$ is constructed from two 1-*qp* bands with configurations: $\pi 1/2[550]$ and $\pi 3/2[541]$. At spin value of $27/2^{-}$, band crossing occurs and the above mentioned 1-*qp* bands get crossed by a 3-*qp* band identified as $\pi 1/2[550] \otimes \upsilon(5/2[532], 7/2[523])$ which contributes to the yrast states up to spin $35/2^{-}$. At spin $35/2^{-}$, this 3-*qp* band gets overlapped with two more 3-*qp* bands with configurations: $\pi 3/2[541] \otimes \upsilon(5/2[532], 7/2[523])$ and $\pi 1/2[550] \otimes \upsilon(3/2[541], 5/2[532])$, which then make the yrast line up to the highest calculated spin.

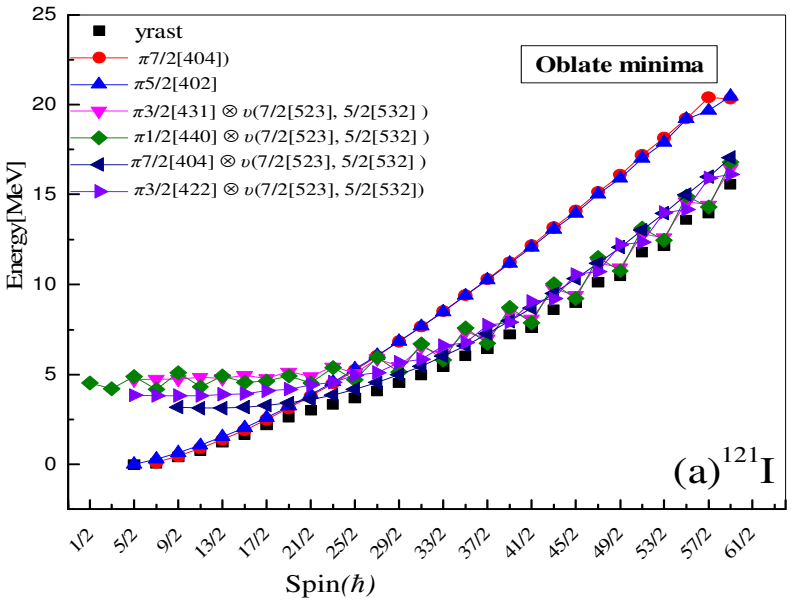

Fig. 3.3.2(a) Band diagram for positive parity for ^{121}I. Only the important lowest lying bands in each configuration are plotted.

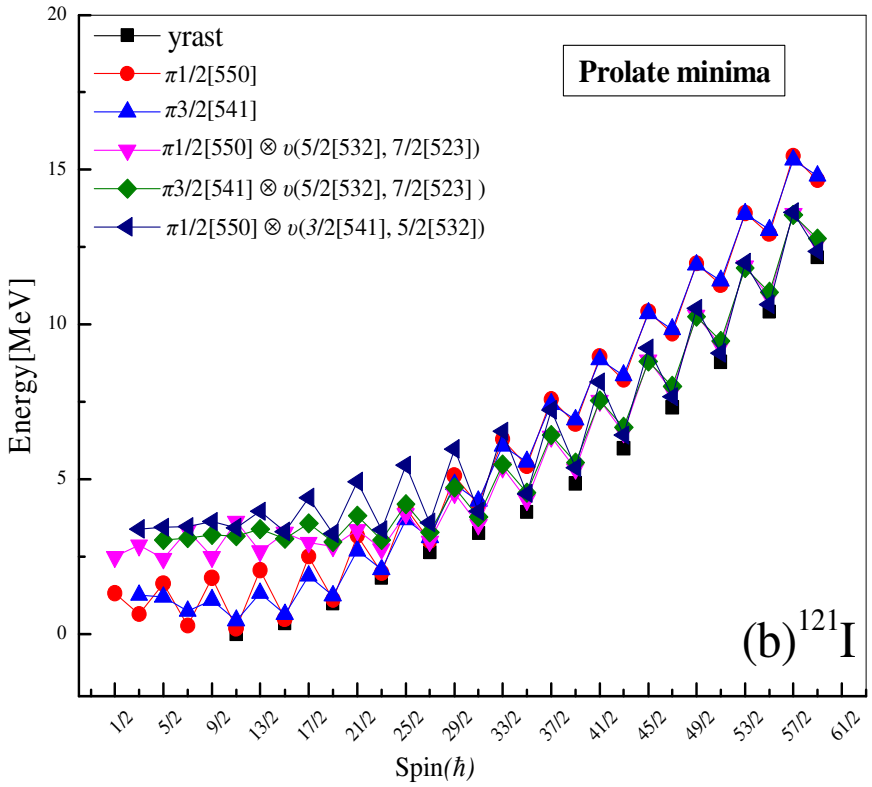

Fig. 3.3.2(b) Band diagram for negative parity for ^{121}I. Only the important lowest lying bands in each configuration are plotted.

^{123}I

(a) Positive parity

For the case of ^{123}I (see Fig. 3.3.3(a)), the yrast states up to the spin $19/2^+$ are arising from two overlapped 1-*qp* bands with configurations: $\pi 7/2[404]$ and $\pi 5/2[402]$. At this spin, a crossing of these bands takes place by a 3-*qp* band identified as $\pi 7/2[404] \otimes \upsilon(7/2[523], 5/2[532])$, which then is found to be responsible for the formation of yrast band up to the spin value of $31/2^+$. After this spin, this 3-*qp* band gets overlapped with another 3-*qp* band identified as $\pi 1/2[440] \otimes \upsilon(7/2[523], 5/2[532])$ and these two 3-*qp* bands then contributes to the formation of yrast states up to spin $35/2^+$. Beyond this spin, above mentioned 3-*qp* bands are superimposed by two more 3-*qp* bands with configurations: $\pi 1/2[440] \otimes \upsilon(7/2[523], 3/2[541])$ and $\pi 1/2[420] \otimes \upsilon(7/2[523], 5/2[532])$ and all these bands move together to give rise to the remaining calculated yrast levels.

(b) Negative parity

From the band diagram of ^{123}I, given in Fig. 3.3.3(b), one can see that the yrast band is formed by the two overlapped 1-*qp* bands $\pi 1/2[550]$ and $\pi 3/2[541]$ up to spin of $27/2^-$. At

the spin $27/2^-$, these superimposed 1-*qp* bands get crossed by a 3-*qp* band identified as $\pi 1/2[550] \otimes \upsilon(5/2[532], 7/2[523])$ which contribute to yrast line up to the spin value of $39/2^-$. After this spin, two more 3-*qp* bands with configurations: $\pi 1/2[550] \otimes \upsilon(3/2[541], 5/2[532])$ and $\pi 3/2[541] \otimes \upsilon(1/2[550], 7/2[523])$ get combined with above mentioned bands and contribute to the formation of the higher calculated yrast states.

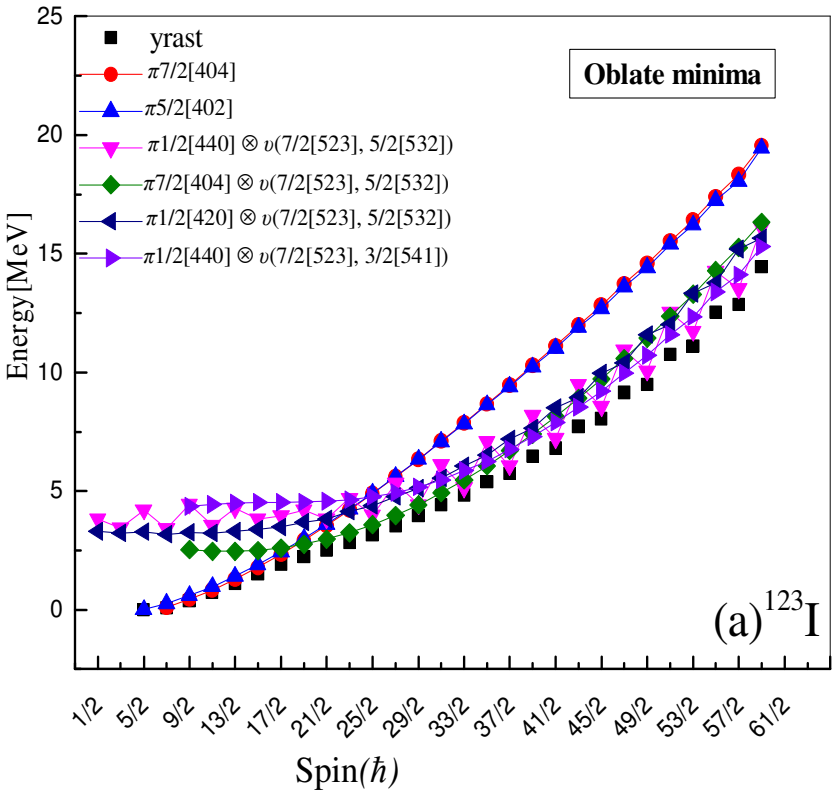

Fig. 3.3.3(a) Band diagram for positive parity for ^{123}I. Only the important lowest lying bands in each configuration are plotted.

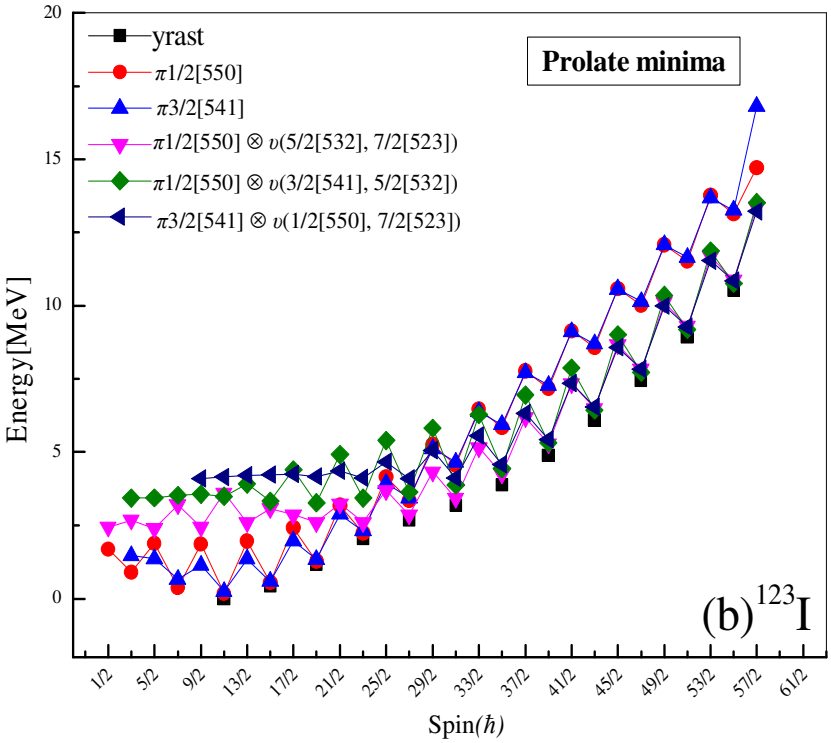

Fig. 3.3.3(b) Band diagram for negative parity for ^{123}I. Only the important lowest lying bands in each configuration are plotted.

^{125}I

(a) Positive parity

Fig. 3.3.4(a) shows the band diagram of ^{125}I for positive parity states. In this case, a combination of two 1-*qp* bands, $\pi 7/2[404]$ and $\pi 5/2[402]$ is contributing towards the formation of yrast line up to the spin value of $19/2^+$, which is then crossed by a 3-*qp* band, $\pi 7/2[404] \otimes \upsilon(7/2[523], 5/2[532])$ and thus forms the yrast line along with one more 3-qp band $\pi 7/2[404] \otimes \upsilon(7/2[523], 1/2[550])$ up to the spin value of $25/2^+$. Subsequently, a 3-*qp* band $\pi 7/2[404] \otimes \upsilon(7/2[523], 1/2[550])$ becomes lower in energy and contributes to the yrast line up to spin $37/2^+$, beyond which two overlapped 3-*qp* bands identified as : $\pi 3/2[431] \otimes \upsilon(7/2[523], 1/2[550])$ and $\pi 1/2[440] \otimes \upsilon(7/2[523], 1/2[550])$, are found to lie lower in energy, thereby leading to the formation of yrast line up to the highest calculated spin value.

(b) Negative parity

For ^{125}I, (see Fig. 3.3.4(b)), up to spin 23/2$^-$, yrast band is formed from the overlapping of two 1-*qp* bands, π1/2[550] and π3/2[541]. At spin 23/2$^-$, band crossing takes place and a mixture of two 3-*qp* bands identified as: π1/2[550] $\otimes$ υ(5/2[532], 7/2[523]) and π3/2[541] $\otimes$ υ(5/2[532], 7/2[523]) becomes lower in energy and contributes to yrast line up to the spin value of 31/2$^-$. At the spin 31/2$^-$, one more 3-*qp* band with configuration: π3/2[541] $\otimes$ υ(1/2[550], 7/2[523]) along with the above mentioned 3-*qp* bands starts contributing towards the formation of yrast band up to the maximum calculated spin.

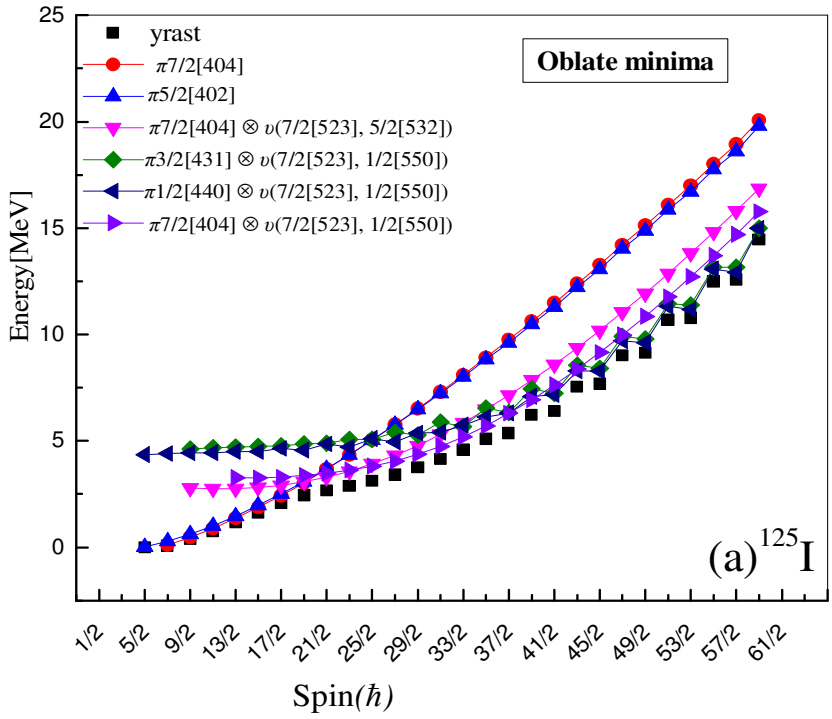

Fig. 3.3.4(a) Band diagram for positive parity for ^{125}I. Only the important lowest lying bands in each configuration are plotted.

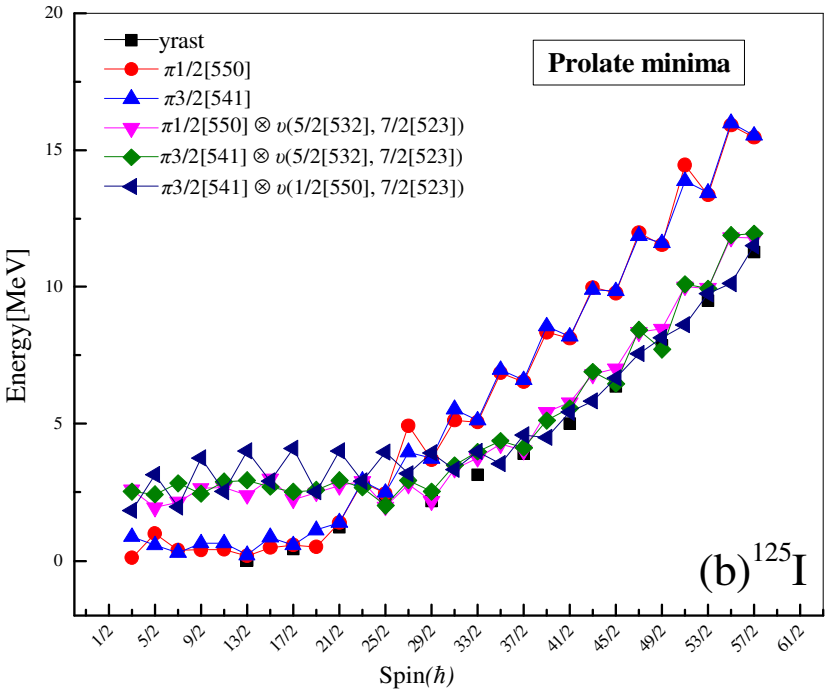

Fig. 3.3.4(b) Band diagram for negative parity for ^{125}I. Only the important lowest lying bands in each configuration are plotted.

^{127}I

(a) Positive parity

Coming onto the band diagram of ^{127}I, as shown in Fig. 3.3.5(a), till the spin of $19/2^+$, the yrast band arises because of the superimposition of two 1-*qp* bands, $\pi 7/2[404]$ and $\pi 5/2[402]$. These overlapped 1-*qp* bands get crossed by a 3-*qp* band having configuration: $\pi 7/2[404] \otimes \upsilon(7/2[523], 1/2[550])$, which then contributes to the yrast band from spin $19/2^+$ to $35/2^+$. After this spin, two more 3-*qp* bands with configurations: $\pi 1/2[440] \otimes \upsilon(7/2[523], 1/2[550])$ and $\pi 3/2[431] \otimes \upsilon(7/2[523], 1/2[550])$ contribute to the remaining calculated yrast levels.

(b) Negative parity

Finally, for ^{127}I (see Fig. 3.3.5(b)), up to the spin of $21/2^-$, the yrast line arises due to two superimposed 1-*qp* bands, $\pi 1/2[550]$ and $\pi 3/2[541]$. After this spin, band crossing occurs at $23/2^-$ and two 3-*qp* bands with configurations: $\pi 1/2[550] \otimes \upsilon(5/2[532], 7/2[523])$ and $\pi 3/2[541] \otimes \upsilon(5/2[532], 7/2[523])$ become lower in energy and contribute towards to the formation of yrast band up to the spin value of $35/2^-$. At higher spin range, another 3-*qp* band with configuration: $\pi 1/2[550] \otimes \upsilon(3/2[541], 9/2[514])$ also starts contributing along

with the above mentioned 3-*qp* bands, thereby leading to the formation of the yrast band up to the maximum calculated spin.

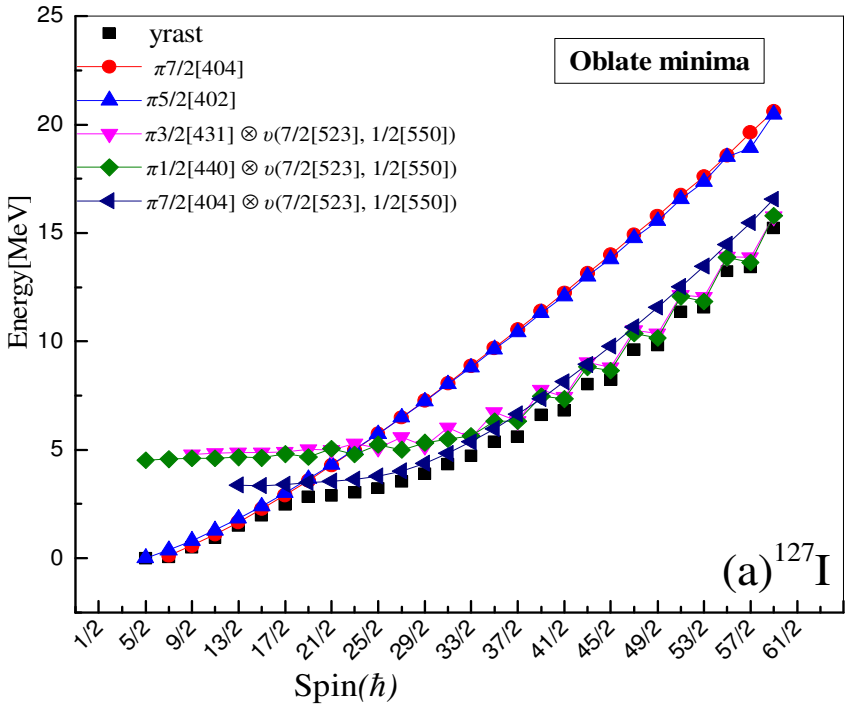

Fig. 3.3.5(a) Band diagram for positive parity for ^{127}I. Only the important lowest lying bands in configuration are plotted.

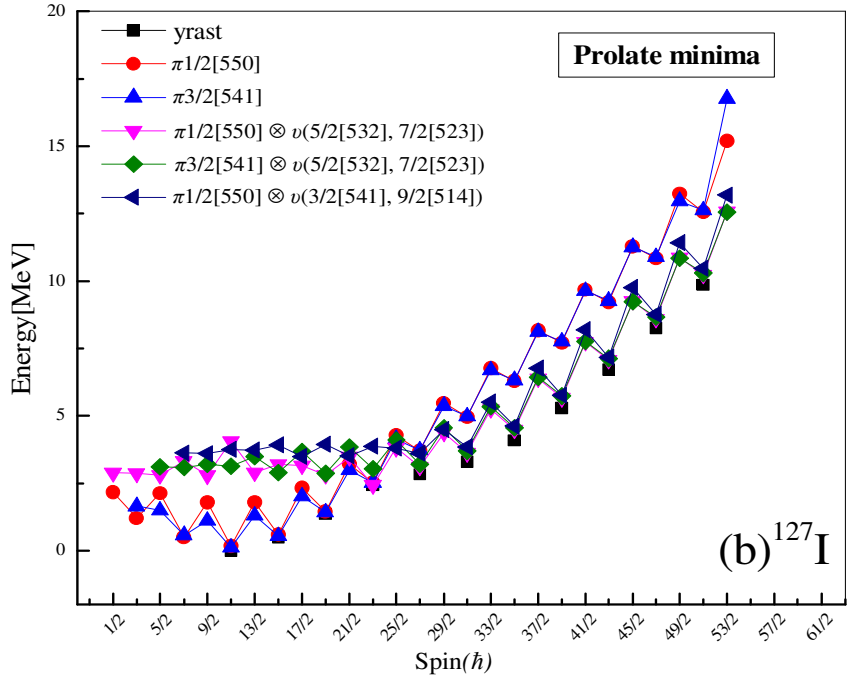

Fig. 3.3.5(b) Band diagram for negative parity for ^{127}I. Only the important lowest lying bands in each configuration are plotted.

3.3.2 Yrast line

The yrast line is defined as a sequence of the lowest energy states of each angular momentum in a nucleus. In PSM, yrast line is obtained through the process of diagonalization of the Hamiltonian in the deformed basis, which in turn, corresponds to the configuration mixing or band mixing in shell model. In the present work, the positive-parity and negative-parity yrast bands have been obtained through Projected Shell Model (PSM) calculations for $^{119-127}$I isotopes and are compared with the corresponding available experimental data. Theoretically, I have been able to obtain the data on positive- and negative-parity yrast states in these nuclei up to a maximum spin of 59/2, whereas experimental data on the positive-parity yrast states in these nuclei are available up to a maximum spin value of $55/2^+$, $49/2^+$, $21/2^+$, $17/2^+$ and $21/2^+$ for ^{119}I, ^{121}I, ^{123}I, ^{125}I and ^{127}I, respectively and up to a maximum spin value of $63/2^-$, $55/2^-$, $23/2^-$, $23/2^-$ and $23/2^-$ for ^{119}I, ^{121}I, ^{123}I, ^{125}I and ^{127}I, respectively for negative-parity yrast states. The comparison of calculated and experimental yrast lines for positive- and negative-parity bands is presented in Figs. 3.3.6(a), 3.3.6(b), 3.3.6(c), 3.3.6(d) and 3.3.6(e) for ^{119,121,123,125,127}I isotopes, respectively. The yrast states (theory and experiment), plotted in these figures, have been obtained as a result of energy differences between the energy of an angular momentum state from the band head energy for positive- and negative-parity bands, separately. From the comparison, the degree of agreement between the theoretical results and experimental ones for yrast states can be considered to be satisfactory for the low-lying states in the iodine isotopes under study. Also, the calculations reproduce successfully the experimental band head spins for positive- and negative-parity yrast bands of $^{119-127}$I isotopes, which have been obtained as $5/2^+$ for positive-parity band and $11/2^-$ for negative-parity band. Furthermore, in case of band head energies of positive- and negative-parity bands taken together, a comparison of results (theory and experiments) for $^{119-127}$I is presented in Table 3, where the relative energies of negative-parity band head spin $11/2^-$ with respect to the positive-parity band head spin of $5/2^+$ are given. Here, the band head energy of $5/2^+$ of all the $^{119-127}$I isotopes is taken as the reference energy with respect to which the band head energies of negative-parity bands are calculated. It may be noted that the calculated PSM results for the relative energies are in a reasonable agreement with the experimentally measured values, for example, in ^{127}I, the PSM relative energy of the band head is 1.18 MeV, whereas the observed value is 1.23 MeV and the values for ^{121}I are 1.11 MeV and 0.81 MeV, respectively.

Again, from the comparison made on yrast energies, it is seen that the low-lying calculated yrast states are following the experimental ones, while there are some disagreements at higher spins. The discrepancy at higher spins could be due to the possibility of presence of some degree of triaxiality in these Iodine nuclei, as reported in Refs. [4,7,18]. The incorporation of triaxiality parameter in the axial PSM framework may help in improving the calculated results for these nuclei. This could also constitute a shortcoming of the present framework. Further, the triaxial calculations of these nuclei would be taken up as a separate project and this is my aim in future.

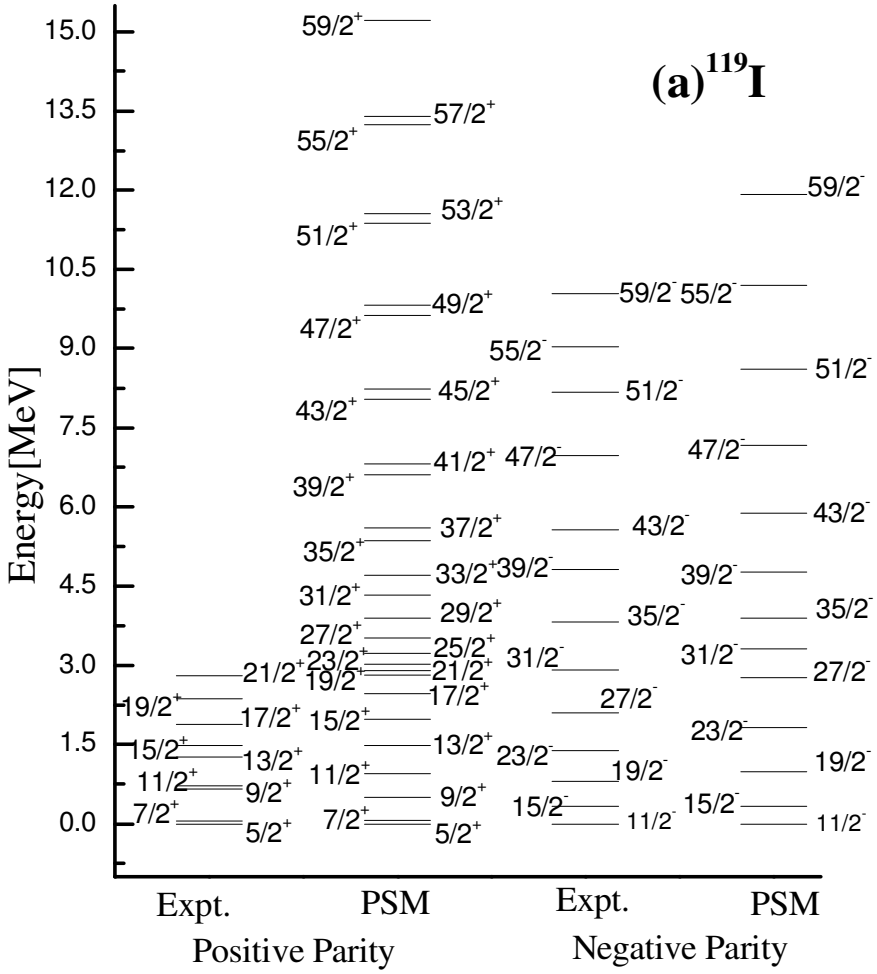

Fig. 3.3.6(a) Comparison of the calculated (PSM) yrast energies of the positive and negative-parity bands with experimental data for ^{119}I.The experimental data of yrast lines for positive- and negative-parity states is taken from Ref. [32].

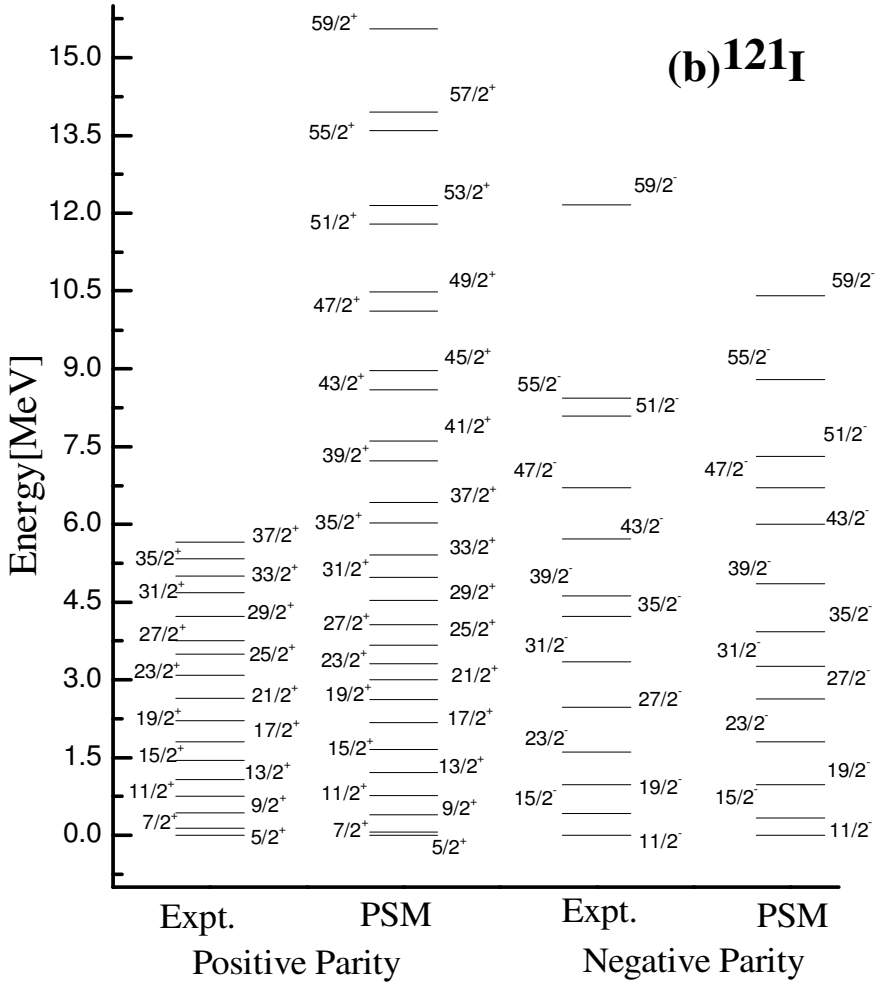

Fig. 3.3.6(b) Comparison of the calculated (PSM) yrast energies of the positive and negative-parity bands with experimental data for ^{121}I. The experimental data of yrast lines for positive- and negative-parity states is taken from Ref. [33].

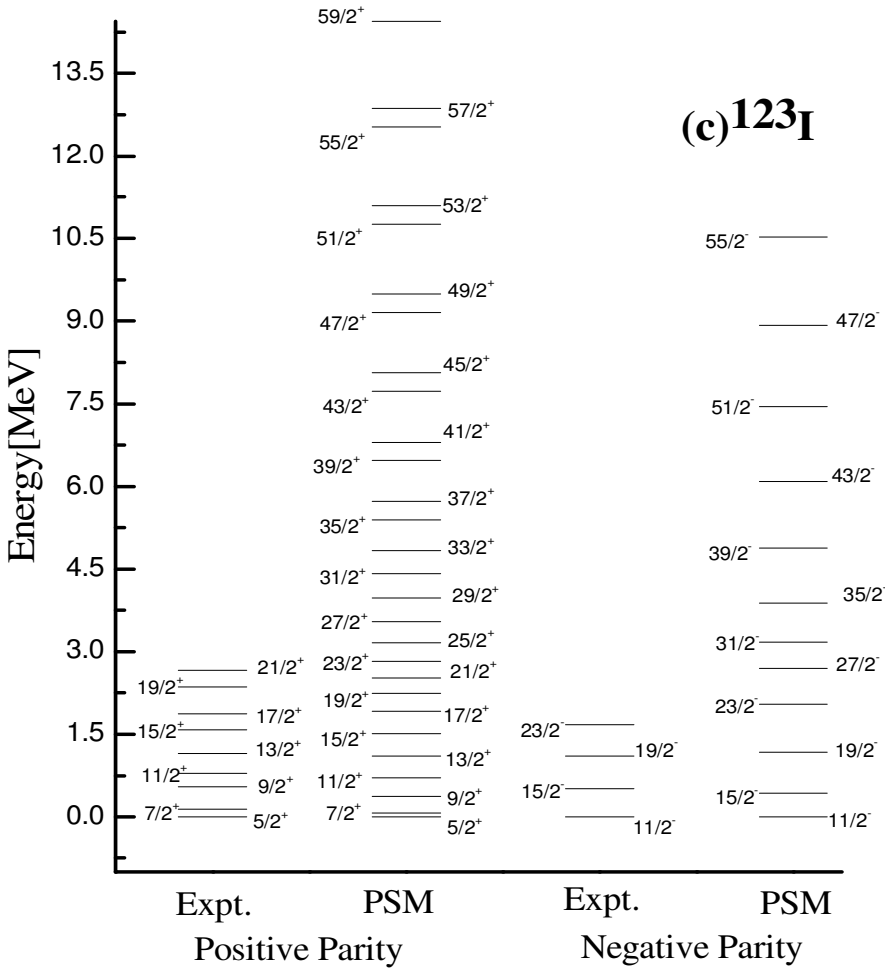

Fig. 3.3.6(c) Comparison of the calculated (PSM) yrast energies of the positive and negative-parity bands with experimental data for ^{123}I. The experimental data of yrast lines for positive- and negative-parity states is taken from Ref. [34].

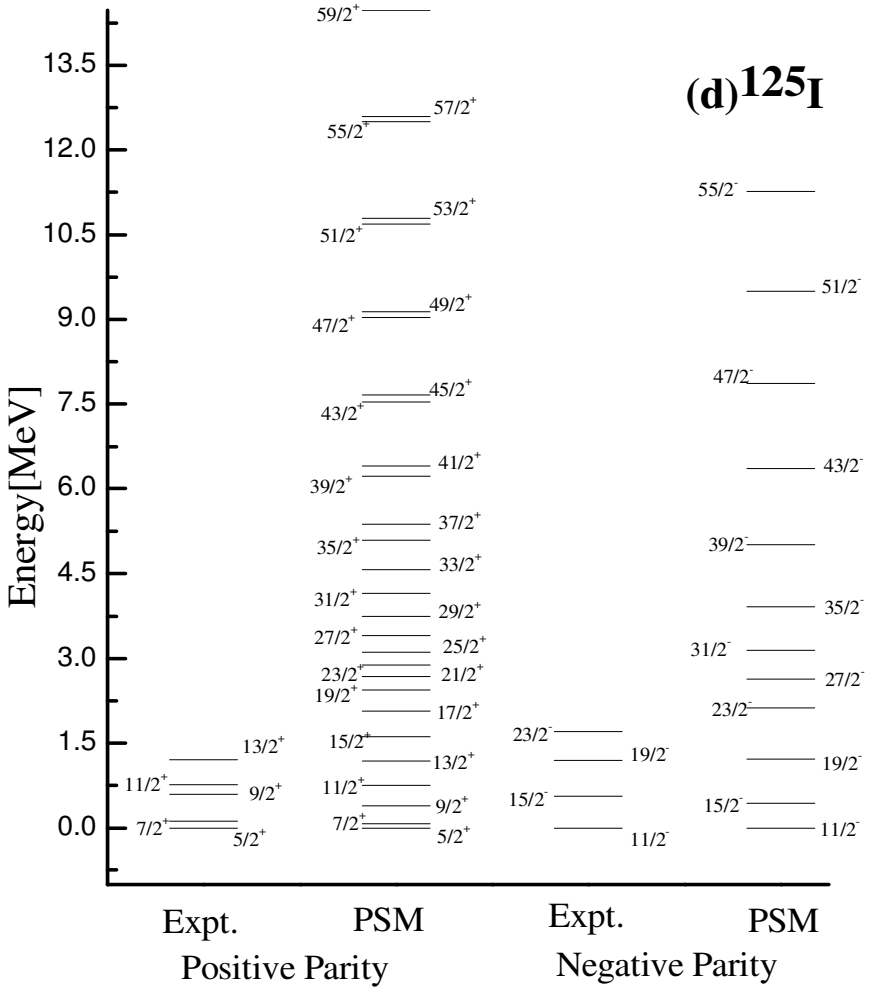

Fig. 3.3.6(d) Comparison of the calculated (PSM) yrast energies of the positive and negative-parity bands with experimental data for ^{125}I. The experimental data of yrast lines for positive- and negative-parity states is taken from Ref. [35].

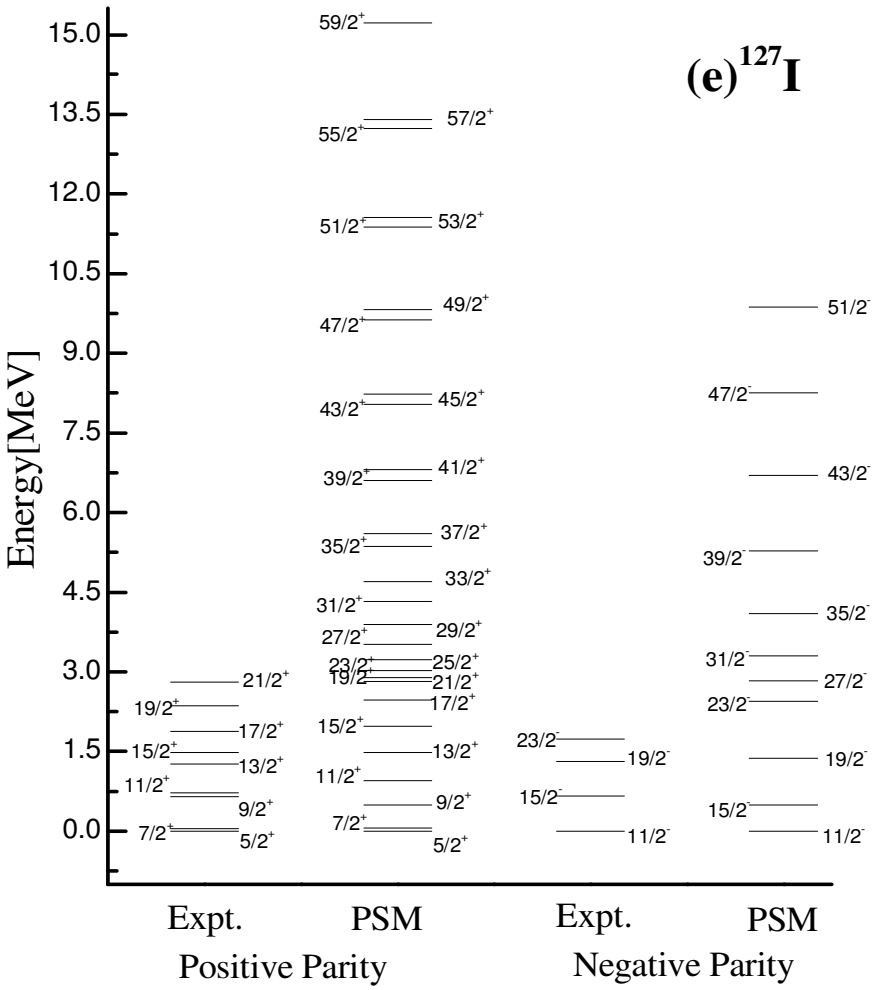

Fig. 3.3.6(e) Comparison of the calculated (PSM) yrast energies of the positive and negative-parity bands with experimental data for ^{127}I. The experimental data of yrast lines for positive- and negative-parity states is taken from Ref. [36].

3.3.3 Backbending in moment of inertia in yrast bands

One can study the behaviour of rotational band by the phenomenon of backbending in moment of inertia. The backbending is defined as the rapid increase of the moment of inertia with the decrease in the rotational frequency at a particular value of spin. For positive and negative-parities backbending in moment of inertia are shown in Figs. 3.3.7(a)-(e) and Figs. 3.3.8(a)-(e), respectively. It can be represented as a plot between twice the kinetic moment of inertia and square of corresponding rotational frequency. The

values of kinetic moment of inertia ($2\Im^{(1)}$) and rotational frequencies ($\hbar^2\omega^2$) are calculated by using the formulae [31] as given below

$$2\Im^{(1)} = \frac{(2I-1)}{\omega} \tag{3.3.2}$$

$$\hbar\omega = \frac{E_\gamma}{\sqrt{(I+1)(I+2)-K^2} - \sqrt{(I-1)I-K^2}} \tag{3.3.3}$$

where, $E_\gamma = E(I) - E(I-2)$

For odd-mass nuclei, backbending is phenomenologically associated with crossings between bands with 1-*qp* and 3-*qp* configurations. In the present case, 1-*qp* configurations are those from the deformed proton $\pi g_{7/2}$, $\pi g_{9/2}$ for positive-parity and $h_{11/2}$ for negative-parity orbit, while 3-*qp* ones consist of these proton 1-*qp* configurations plus a pair of $h_{11/2}$ neutrons for positive as well as for negative-parity. With the band mixing, the yrast line jumps from a given angular momentum with a small deformation to a higher angular momentum with a large deformation, resulting in a drastic increase in the moment of inertia at this angular momentum. In following sub-sections 3.3.3.1 and 3.3.3.2, backbending phenomenon for positive as well as negative-parity yrast bands in $^{119-127}$I has been discussed.

3.3.3.1 For positive-parity bands

The experimental and theoretical backbending data for $^{119-127}$I isotopes are plotted for positive- parity in Figs. 3.3.7 (a) - (e). First of all, for ^{119}I (see Fig. 3.3.7(a)), the experimental backbending occurs at the spin of $25/2^+$, whereas PSM results predict backbending at the spin of $19/2^+$, which correspond to the rotational frequencies ($\hbar^2\omega^2$) of 0.175 MeV^2 and 0.247 MeV^2 respectively. Moreover, it is also observed from the band diagram (Fig. 3.3.7(a)) for ^{119}I that the band crossing occurring at $17/2^+$ is in consistent with the phenomenon of backbending taking place at the same spin, which supports the accuracy of calculated results. In case of ^{121}I isotope, the experimental backbending is observed at the spin of $25/2^+$ and theoretical backbending calculated by PSM occurs at the spin of $19/2^+$ corresponding to the rotational frequencies of 0.175 MeV^2 and 0.216 MeV^2, respectively. Also, it is observed from the band diagram that the band crossing for ^{121}I (See Fig. 3.3.7(b)) occurs at $19/2^+$, which confirms the accuracy of calculated results. Next, for ^{123}I isotope, the experimental backbending occurs at the spin of $15/2^+$, whereas theoretically calculated backbending occurs at the spin of $17/2^+$ corresponding to the rotational frequencies for experimental and theoretical backbendings at 0.137 MeV^2 and

0.152 MeV^2, respectively. In case of ^{125}I, there is no experimental backbending but theoretical backbending has been found to occur at the spin value of $17/2^+$ corresponding to rotational frequency of 0.179 MeV^2, which is happening at the same spin at which the crossing of bands occurs, as shown in the band diagram of ^{125}I (see Fig. 3.3.7(d)). Lastly, for ^{127}I (Fig. 3.3.7(e)), the experimental and theoretical backbendings are found at the spin value of $15/2^+$ and $19/2^+$ with the corresponding rotational frequencies 0.130 MeV^2 and 0.168 MeV^2, respectively.

Table 3.3.1 Relative energies of negative-parity band head spin ($11/2^-$) with respect to positive-parity band head spin ($5/2^+$) of $^{119-127}$I isotopes.

Isotopes	**Relative energies of negative-parity band head spin ($11/2^-$) with respect to positive-parity band head spin ($5/2^+$)**	
	Exp.	**PSM**
^{119}I	0.69	1.18
^{121}I	0.81	1.11
^{123}I	0.94	1.44
^{125}I	1.08	1.50
^{127}I	1.23	1.18

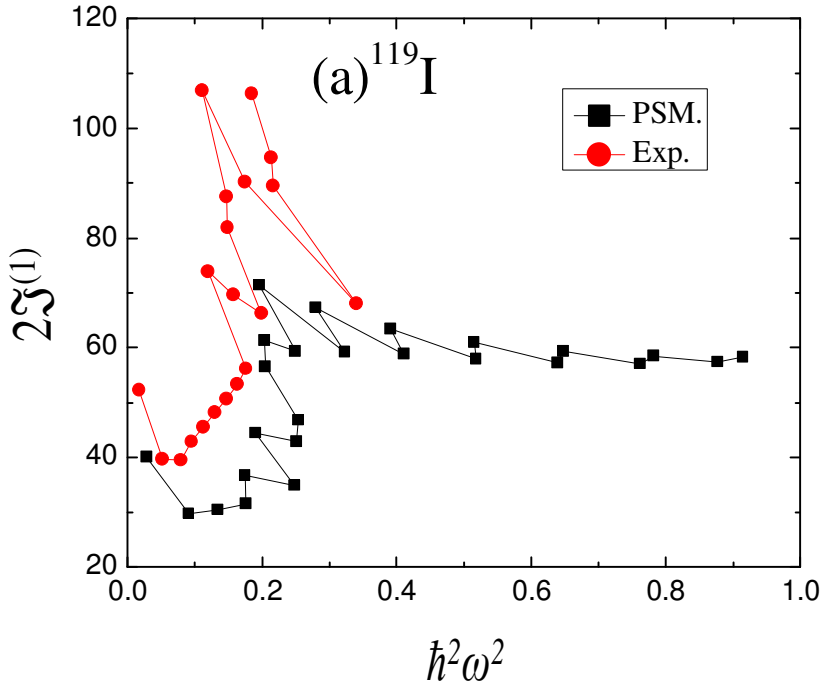

Fig. 3.3.7(a) Twice the kinetic moment of inertia ($2\Im^{(1)}$) plotted against angular frequency squared ($\hbar^2\omega^2$) in comparison with the experimental data for ^{119}I, for positive-parity yrast band.

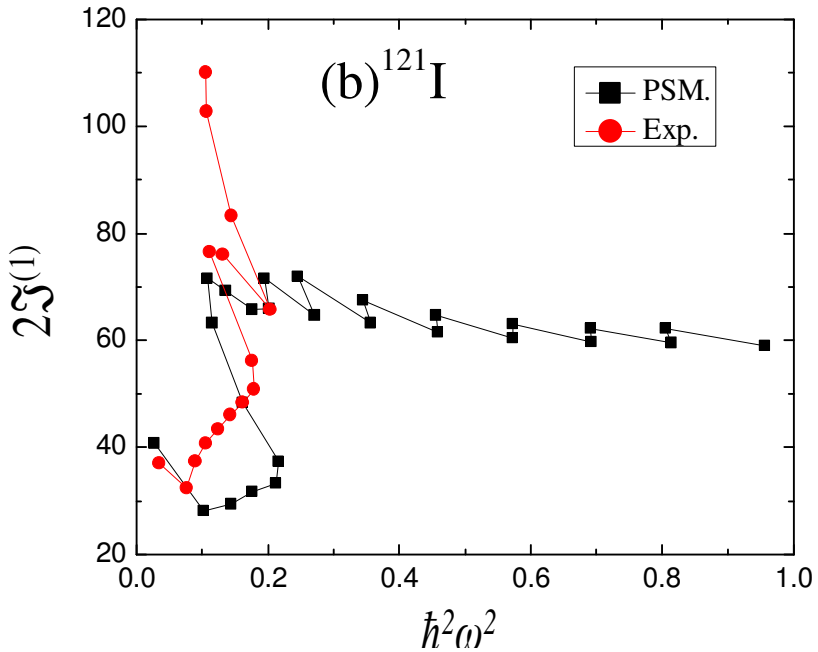

Fig. 3.3.7(b) Twice the kinetic moment of inertia ($2\Im^{(1)}$) plotted against angular frequency squared ($\hbar^2\omega^2$) in comparison with the experimental data for ^{121}I, for positive-parity yrast band.

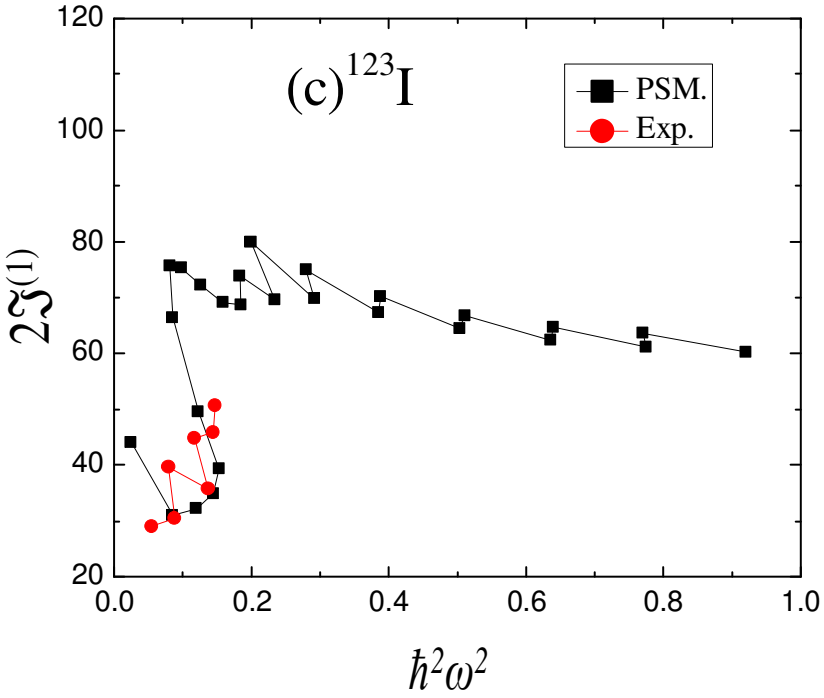

Fig. 3.3.7(c) Twice the kinetic moment of inertia ($2\Im^{(1)}$) plotted against angular frequency squared ($\hbar^2\omega^2$) in comparison with the experimental data for ^{123}I, for positive-parity yrast band.

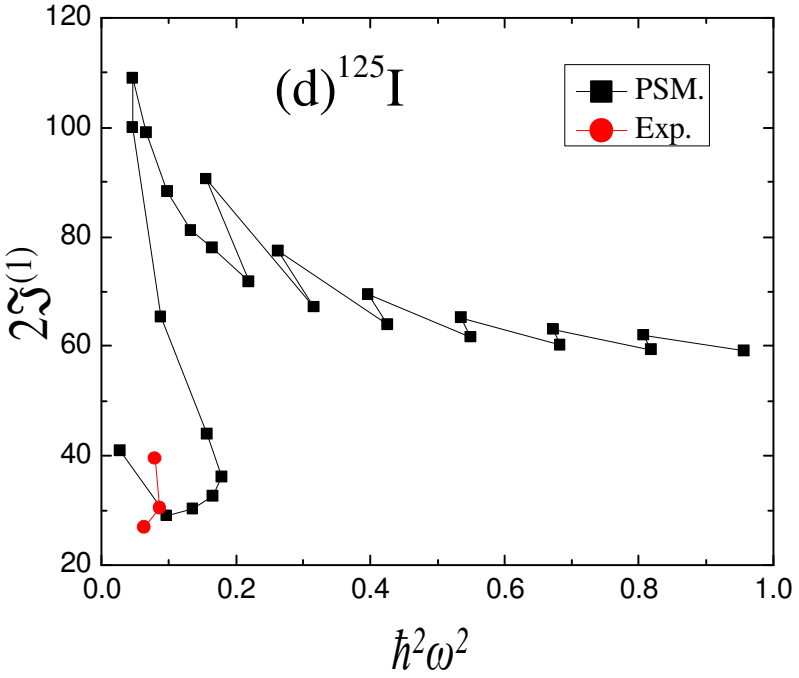

Fig. 3.3.7(d) Twice the kinetic moment of inertia ($2\Im^{(1)}$) plotted against angular frequency squared ($\hbar^2\omega^2$) in comparison with the experimental data for ^{125}I, for positive-parity yrast band.

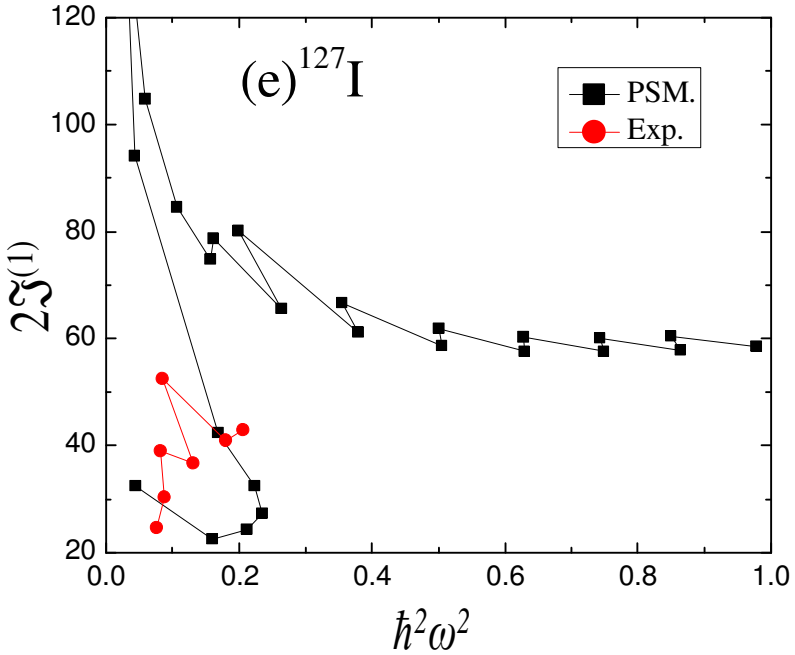

Fig. 3.3.7(e) Twice the kinetic moment of inertia ($2\Im^{(1)}$) plotted against angular frequency squared ($\hbar^2\omega^2$) in comparison with the experimental data for ^{127}I, for positive-parity yrast band.

3.3.3.2 For negative-parity bands

The experimental and theoretical data of backbending in moment of inertia for negative-parity states of $^{119\text{-}127}I$ isotopes are shown in Figs. 3.3.8 (a) -(e). In case of ^{119}I, the experimental and theoretical backbendings are found to occur at spins of $35/2^-$ and $27/2^-$, with corresponding rotational frequencies ($\hbar^2\omega^2$) of 0.837 MeV^2 and 0.557 MeV^2 respectively. For ^{121}I isotope, the experimental and theoretical backbendings are observed at the rotational frequencies of 0.706 MeV^2 and 0.511 MeV^2 at spins of $31/2^-$ and $27/2^-$, respectively. For ^{123}I, there is no experimental backbending but theoretical backbending has been found to occur at the spin value of $27/2^-$, at the rotational frequency of 0.607 MeV^2. Also for ^{125}I, there is no experimental backbending but calculated results show backbending to occur at the spin value of $23/2^-$, at the rotational frequency of 0.483 MeV^2. Lastly, for ^{127}I, theoretical results show backbending at the spin $23/2^-$, at the rotational frequency of 0.496 MeV^2, but experimental data does not confirm any backbending to occur for this isotope.

Further, it has been found from the present calculations that backbending in moment of inertia (shown in Figs. 3.3.7 and 3.3.8) occurs at the same spin value at which band crossing takes place in all the $^{119\text{-}127}I$ isotopes, for positive as well as negative-parity states, respectively.

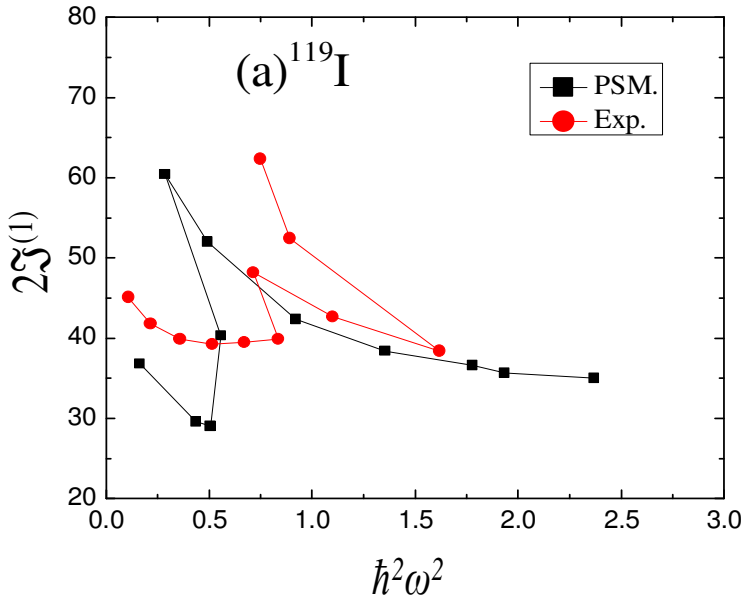

Fig. 3.3.8(a) Twice the kinetic moment of inertia ($2\Im^{(1)}$) plotted against angular frequency squared ($\hbar^2\omega^2$) in comparison with the experimental data for ^{119}I, for negative-parity yrast band.

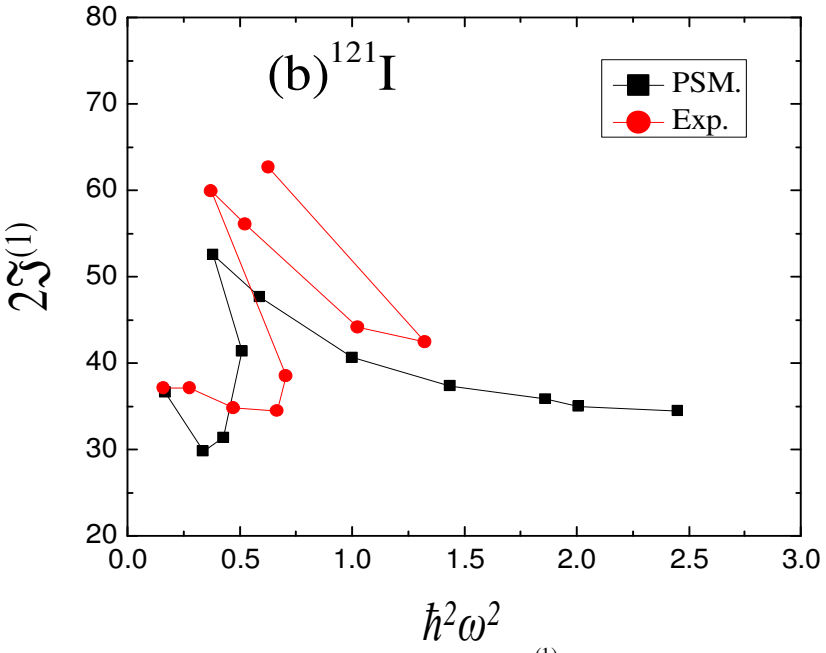

Fig. 3.3.8(b) Twice the kinetic moment of inertia ($2\Im^{(1)}$) plotted against angular frequency squared ($\hbar^2\omega^2$) in comparison with the experimental data for ^{121}I, for negative-parity yrast band.

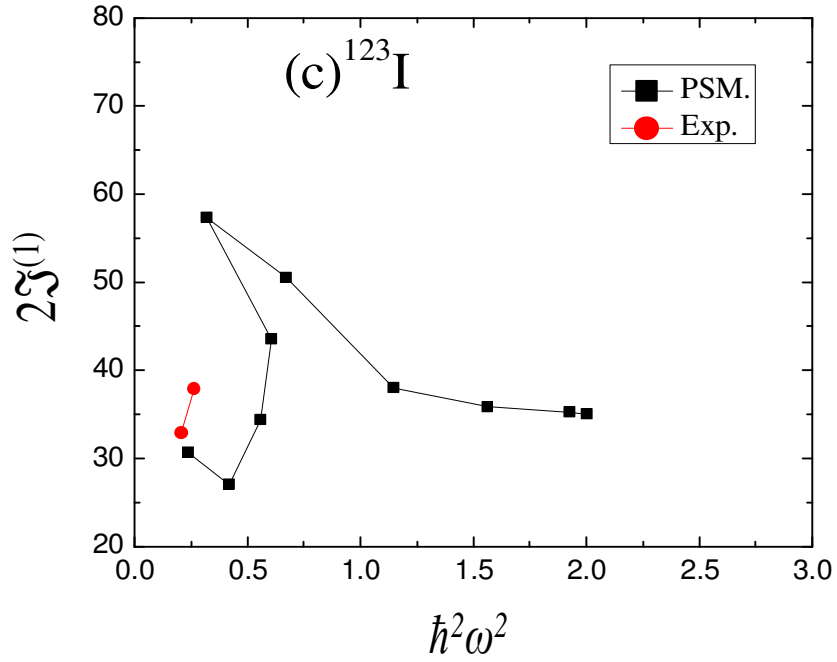

Fig. 3.3.8(c) Twice the kinetic moment of inertia ($2\Im^{(1)}$) plotted against angular frequency squared ($\hbar^2\omega^2$) in comparison with the experimental data for ^{123}I, for negative-parity yrast band.

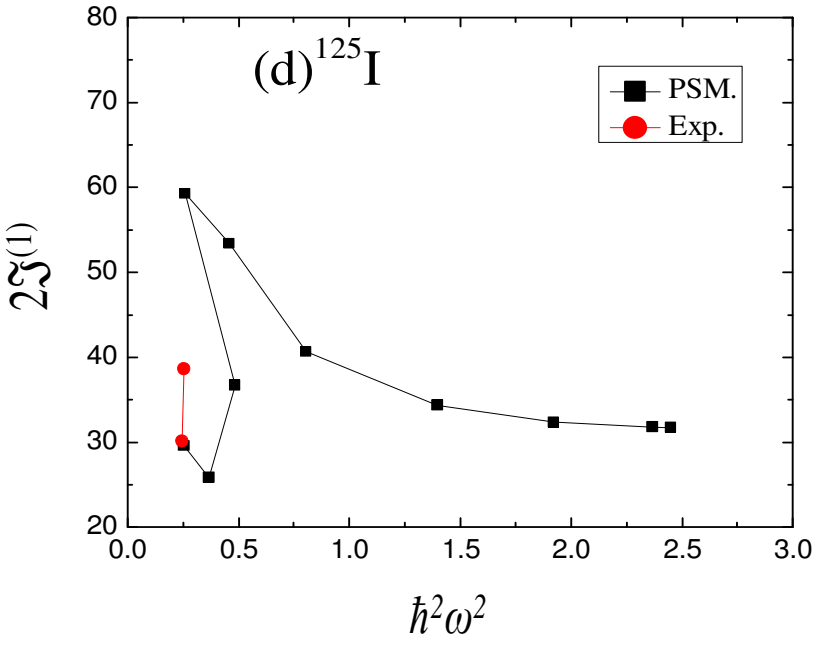

Fig. 3.3.8(d) Twice the kinetic moment of inertia ($2\Im^{(1)}$) plotted against angular frequency squared ($\hbar^2\omega^2$) in comparison with the experimental data for ^{125}I for negative-parity yrast band.

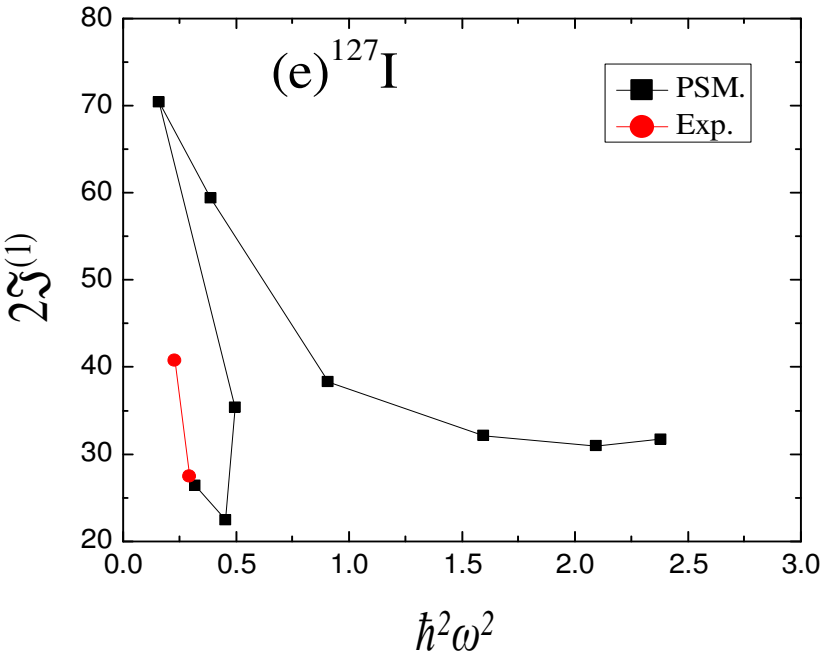

Fig. 3.3.8(e) Twice the kinetic moment of inertia ($2\Im^{(1)}$) plotted against angular frequency squared ($\hbar^2\omega^2$) in comparison with the experimental data for ^{127}I for negative-parity yrast band.

3.3.4 Reduced transition probability

One of the vital nuclear structure properties which give important information on the nuclear structure are the reduced electromagnetic transition probabilities, $B(E2)$ and $B(M1)$. These values represent basic nuclear information complementary to our knowledge of the energies of low-lying levels in nuclides. This is one of the most important tools available to investigate the wavefunctions of nuclei. Generally, these values highlight the extent to which quadrupole distortions are present in the structure of the nuclei and in the present work, reduced transition probabilities have been calculated using wavefunctions obtained by the projection technique implemented in PSM.

The reduced electric quadrupole transition probability $B(E2)$ from an initial state (I_i=I) to a final state ($I_f = I - 2$) is given by

$$B(E2, I_i \rightarrow I_f) = \frac{e^2}{2I_i + 1} \left| \left\langle \sigma_f, I_f \right| \left| \hat{Q}_2 \right| \left| \sigma_i, I_i \right\rangle \right|^2 \tag{3.3.4}$$

where, the operator $\hat{Q}_2$ is related to the quadrupole operators. For the calculation of B(E2) values, I have used the empirical relations for obtaining the numerical values for proton (neutron) effective charges as e_π (e_ν), which are defined as:

$$e_\pi = 1 + e_{eff} \quad \text{and} \quad e_\upsilon = e_{eff}$$

and in the present set of calculations, I have taken e_{eff}=0.6.

In a similar way, one can also calculate reduced magnetic transition probability $B(M1)$ using PSM wavefunctions. Magnetic dipole transition strengths are sensitive to the single-particle nuclear wavefunction. The reduced magnetic dipole transition probability $B(M1)$ from initial state (I_i=I) to final state (I_f=I-1) is calculated by

$$B\left(M1, I_i \rightarrow I_f\right) = \frac{\mu_N^2}{2I_i + 1} \left| \left\langle \sigma_f, I_f \right| \left| \hat{\mathrm{M}}_1 \right| \left| \sigma_i, I_i \right\rangle \right|^2 \tag{3.3.5}$$

where the magnetic dipole operator is defined as

$$\hat{\mathrm{M}}_1^\tau = g_l^\tau \hat{j}^\tau + \left(g_s^\tau - g_l^\tau\right) \hat{s}^\tau$$

here τ denotes for either π or ν ; g_l and g_s are the orbital and the spin gyromagnetic factors, respectively and are defined as:

$$g_\tau(\sigma, I) = \frac{1}{\left[I(I+1)(2I+1)\right]^{1/2}} \left(g_l^\tau \left\langle \sigma, I \middle\| J^\tau \middle\| \sigma, I \right\rangle + (g_s^\tau - g_l^\tau) \left\langle \sigma, I \middle\| S^\tau \middle\| \sigma, I \right\rangle\right)$$

(3.3.6)

and in the present calculations, one can use the free values for g_l, whereas for g_s, the free values are damped by a factor of 0.85. The standard free values of g_l and g_s for protons and neutrons are

$$g_l^{\pi} = 1,\ g_l^{\nu} = 0,\ g_s^{\pi} = 5.586 \times 0.85,\ g_s^{\nu} = -3.826 \times 0.85$$

In the present calculations, the effective charges as well as damping of free values of g_s have been used to take into account the effect of core-polarization and meson-exchange current corrections.

The reduced matrix element of an operator $\hat{O}$($\hat{O}$ is either $\hat{Q}$ or $\hat{\mathrm{M}}$) is expressed by

$$\left\langle \sigma_f, I_f \right\| \hat{O}_L \left\| \sigma_i, I_i \right\rangle = \sum_{\kappa_i, \kappa_f} f^{\sigma_i}_{I_i \kappa_i} f^{\sigma_f}_{I_f \kappa_f} \sum_{M_i, M_f, M} (-1)^{I_f - M_f} \begin{pmatrix} \mathrm{I_f} & \mathrm{L} & \mathrm{I_i} \\ -\mathrm{M_f} & \mathrm{M} & \mathrm{M_i} \end{pmatrix}$$

$$\times \left\langle \phi_{\kappa_f} \left| \hat{P}^{I_f}_{K_{\kappa_f} M_f} \hat{O}_{LM} \hat{P}^{I_i}_{K_{\kappa_i} M_i} \right| \phi_{\kappa_i} \right\rangle$$

The theoretical results on the reduced electric transition probabilities, ($B(E2)$) for positive and negative-parity yrast band in $^{119\text{-}127}$I isotopes are shown respectively in Figs. 3.3.9 and 3.3.10, whereas magnetic transition probabilities ($B(M1)$) for positive and negative-parity yrast band are shown in Figs. 3.3.11 and 3.3.12, respectively. In Figs. 3.3.11 and 3.3.12, the usual staggering pattern of $B(M1)$ values is quite visible for the whole spin range corresponding to the data being plotted with the present scale along the two axes.

Further, due to non-availability of experimental data on $B(E2)$ and $B(M1)$ values for positive- as well as negative-parity yrast bands on these nuclei, one cannot make any comment on their degree of accuracy. However, these results could serve as motivation for experimentalists to look for this data.

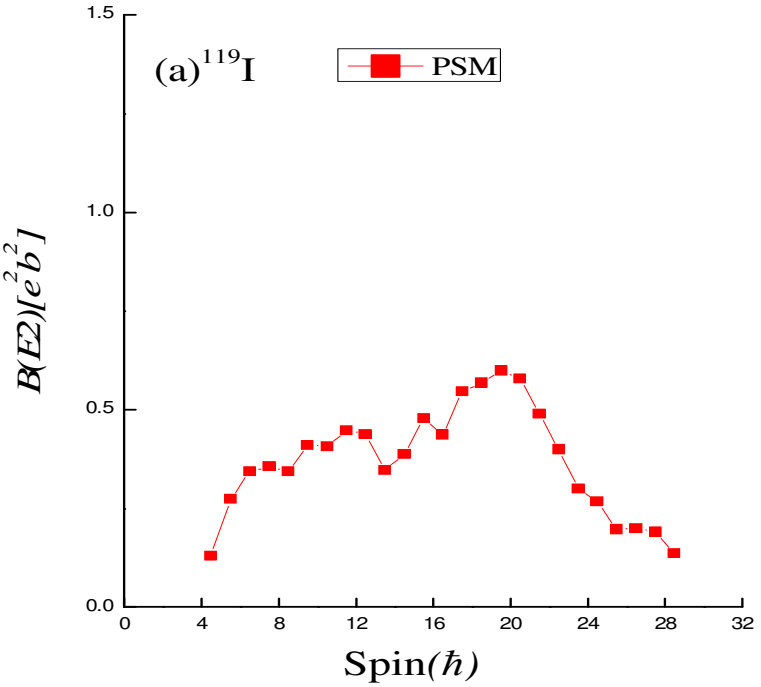

Fig. 3.3.9(a) Calculated *B(E2)* transition probabilities for the positive-parity yrast band for ^{119}I

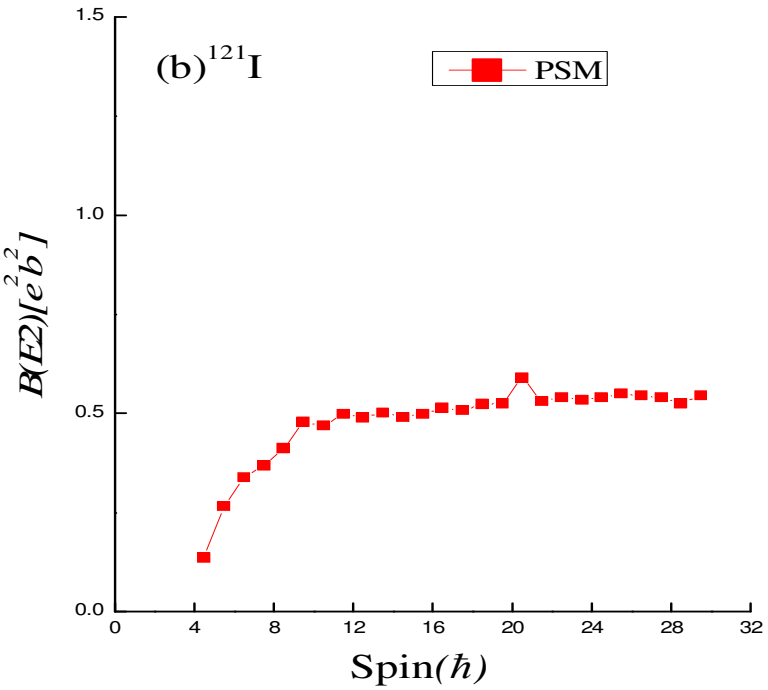

Fig. 3.3.9(b) Calculated *B(E2)* transition probabilities for the positive-parity yrast band for ^{121}I.

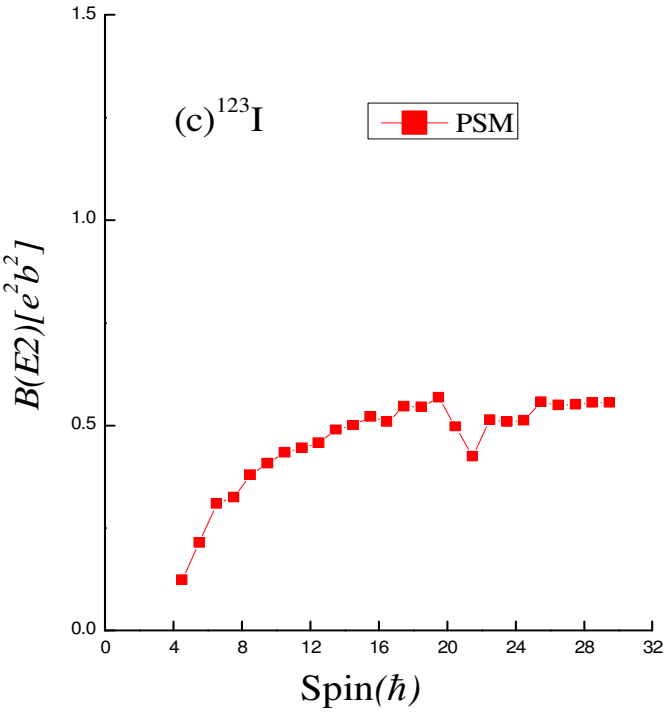

Fig. 3.3.9(c) Calculated *B(E2)* transition probabilities for the positive-parity yrast band for ^{123}I.

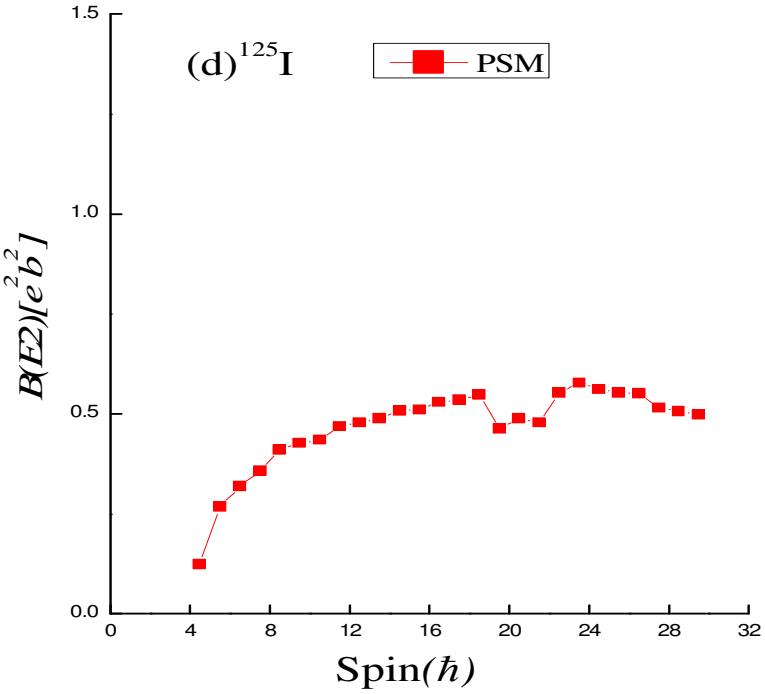

Fig. 3.3.9(d) Calculated *B(E2)* transition probabilities for the positive-parity yrast band for ^{125}I.

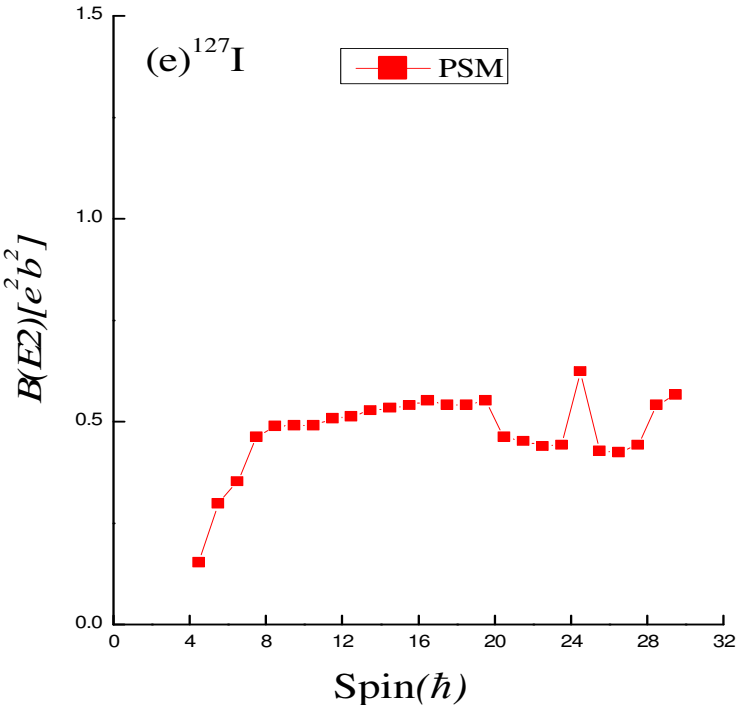

Fig. 3.3.9(e) Calculated *B(E2)* transition probabilities for the positive-parity yrast band for ^{127}I.

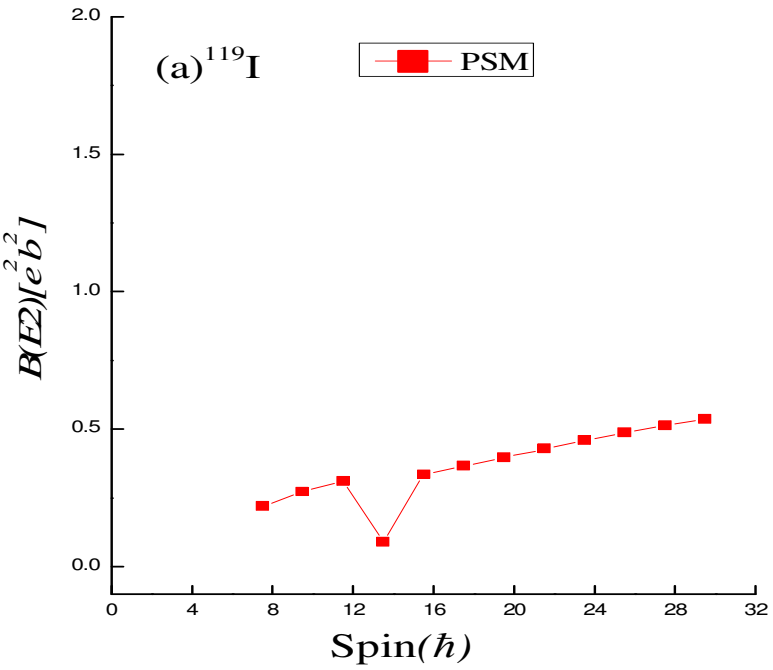

Fig. 3.3.10(a) Calculated *B(E2)* transition probabilities for the negative-parity yrast band for ^{119}I.

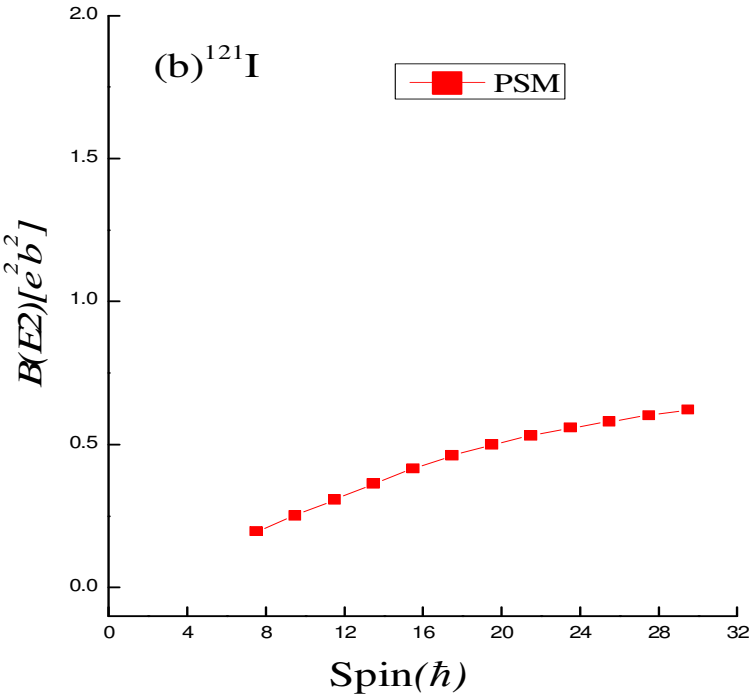

Fig. 3.3.10(b) Calculated *B(E2)* transition probabilities for the negative-parity yrast band for ^{121}I.

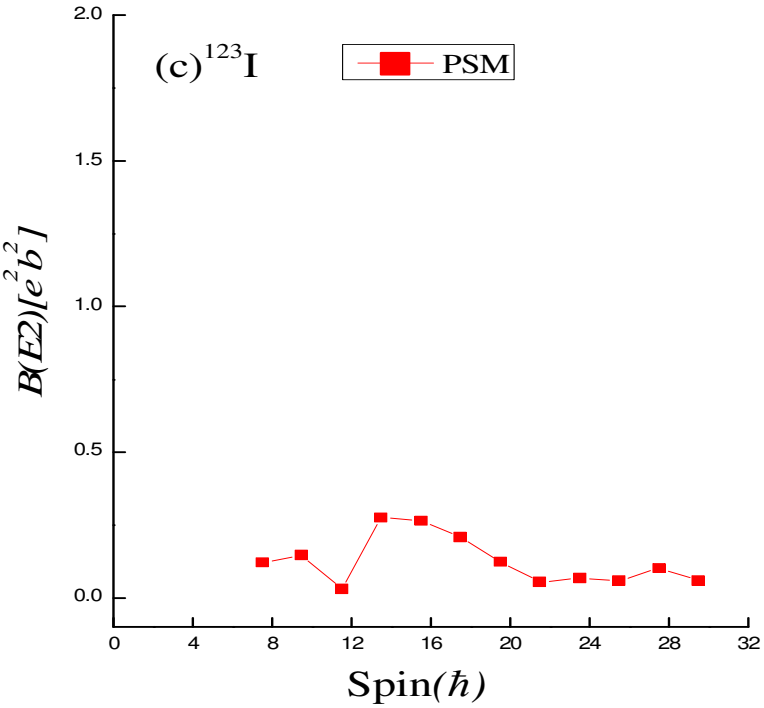

Fig. 3.3.10(c). Calculated *B(E2)* transition probabilities for the negative-parity yrast band for ^{123}I.

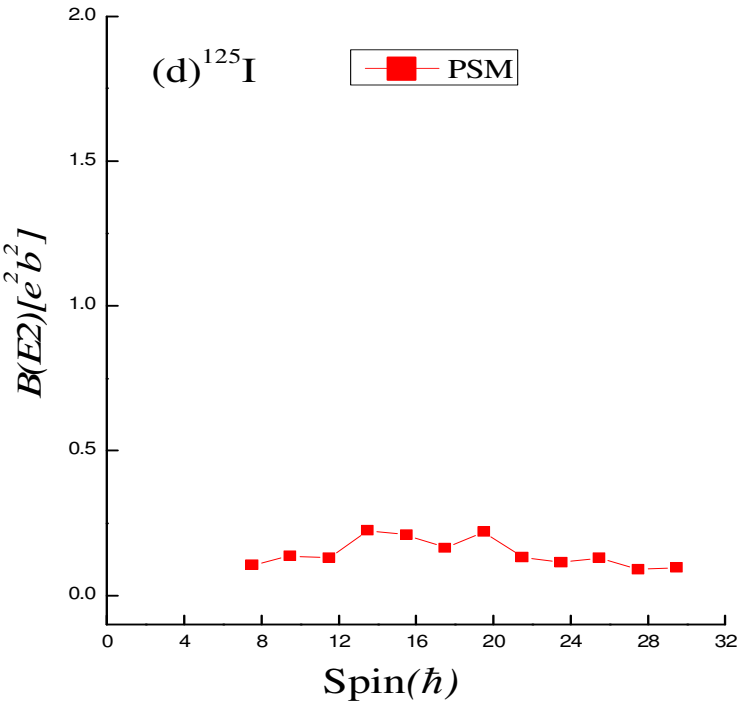

Fig. 3.3.10(d) Calculated *B(E2)* transition probabilities for the negative-parity yrast band for ^{125}I.

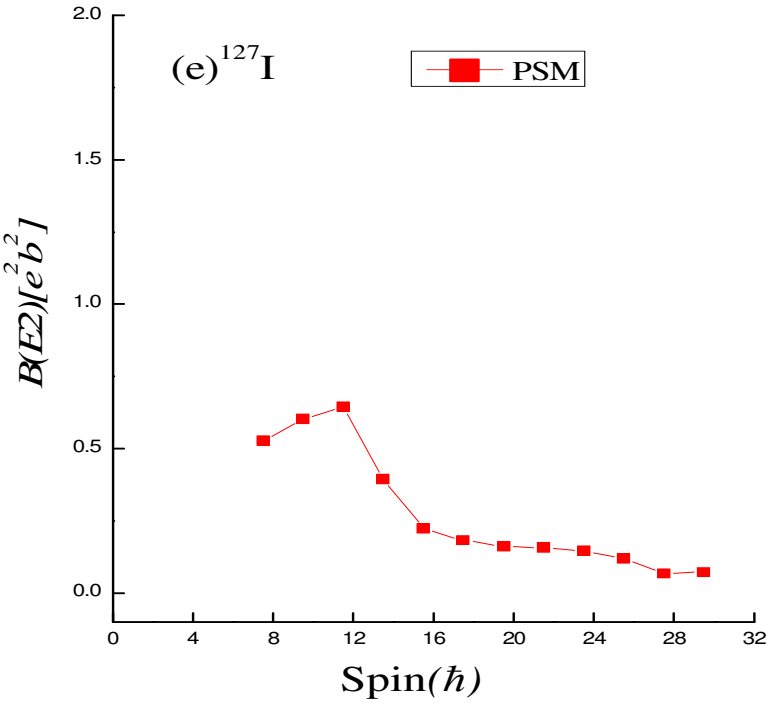

Fig. 3.3.10(e) Calculated *B(E2)* transition probabilities for the negative-parity yrast band for ^{127}I.

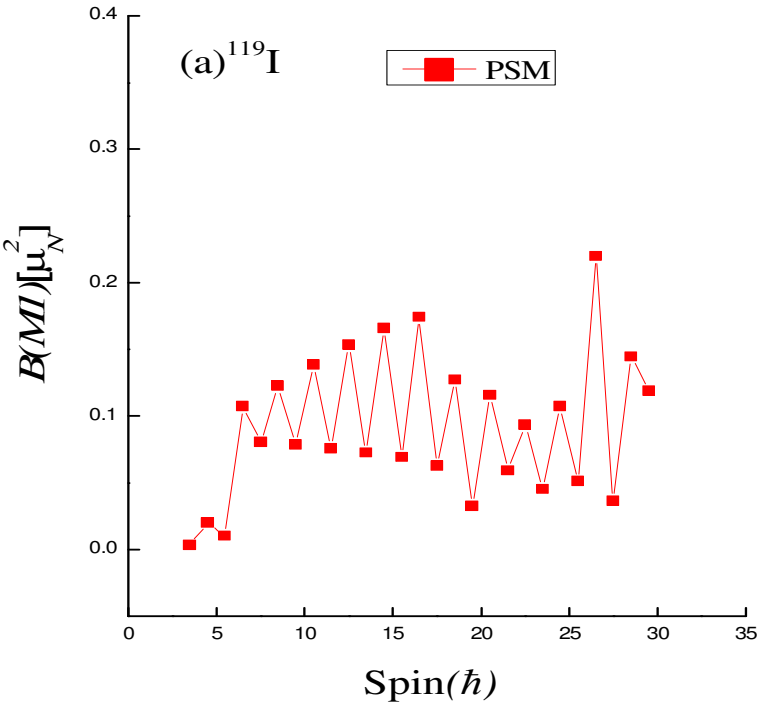

Fig. 3.3.11(a) Calculated $B(M1)$ transition probabilities for the positive-parity yrast band in ^{119}I.

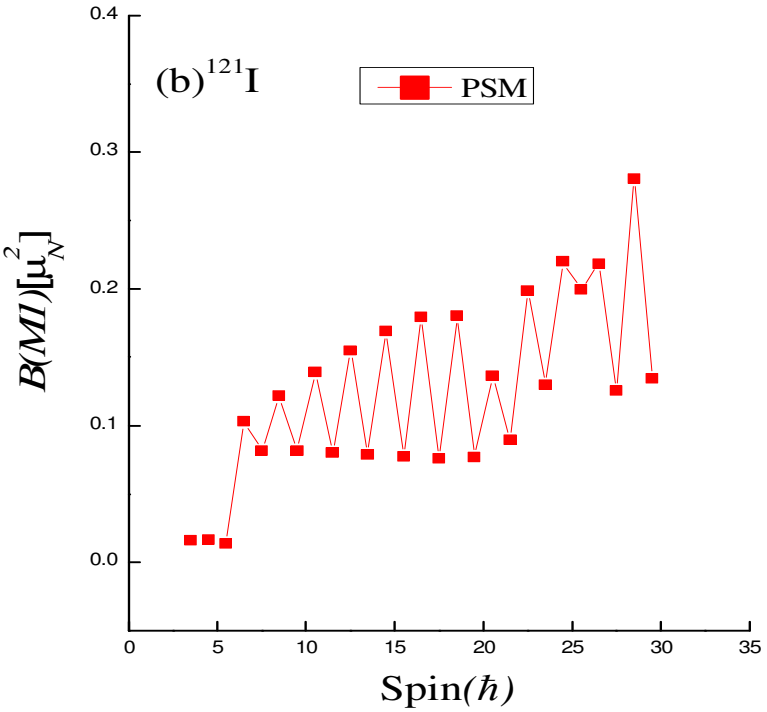

Fig. 3.3.11(b) Calculated $B(M1)$ transition probabilities for the positive-parity yrast band in ^{121}I.

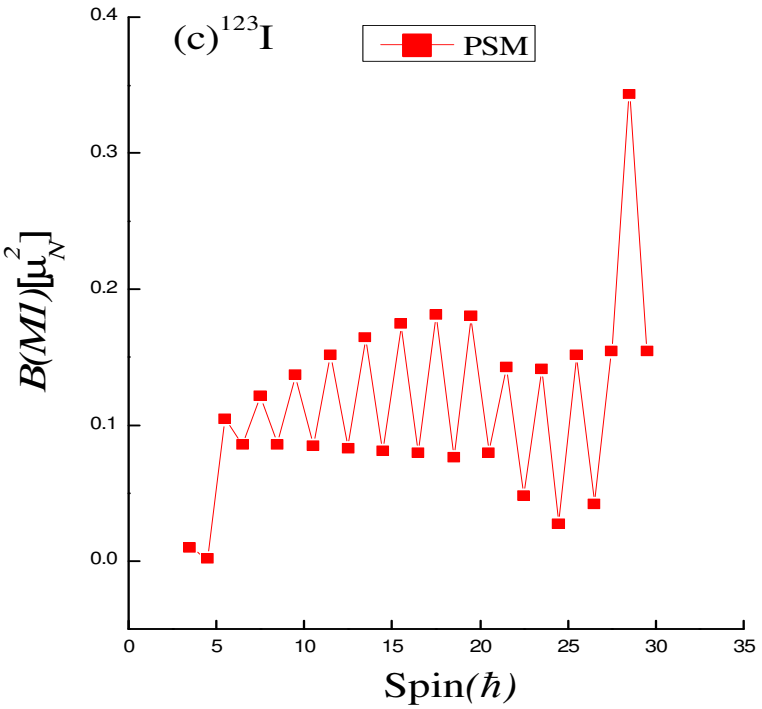

Fig. 3.3.11(c) Calculated $B(M1)$ transition probabilities for the positive-parity yrast band in ^{123}I.

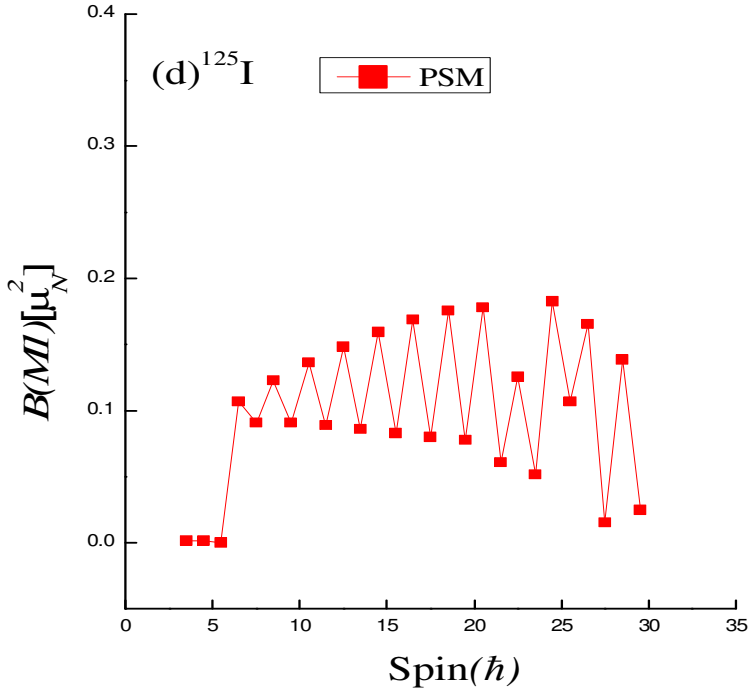

Fig. 3.3.11(d) Calculated $B(M1)$ transition probabilities for the positive-parity yrast band in ^{125}I.

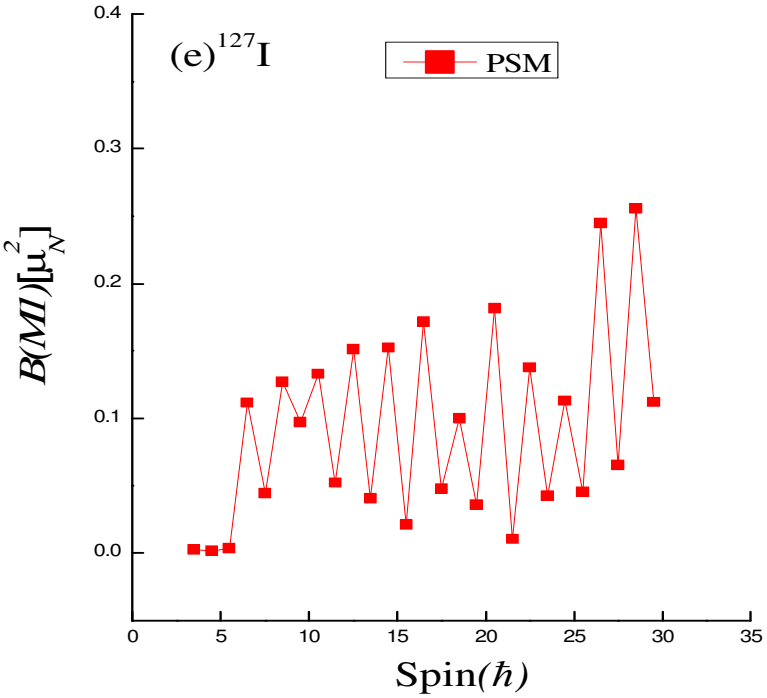

Fig. 3.3.11(e) Calculated $B(M1)$ transition probabilities for the positive-parity yrast band in ^{127}I.

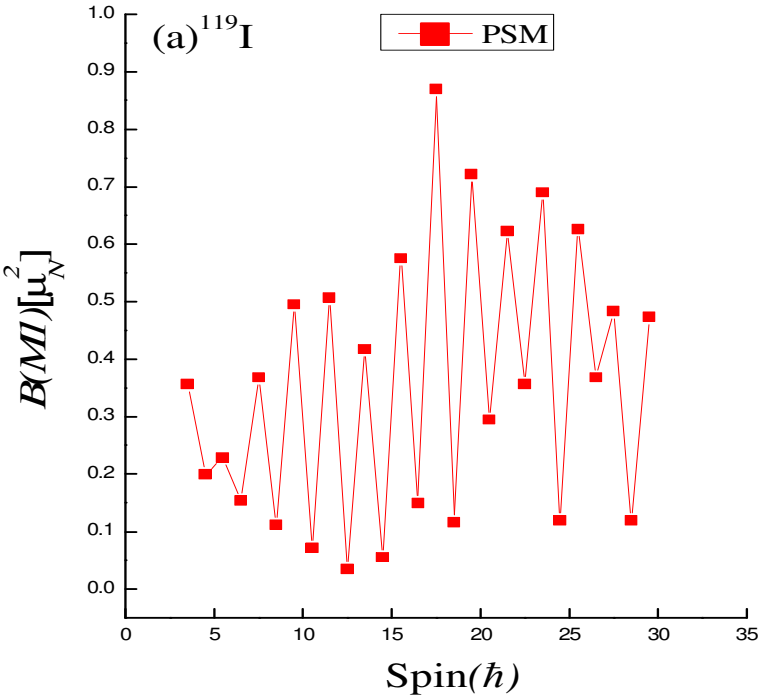

Fig. 3.3.12(a) Calculated $B(M1)$ transition probabilities for the negative-parity yrast band in ^{119}I.

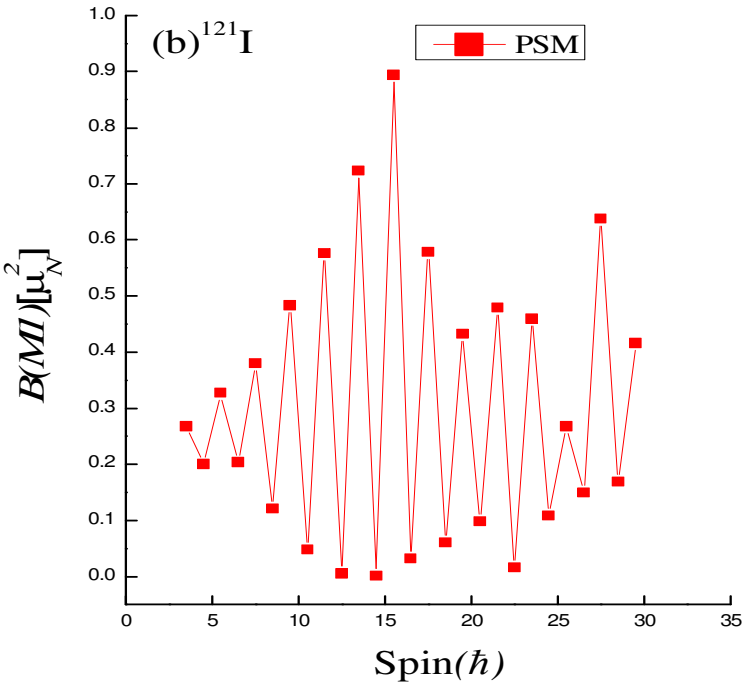

Fig. 3.3.12(b) Calculated $B(M1)$ transition probabilities for the negative-parity yrast band in ^{121}I.

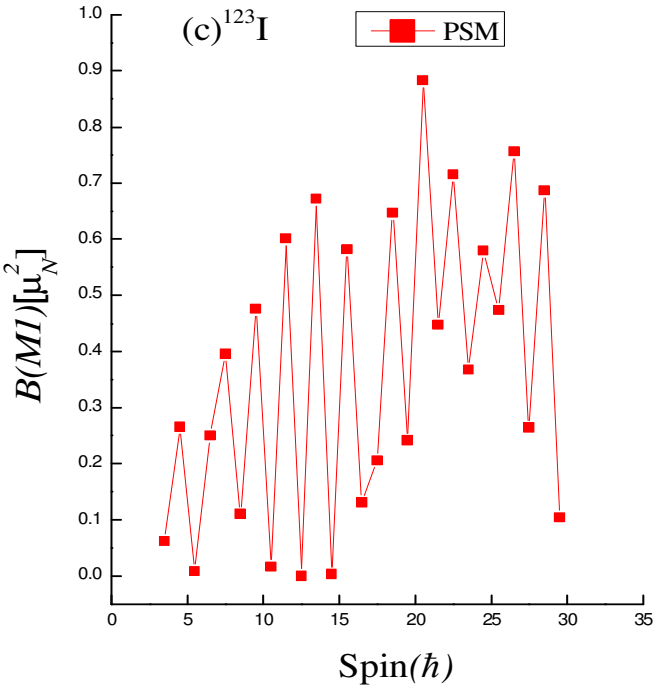

Fig. 3.3.12(c) Calculated $B(M1)$ transition probabilities for the negative-parity yrast band in ^{123}I.

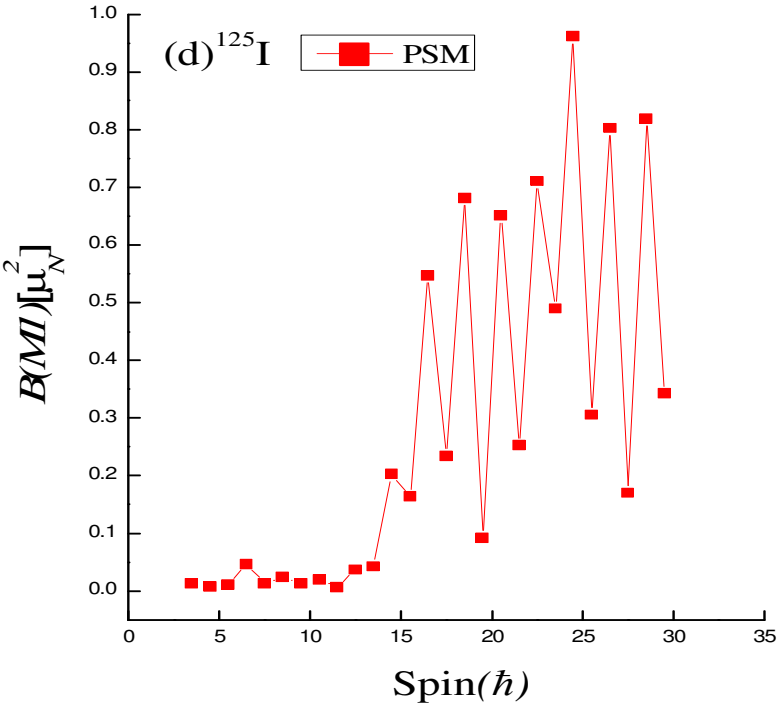

Fig. 3.3.12(d) Calculated *B*(*M1*) transition probabilities for the negative-parity yrast band in ^{125}I.

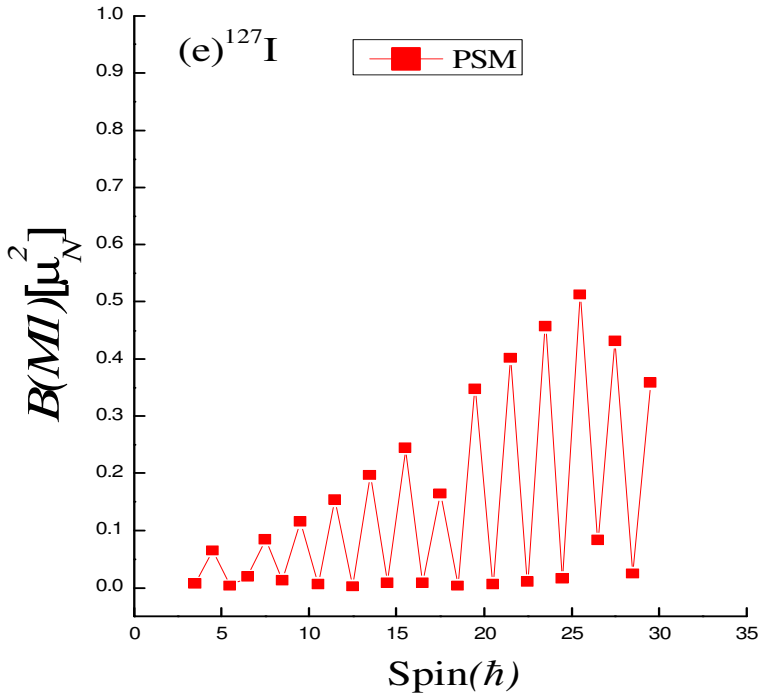

Fig. 3.3.12(e) Calculated *B*(*M1*) transition probabilities for the negative-parity yrast band in ^{127}I.

3.4 Conclusions

Conclusions which are drawn from the present study on $^{119-127}$I nuclei are as under:

(i) The PSM calculations, carried out for yrast line in $^{119-127}$I isotopes for positive as well as negative-parity, show satisfactory agreement with experimental data. The calculations reproduce the experimental band head spins ($5/2^+$ for positive-parity and $11/2^-$ for negative-parity) of the $^{119-127}$I isotopes successfully. The degree of agreement from the comparative study of yrast states of $^{119-127}$I nuclei indicates that the applied PSM framework is quite reliable for the nuclei lying in this mass region.

(ii) The results on band diagrams show that the yrast lines in $^{119-127}$I isotopes for positive as well as negative-parity arise not only from 1-qp states but also from the multi-quasiparticle states. The low lying yrast states are found to arise from 1-qp states. As one goes to higher angular momentum states, it is found that the intrinsic state changes and has 3-*qp* configurations.

(iii) The calculations on backbending for $^{119-127}$I isotopes, for positive as well as negative-parity, predict their occurrence at the spins which are very close to those at which experimental ones are observed.

(iv) In the present work, the reduced electromagnetic transition probabilities, ($B(E2)$ and $B(M1)$) for yrast states are calculated for the first time. As there is no experimental as well as other theoretical data available on reduced transition probabilities for $^{119-127}$I isotopes for positive as well as negative-parity, so one cannot make any comment on their degree of accuracy. Further, it will provide an opportunity to the experimentalists to work for this data.

To summarise, it is well understood that a systematic study for a chain of nuclei is always a serious test for phenomenological nuclear models before they can be used to explain or predict an isolated observation in specific isotopes and the present study of odd-mass $^{119-127}$I nuclei in the PSM framework has quite satisfactorily explained the results as far as essence of physics has been understood.

Furthermore, the results presented in this chapter-3 have been published in an international journal with the details: **Nuclear Physics A, 952 (2016) 41**.

Bibliography

[1] C.B. Moon, J. Korean Phys. Soc. **45** (2004) 859.

[2] C.B. Moon and J. U. Kwon, J. Korean Phys. Soc. **32** (1998) 666.

[3] E.S. Paul, et al., Phys. Rev. **C59** (1999) 1984.

[4] S. Tormanen, et al., Nucl. Phys. **A613** (1997) 282.

[5] Y. Liang, D.B. Fossan, J.R. Hughes, D.R. La Fosse, T. Lauritsen, R. Ma, E.S. Paul, P.Vaska, M.P. Waring and N. Xu, Phys.Rev. **C45** (1992) 1041.

[6] Ranjana Goswami, B. Sethi, P. Banerjee and R.K. Chattopadhyay, Phys. Rev. **C47** (1993) 1013.

[7] Hariprakash Sharma, B. Sethi, Ranjana Goswami, P. Banerjee, R.K. Bhandari and Jahan Singh, Phys. Rev. **C59** (1999) 2446.

[8] Hariprakash Sharma, B. Sethi, P. Banerjee, Ranjana Goswami, R.K. Bhandari and Jahan Singh, Phys. Rev. **C63** (2000) 014313.

[9] M.P.Waring, et al. Phys. Rev. **C48** (1993) 2629.

[10] Y. Liang, et al., in Proceedings of the International Conference on High Spin Physics and Gamma-Soft Nuclei, Pittsburgh, 1990, edited by J.X. Saladin, R.A. Sorensen and C.M.Vincent (World Scientific, Singapore, 1991), p. 308.

[11] J. S. Geiger, Phys. Rev. **C158** (1967) 1094.

[12] J. Ludziejewaki, J. Kownacki, W. Klamra, J. Chwaszczewaka and W. Przybski, Acta Phys. Pol. **36** (1969) 939.

[13] J. R. Lien, J. Gard, C. Lunde Nilsen, G. Lovhoiden and P. B.Vold, Nucl. Phys. **A281** (1977) 443.

[14] U. Hagemann, H.-J. Keller and H.-F. Brinckmann, Nucl. Phys. **A289** (1977) 292.

[15] L. G. Kostova, W. Andrejtscheff, L. K. Kostov, F. Dönau, L. Kaubler, H. Prade and H. Rotter, Nucl. Phys. **A485** (1988) 31.

[16] C.B.Moon and T. Komatsubara, J. Korean Phys. Soc. **45** (2004) L791.

[17] P. Singh, Somnath Nag and A. K. Singh et al., Phys. Rev. **C82** (2010) 034301.

[18] R.E. Shroy, D.M. Gordon, M. Gai, D.B. Fossan and A.K.Gaigalas, Phys. Rev. **C26** (1982) 1089.

[19] J. Katakura, M. Oshima, K. Kitao and H. Iimura, Nucl. Data Sheets **70** (1993) 217.

[20] D. L. Balabanski et al., Phys. Rev. **C56** (1997) 1629.

[21] P. Singh and A. K. Singh et al., Phys. Rev. **C85** (2012) 034319.

[22] D. M. Gordon, M. Gai, A. K. Gaigalas, R. E. Shroy and D. B.Fossan, Phys. Lett. **B67** (1977) 161.

[23] M. Gai, D. M. Gordon, R. E. Shroy, D. B. Fossan and A. K.Gaigalas, Phys. Rev. **C26** (1982) 1101.

[24] B. Ding et al., Phys. Rev. **C85** (2012) 044306.

[25] K. Hara, Y. Sun, Int. J. Mod. Phys. **E4** (1995) 637.

[26] R. Palit, J.A. Sheikh, Y. Sun, H.C. Jain, Nucl. Phys. **A686** (2001) 141.

[27] Y. Sun, J.L. Egido, Nucl. Phys. **A580** (1994) 1.

[28] Y. Sun, J. Zhang, M. Guidry, J. Meng, S. Im, Phys. Rev. **C62** (2000) 021601(R).

[29] K. Hara, Y. Sun, Nucl. Phys. **A529** (1991) 445.

[30] Jing-ye Zhang, A.J. Larabee, L.L. Riedinger, J. Phys. **G13** (1987) 75.

[31] A.Ibannez-Sandoval, M.E. Ortiz, V.Velazquez, A. Galindo-Uribarri, P.O. Hess, Y. Sun, Phys. Rev. **C83** (2011) 034308.

[32] D.M. Symochko, E.Browne, J.K.Tuli, Nucl.Data Sheets **110** (2009) 2945.

[33] S.Ohya, Nucl.Data Sheets **111** (2010) 1619.

[34] S.Ohya, Nucl.Data Sheets **102** (2004) 547.

[35] J.Katakura, Nucl.Data Sheets **112** (2011) 495.

[36] A.Hashizume, Nucl.Data Sheets **112** (2011) 1647.

4. Projected Shell Model study of odd-mass $^{115\text{-}125}$Sb isotopes.

4.1 Introduction

The structure of high-spin states in neutron deficient nuclei near Z=50 major shell closure has explored quite informative results in nuclear physics. Nuclei near this closed proton-shell exhibit a variety of collective structures that coexist with the expected single-particle structure. The experimental information about the nature of collectivity in this region has been provided by the spectroscopic studies of high spin states of odd-A nuclei lying above the Z=50 shell closure [1]. The presence of coexistence of states with different degrees of collectivity in these transitional nuclei has generated considerable interest because these nuclei are near to closed shells, thereby, providing an excellent opportunity to probe important features of nuclear structure. Also, these nuclei are found to be particularly good for spectroscopic investigations due to the experimental accessibility of many Z = 50, tin nuclei across the N = 50–82 shell. Thus, to have some more information about the structure of nuclei lying in the vicinity of Z=50 closed shell, an attempt has been made in the present work to study an isotropic chain of odd mass $^{115\text{-}125}$Sb nuclei in the PSM framework of calculations. Further, before discussing the physics of present work and correlating the same with the outcome of the other research groups, a brief discussion of the work carried out earlier by various other groups [2-22] has been presented below.

It has been found from the study of literature on odd-A Sb nuclei that there are significant underlying structural changes along with the superficially smooth variation of low-energy properties as a function of the neutron number [2,3]. The properties of the low-lying levels of these odd-proton Sb isotopes with 115≤A≤125 are reproduced well in theoretical calculations [4,5] that take into account an odd proton in the spherical orbitals of the Z = 50–82 major shell coupled to the quadrupole and octupole phonon excitations of the Z = 50 Sn core. The Antimony isotopes, with only one proton outside the closed shell, are expected to behave like spherical shell-model nuclei with the valence proton occupying the $d_{5/2}$, $g_{7/2}$, and $h_{11/2}$ orbitals and the neutrons outside of N=50 occupy a similar shell-model space with the Fermi level depending on the neutron number N. A large number of new single-particle states are found in these isotopes of Antimony [6]

and these states show the irregular energies typical of shell-model nuclei. Thus, these nuclei have been observed to possess a wide range of both spherical and deformed states, all of which relate to a coupling of the valence proton to the different structures in the Sn core nuclei.

An investigation of odd-*A* Sb nuclei [7] has revealed a collective structure that involves the coupling of 2p-2h Sn-core deformed states to the low-*K* valence $d_{5/2}$, $g_{7/2}$, and $h_{11/2}$ proton orbitals above the Z = 50 shell gap. The rotational bands in this *Z*=50 region regarding these collective structures has been explored in several *Z*=51 [8-13] and *Z*=50 [13-15] nuclei. Intruder bands in these nuclei based on 2p-2h excitations across the shell gap were observed to extremely high frequency approaching $\hbar\omega$ = 1.5MeV with gradually decreasing dynamic moments of inertia ($\Im^{(2)}$) to values well below the rigid body moment of inertia.

Several experimental studies [16-22] have been devoted to study the level schemes of odd-A $^{115-125}$Sb nuclei in the past few decades. For example, the previously known [1,16] level scheme of ^{115}Sb has been further extended by Chakrawarthy *et al.* [17] to an excitation energy of ≈10 MeV and a spin of I=51/2$^-$. Moreover, the already known energy levels have also been confirmed in this study. Further, this study has also reported an interesting excited intruder band based on aligned neutrons in the $h_{11/2}$ orbital. The low-spin studies [1,18,19] in ^{117,119}Sb have identified a number of spherical levels of multi-quasiparticle nature whereas, the high-spin [6] level schemes for ^{117,119}Sb have been observed to possess a wide range of both spherical and deformed states. This study [6] has also reported a negative parity band based on $\pi h_{11/2}$ sub-shell in ^{117,119}Sb nuclei.

Many new transitions were observed [20] for the first time in high-spin study of ^{121,123}Sb using γ-ray and electron spectroscopy. Jones *et al.* [21] have used multi-dimensional γ-ray coincidence techniques to identify a number of states, and angular correlation measurements have been used with intensity-balance techniques to identify spins and parities of states in these nuclei. The multiparticle states reported in this study are found to be arising from the coupling of a $d_{5/2}$ or $g_{7/2}$ proton with $\nu h_{11/2}$, $\nu s_{1/2}$, and

$\nu d_{3/2}$ excitations, observed in neighbouring tin nuclei. Proquet *et al.* [22] identified the high spin states upto $31/2^-$ in ^{125}Sb for the first time and the isomeric states lying around 2.3 MeV have been established in ^{125}Sb from the delayed coincidences between the fission fragment detector SAPHIR and the gamma array. All the observed states have been described by coupling a $d_{5/2}$ or $g_{7/2}$ proton to an excited Sn core involving either vibrational states or broken neutron pairs.

The overall study made in the past on odd-mass $^{115-125}$Sb nuclei reveal that the negative parity yrast states in these nuclei have been studied upto spins of $51/2^-$, $43/2^-$, $35/2^-$, $19/2^-$, $27/2^-$ and $31/2^-$ respectively. Thus, the present work is mainly focussed on the PSM study of high spin structure of these nuclei and the available range of experimental high spins of these nuclei has been further extended upto $59/2^-$ in all these nuclei. Further, it has also been found from the available experimental data on these nuclei that the ground state spin of these nuclei is $11/2^-$ and the present PSM calculations have also reproduced the same band head spin for these nuclei. In the present study, the results are obtained for the energy spectrum, back-bending and transition probabilities like $B(M1)$, $B(E2)$.

This chapter is planned in the following way. In this chapter, Section 4.2 deals with the formal aspects of the theory of applied approach, PSM. In Section 4.3, I have discussed various nuclear structure properties that have been obtained by using PSM wave-functions and these results have also been compared with the corresponding available experimental ones. Section 4.4 of this chapter contains the concluding remarks of the present work.

4.2 Input parameters used in PSM calculations for $^{115-125}$Sb isotopes

In order to calculate the nuclear structure properties, I have applied a microscopic method known as projected shell model (PSM). The PSM has been developed as a shell model truncation scheme which is implemented in a deformed single-particle basis [23]. Detail of this model is given in chapter 2 of this thesis. The Hamiltonian employed in the calculation is

$$\hat{H} = \hat{H}_o - \frac{\chi}{2}\sum_{\mu}\hat{Q}^{\dagger}_{\mu}\hat{Q}_{\mu} - G_M\hat{P}^{\dagger}\hat{P} - G_Q\sum_{\mu}\hat{P}^{\dagger}_{\mu}\hat{P}_{\mu} \quad (4.2.1)$$

where $\hat{H}_o$ is the spherical single-particle Hamiltonian which contains a proper spin-orbit force. The second, third and fourth terms represent quadrupole-quadrupole (QQ), monopole- pairing and quadrupole-pairing interactions, respectively. The parameter χ represents the strength of quadrupole-quadrupole interaction and its value is adjusted via self-consistent conditions with a given quadrupole deformation ε_2. There is another input parameter known as hexadecapole deformation ε_4, which is normally used to reproduce the experimental energies correctly, but in the present calculations, its value has been set as zero for all the $^{115-125}$Sb nuclei to reproduce the experimental data correctly. The values of the empirical deformation, ε_2, along with hexadecapole deformations, ε_4, which have been used as an input in the PSM calculations for these Antimony nuclei, are given in Table 4.2.1. Spin-orbit force parameters (κ and μ) appearing in Nilsson potential are essential to reproduce the correct shell filling and are taken from Zhang *et al*. [24] for the present set of calculations, as given in Table 4.2.2. All pairing interactions are assumed to occur between the like nucleons. The monopole interaction, G_M, is given as

$$G_M = \left(G_1 \mp G_2\frac{N-Z}{A}\right)\frac{1}{A}(\text{MeV}) \quad (4.2.2)$$

with − (+) for neutrons (protons). Here, G_1 and G_2 are the two adjustable constants. The adjustment of the parameters ε_2, G_1 and G_2, will change the energy gap for each shell and, thus, will affect the selection of the quasiparticle basis. In the present calculations, G_1 and G_2 are taken as 18.00 and 12.14, respectively for each of the odd-mass $^{115-125}$Sb isotopes. These calculations are performed by considering three major oscillator shells (N = 3, 4 and 5) for both neutrons and protons.

The following set of multi-qp configurations is used for odd-proton nuclei:

$$\{|\varphi_k\rangle\} = \{a^{\dagger}_{\pi}|0\rangle, a^{\dagger}_{\pi}a^{\dagger}_{\upsilon_1}a^{\dagger}_{\upsilon_2}|0\rangle\} \quad (4.2.3)$$

where $a^{\dagger}$'s are the quasi-particle (qp) creation operators, ν's (π's) denote the neutron (proton) Nilsson quantum numbers which run over low-lying orbitals and $|0\rangle$ is the

Nilsson + BCS vacuum (0-*qp* state). In Eq. (4.2.3), the low-lying 3-*qp* states selected for the many-body basis are those consisting of 1-*qp* plus a pair of *qp*'s from nucleons of another kind and this selection is based on physical considerations. In general, 3-*qp* states made by three nucleons of the same kind are also allowed, but such states usually lie higher in energy. The inclusion of the 3-*qp* configurations is important for odd-mass nuclei for a description of the band-crossing phenomenon which is caused by a rotation alignment of a pair of quasi-neutrons.

In the present PSM calculations, one-dimensional angular momentum projection method for axially deformed nuclei is applied to project the intrinsic axial basis onto good angular momentum states. Here, the many-body wave function is a superposition of (angular momentum) projected multi-quasi-particle states and angular momentum projection transforms the wave function from the intrinsic frame to the laboratory frame.

The total wave function is can be written as

$$\left|\Psi^{\sigma}_{IM}\right\rangle = \sum_{K\kappa} f^{\sigma}_{\kappa} \hat{P}^{I}_{MK} \left|\varphi_{\kappa}\right\rangle,$$
$$\text{with} \quad \hat{P}^{I}_{MK} = \frac{2I+1}{8\pi^2} \int d\Omega D^{I}_{MK}(\Omega) \hat{R}(\Omega) \tag{4.2.4}$$

where, the index σ labels the states with same angular momentum and κ labels the basis states. $\hat{P}^{I}_{MK}$ is the angular momentum projection operator and f^{σ}_{κ} are the weights of the basis state κ. In my calculations, I have not included the particle number projection and I have used only angular momentum projection $\hat{P}^{I}_{MK}$, as all essential features of the PSM are very well described by angular momentum projection alone and particle number projection adds no new physics. Although, the particle number projection may improve the results, the essential physics of the yrast spectroscopy can be described even without taking it into consideration. Further, violation of the particle number caused by the BCS (or HFB) approximation is not so dangerous for the Projected Shell Model as usually believed in the sense that the essence of the physics obtained by the angular momentum projection alone is not altered even if the particle number projection is carried out in

addition. I, therefore, do not consider it to be of absolute necessity for understanding various phenomena related to nuclear rotational motion.

Table 4.2.1 Deformation parameters used in present calculations for $^{115-125}$Sb nuclei.

	^{115}Sb	^{117}Sb	^{119}Sb	^{121}Sb	^{123}Sb	^{125}Sb
ε_2	-0.190	-0.190	-0.180	-0.190	-0.170	-0.170
ε_4	0.000	0.000	0.000	0.000	0.000	0.000

Table 4.2.2 Nilsson parameters (κ and μ) used as input parameters in present calculations for $^{115-125}$Sb nuclei .

Major Shell N	**Protons**		**Neutrons**	
	κ	μ	κ	μ
3	0.090	0.300	0.090	0.250
4	0.070	0.480	0.070	0.390
5	0.560	0.540	0.062	0.430

4.3 Results and Discussions

4.3.1 Yrast spectra

The spectra comprising of lowest energy states of each angular momentum in a nucleus is known as yrast spectra and it is obtained by a diagonalization of the Hamiltonian (Eq.(4.2.1)) in the deformed basis (Eq.(4.2.3)). A quantitative prediction for the yrast energies of rotational bands in $^{115-125}$Sb are presented in this section. By using PSM, rotational bands are calculated upto the maximum spin of $59/2^-$ for negative parity in these isotopes and are plotted in the Figs. 4.3.1(a)-4.3.1(f). Experimental data for the yrast states for the negative-parity in these nuclei are available up to a maximum spin value $51/2^-$, $43/2^-$, $35/2^-$, $19/2^-$, $27/2^-$ and $31/2^-$ for ^{115}Sb, ^{117}Sb, ^{119}Sb, ^{121}Sb, ^{123}Sb, and ^{125}Sb

respectively. This data has been taken from Refs. [25-30] and is also shown for comparison in the same figures. The comparison of the theoretical yrast spectra with the corresponding experimental one indicates that the range of low-spin yrast states has been reproduced quite satisfactorily in $^{115-125}$Sb nuclei, whereas some discrepancies have been observed at intermediate and high spins which could be due to the fact that I have employed the same set of input parameters for all these Sb nuclei. Moreover, in order to make the calculations consistent for any isotopic mass chain of nuclei, the use of same set of interaction parameters is the basic requirement of PSM approach and this could be constructed as the limitation of PSM method. Further, one more interesting feature which is quite noticeable from PSM results on yrast states is that, the band head spin of all these $^{115-125}$Sb has been calculated as $11/2^-$.The experimental data on negative-parity yrast states also gives the band head spin for $^{115-125}$Sb to be $11/2^-$, which clearly indicates that the PSM results on yrast states have successfully reproduced the band head spins of $^{115-125}$Sb nuclei.

Furthermore, the discussion about the origin of different yrast states in these odd-mass $^{115-125}$Sb nuclei using PSM is explained in the next section 4.3.2 of this chapter, where the arise of yrast states has been explained on the basis of band diagrams.

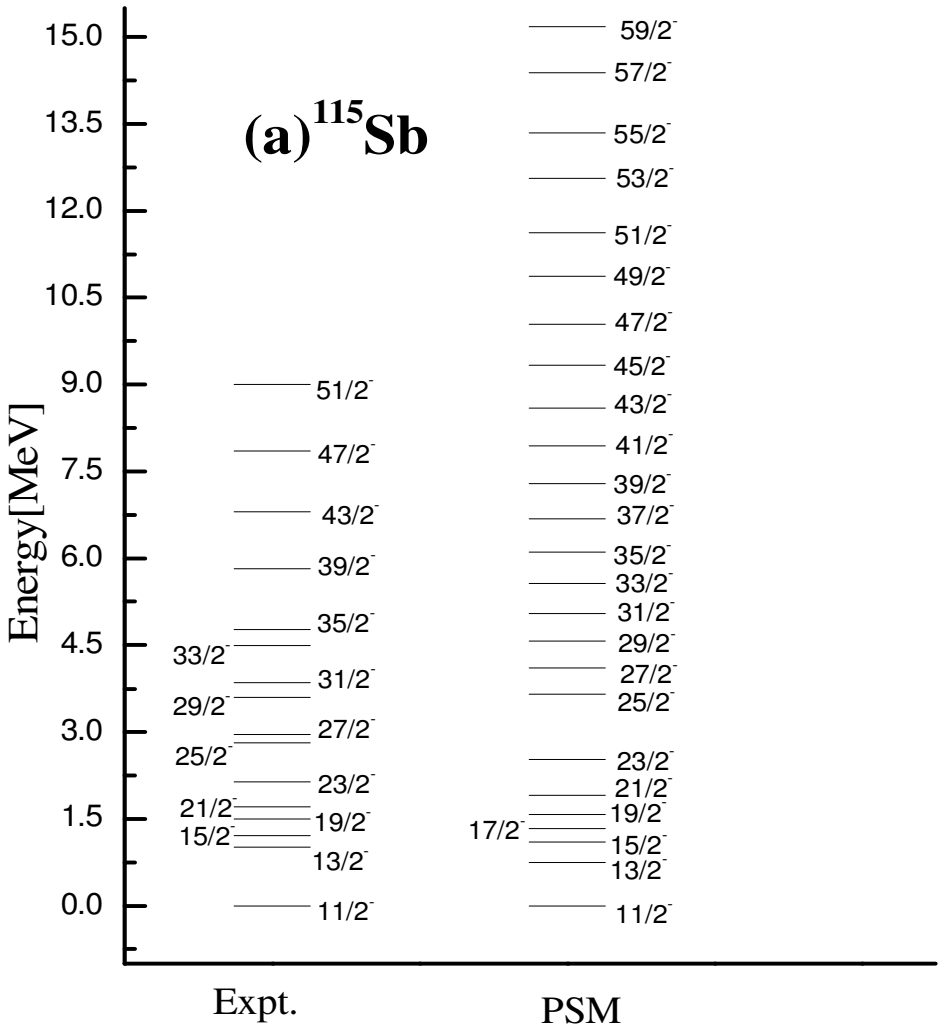

Fig. 4.3.1(a) Comparison of calculated energies of yrast band with experimental data [25] for ^{115}Sb.

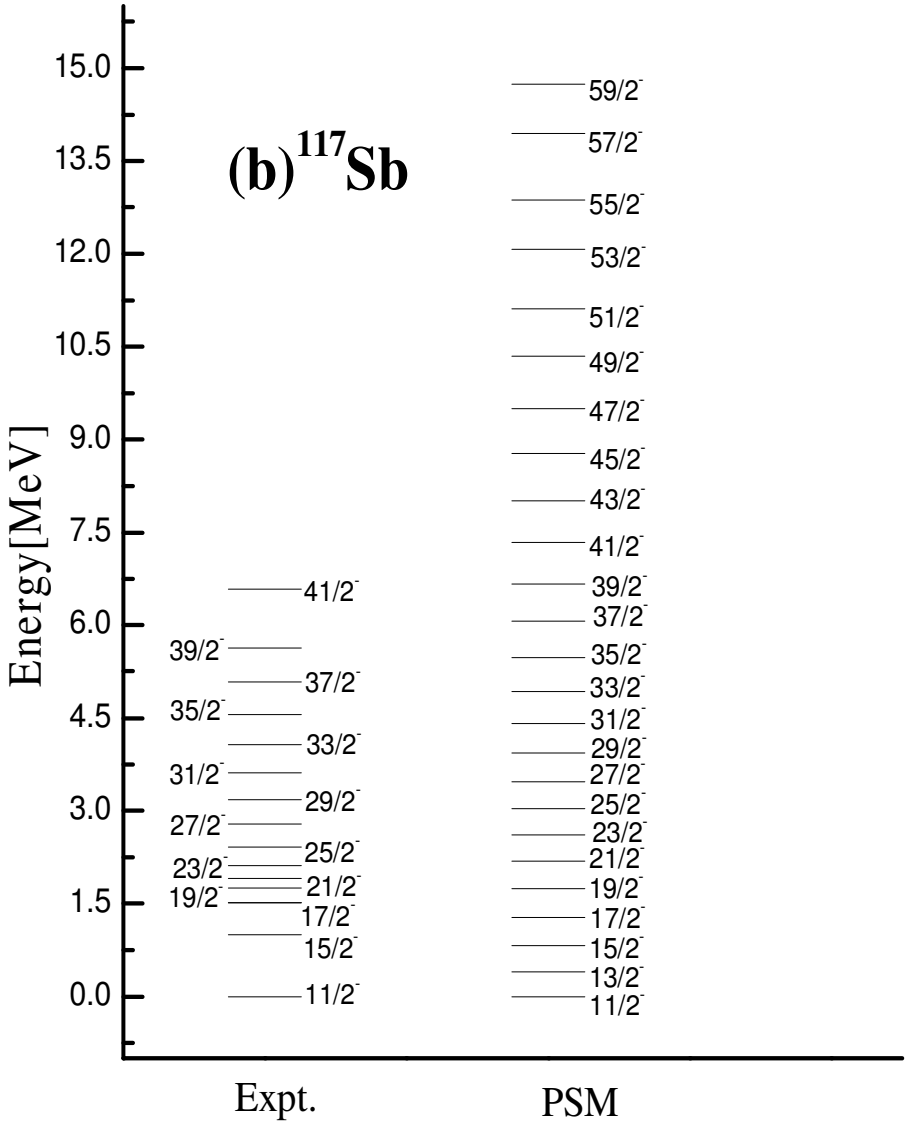

Fig. 4.3.1(b) Comparison of calculated energies of yrast band with experimental data [26] for ^{117}Sb.

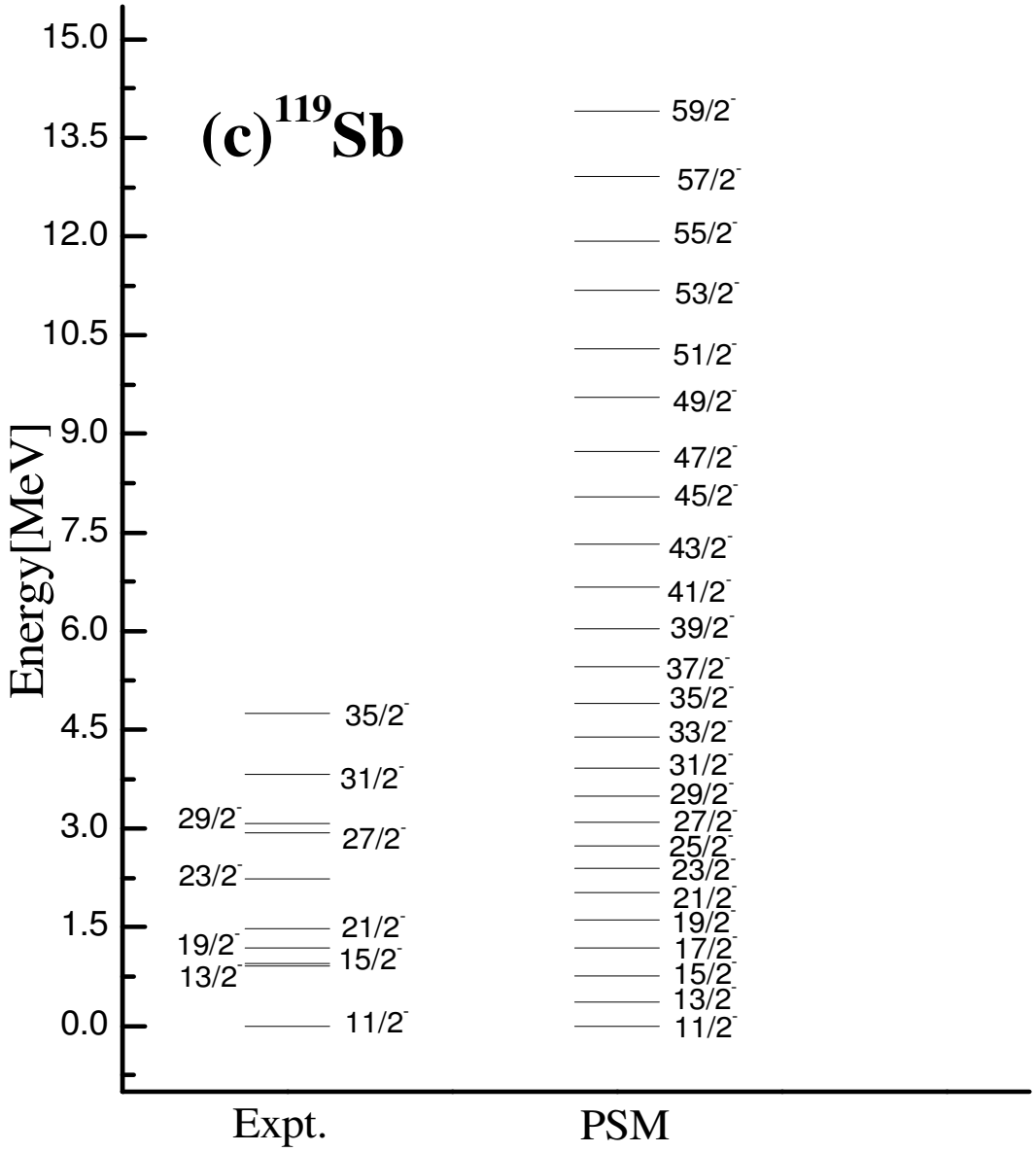

Fig. 4.3.1(c) Comparison of calculated energies of yrast band with experimental data [27] for ^{119}Sb.

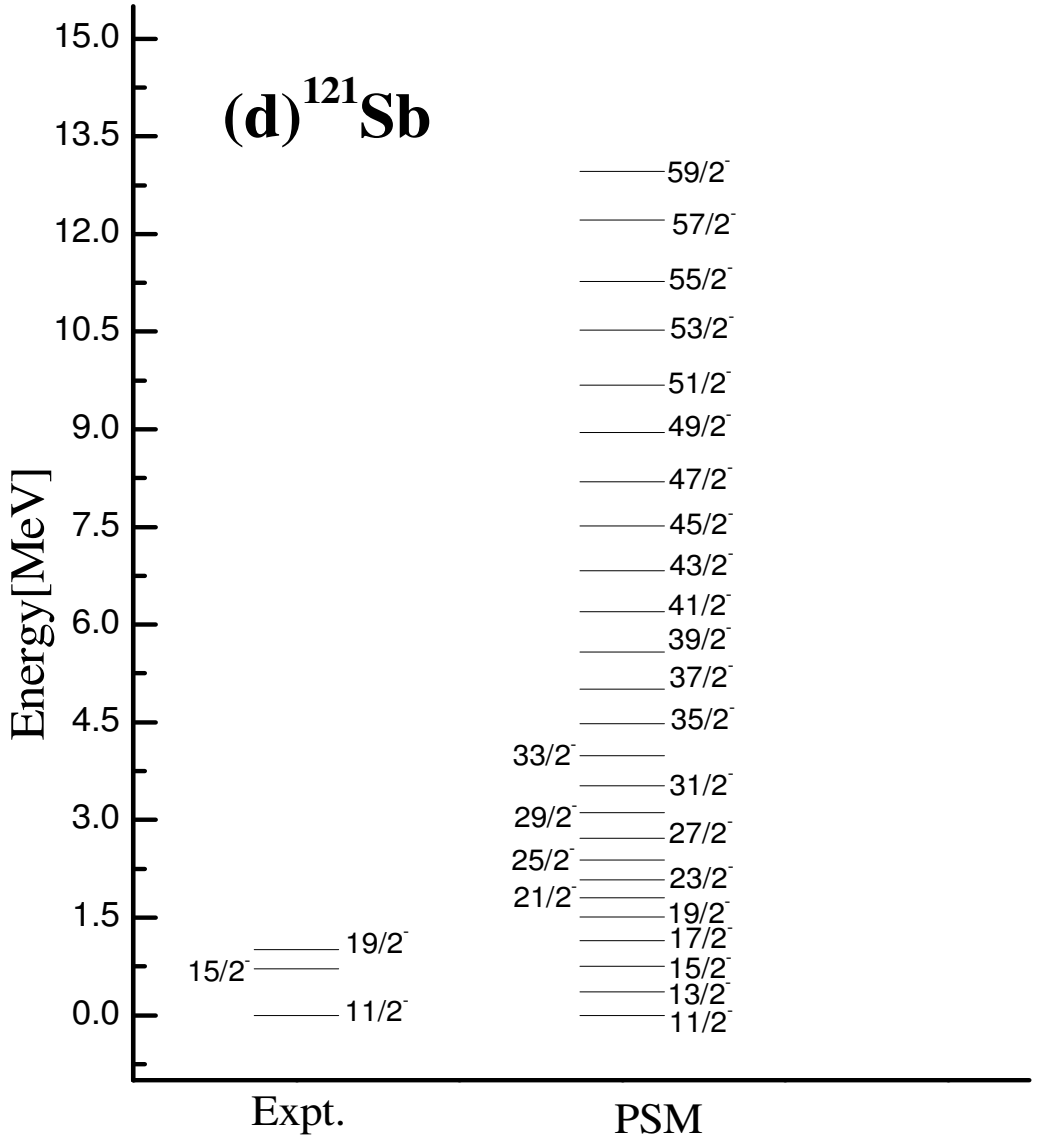

.

Fig. 4.3.1(d) Comparison of calculated energies of yrast band with experimental data [28] for ^{121}Sb.

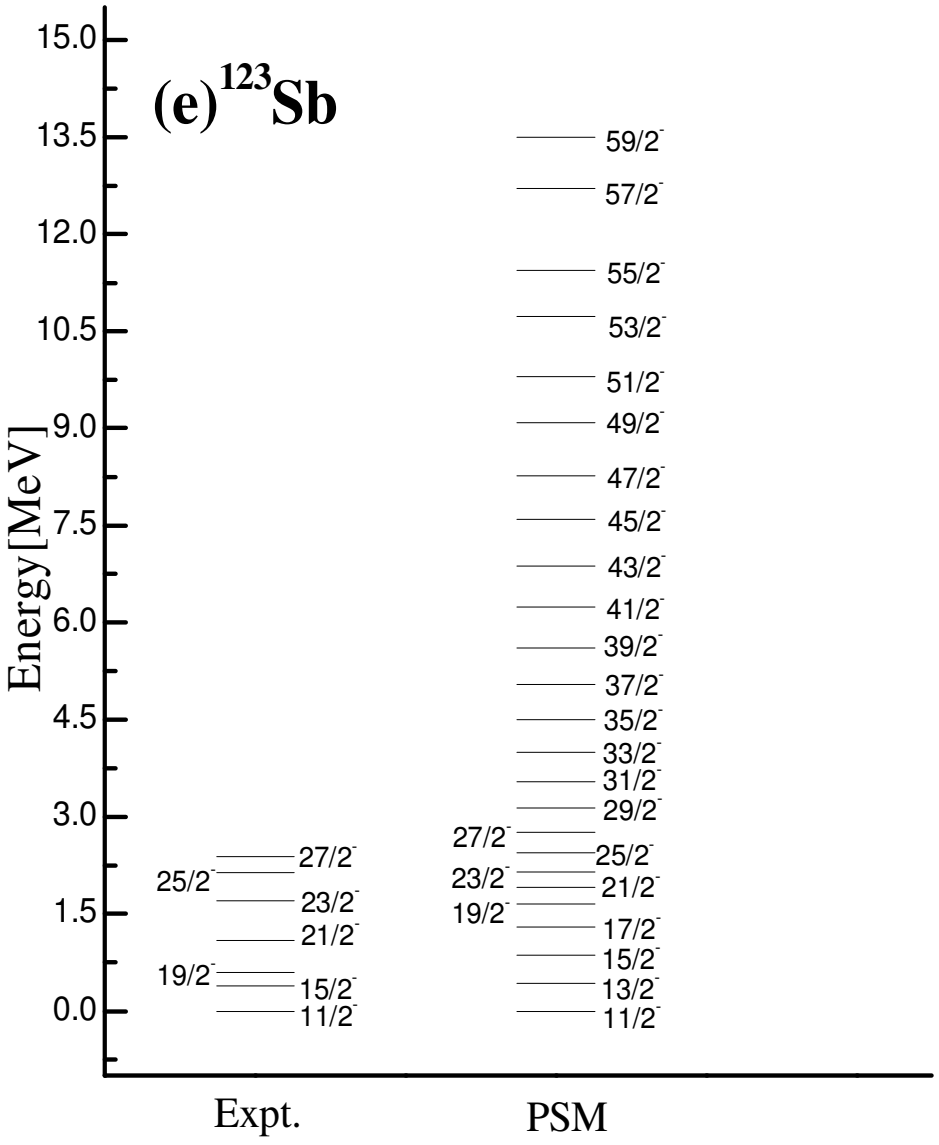

Fig. 4.3.1(e) Comparison of calculated energies of yrast band with experimental data [29] for ^{123}Sb.

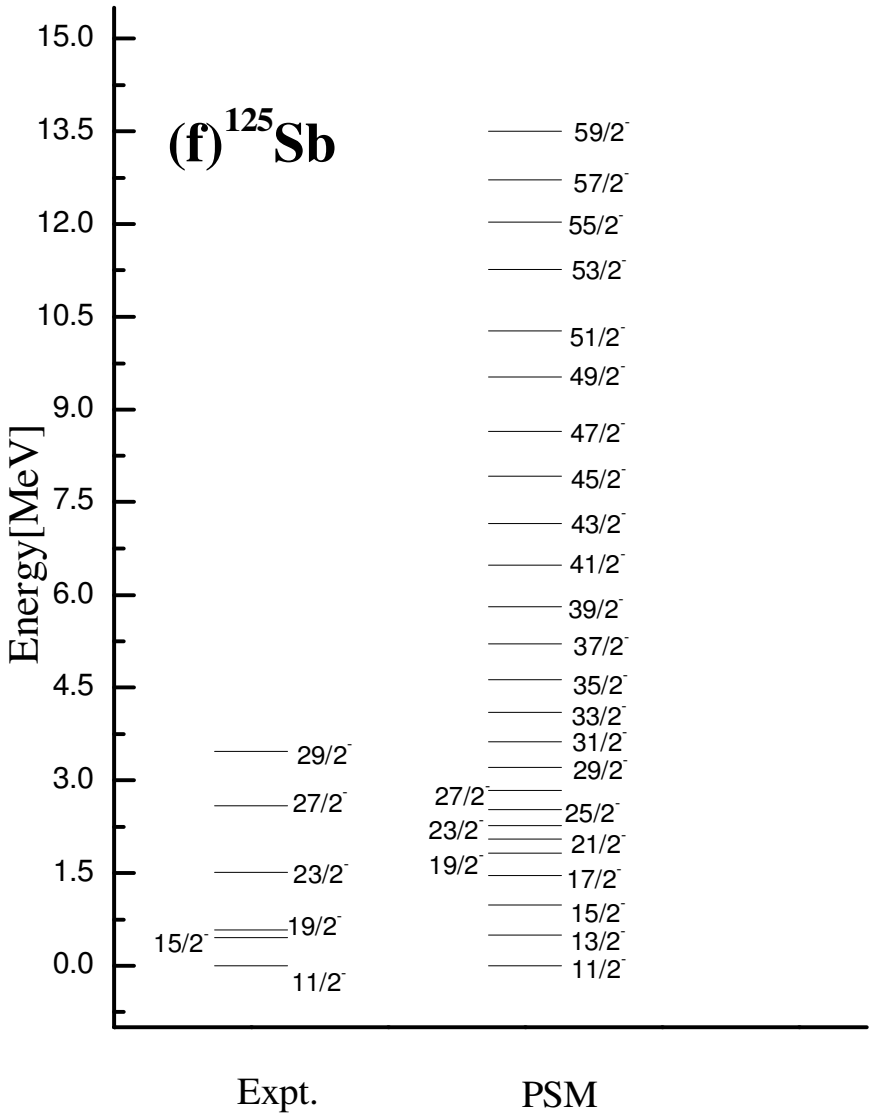

Fig. 4.3.1(f) Comparison of calculated energies of yrast band with experimental data [30] for ^{125}Sb.

4.3.2 Quasi-particle structure of antimony isotopes.

Band diagram is a collection of the band energies and is obtained by plotting different energy bands with respect to spin. It is an indispensable tool which helps in checking the adequacy of the multi-quasi particle configurations involved in the calculations. The band diagrams, presented in Figs. 4.3.2 (a)–4.3.2(f), show the composition of negative-parity yrast bands in $^{115-125}$Sb isotopes.

In case of ^{115}Sb isotope Fig. 4.3.2(a), the low lying yrast states are generated by 1-quasi proton band $1\pi h_{11/2}$ [-11/2], K = -11/2 upto the spin $25/2^-$. After that, a 3-qp band identified as $1\pi h_{11/2}$ [-11/ 2] + $2\upsilon h_{11/2}$ [9/2, -7/2], K = -9/ 2 crosses this 1-qp band at spin $25/2^-$ and remains lowest in energy upto the spin $31/2^-$. At this spin of $31/2^-$, another 3-qp band with configuration: $1\pi h_{11/2}$ [-11/2] + $2\upsilon h_{11/2}$ [-7/2,5/2], K = -13/2 crosses the above mentioned 3-qp band and becomes lower in energy, which then forms the remaining part of the calculated yrast band.

For ^{117}Sb isotope (see Fig. 4.3.2(b)), the yrast band upto spin $21/2^-$ is formed by a 1-qp band with configuration: $1\pi h_{11/2}$ [-11/2], K = -11/2 .This 1-qp band is then crossed by a 3-qp band with configuration $1\pi h_{11/2}$ [-11/2] + $2\upsilon h_{11/2}$ [9/2, -7/2], K = -9/2 and this 3-qp band is responsible for the formation of yrast states from $21/2^-$ to $27/2^-$. At this spin $27/2^-$, this 3-qp band is overlapped with one more 3-*qp* band with configuration: $1\pi h_{11/2}$ [-11/ 2] + $2\upsilon h_{11/2}$ [-7/2, 5/ 2], K = -13/2 and their combination then contributes to the arise of yrast states upto the spin of $31/2^-$. Thereafter, one of the above mentioned two overlapped 3-*qp* bands with configuration $1\pi h_{11/2}$ [-11/ 2] + $2\upsilon h_{11/2}$ [-7/2, 5/ 2], K = -13/ 2 is found to be contributing for the formation of yrast band all alone and makes the yrast spectra upto the last calculated spin.

Further, Fig. 4.3.2(c) represents the band diagram of ^{119}Sb, in which the yrast band arises due to one 1-*qp* band with configuration $1\pi h_{11/2}$ [-11/2], K = -11/2] up to a spin of $21/2^-$. At this spin $21/2^-$, this 1-*qp* band gets crossed by a 3-*qp* band identified as $1\pi h_{11/2}$ [-11/ 2] + $2\upsilon h_{11/2}$ [-7/2, 5/ 2], K = -13/ 2 which contributes to yrast spectra upto the spin value of $51/2^-$. After this spin, a mixture of two more 3-*qp* bands with configurations: $1\pi h_{11/2}$ [9/2] + $2\upsilon h_{11/2}$ [-7/2,5/2], K = 7/ 2 and $1\pi h_{11/2}$ [-7/2] + $2\upsilon h_{11/2}$, [-7/2,5/2], K =

-9/2 gets superimposed with above mentioned 3-qp band, which then collectively make the yrast line up to the last calculated spin.

Furthermore, in case of ^{121}Sb isotope (see Fig. 4.3.2(d)), PSM calculations predict that, a 1-qp band with configuration $1\pi h_{11/2}$ [-11/2], K = -11/2 is contributing towards the formation of yrast line up to the spin value of $19/2^-$, which is then crossed by a 3–qp band identified as $1\pi h_{11/2}$ [-11/ 2] + $2\upsilon h_{11/2}$ [-7/2, 5/ 2], K = -13/ 2, and contributes to yrast spectra upto the spin value of $49/2^-$. At this spin $49/2^-$, a mixture of two overlapped 3-*qp* bands with configurations: $1\pi h_{11/2}$ [9/2] + $2\upsilon h_{11/2}$ [-7/2,5/2], K = 7/ 2 and $1\pi h_{11/2}$ [-7/2] + $2\upsilon h_{11/2}$, [-7/2,5/2], K = -9/2 joins the above mentioned 3-qp band and afterwards forms the ground states upto the last calculated spins.

Now coming to ^{123}Sb, given in Fig. 4.3.2(e). In this case, yrast is contributed by a 1-qp band with configuration $1\pi h_{11/2}$ [-11/2] , K = -11/2 upto spin $19/2^-$. Afterwards, band crossing occurs at I = $19/2^-$ and a 3-qp band which is responsible for this crossing is $1\pi h_{11/2}$ [-11/ 2] + $2\upsilon h_{11/2}$ [-7/2, 5/ 2], K = -13/ 2, becomes lower in energy for giving rise to yrast spectra upto the spin value of $49/2^-$. At this spin, a set of two overlapped 3-*qp* bands with configurations: $1\pi h_{11/2}$ [9/2] + $2\upsilon h_{11/2}$ [-7/2,5/2], K = 7/ 2 and $1\pi h_{11/2}$ [-7/2] + $2\upsilon h_{11/2}$, [-7/2,5/2], K = -9/2 along with the above mentioned 3–qp band starts contributing towards the formation of yrast band up to the maximum calculated spin.

Lastly, for ^{125}Sb (see Fig. 4.3.2(f)), upto the spin of $19/2^-$, the yrast spectra arises because of one 1-*qp* band, $1\pi h_{11/2}$ [-11/2], K = -11/2. After this spin, band crossing occurs due to a 3-*qp* band with configuration: $1\pi h_{11/2}$ [-11/2] +$2\upsilon h_{11/2}$ [-7/2,5/2], K = -13/2 which becomes lower in energy and contributes towards to the formation of yrast band upto the spin value of $47/2^-$. At next higher spin range, two more overlapped 3-*qp* bands with configurations: $1\pi h_{11/2}$ [9/2] + $2\upsilon h_{11/2}$ [-7/2,5/2], K = 7/ 2 and $1\pi h_{11/2}$ [-7/2] + $2\upsilon h_{11/2}$, [-7/2,5/2], K = -9/2 also take part in contributing towards the formation of the yrast band along with the above mentioned 3–qp band up to the maximum calculated spins.

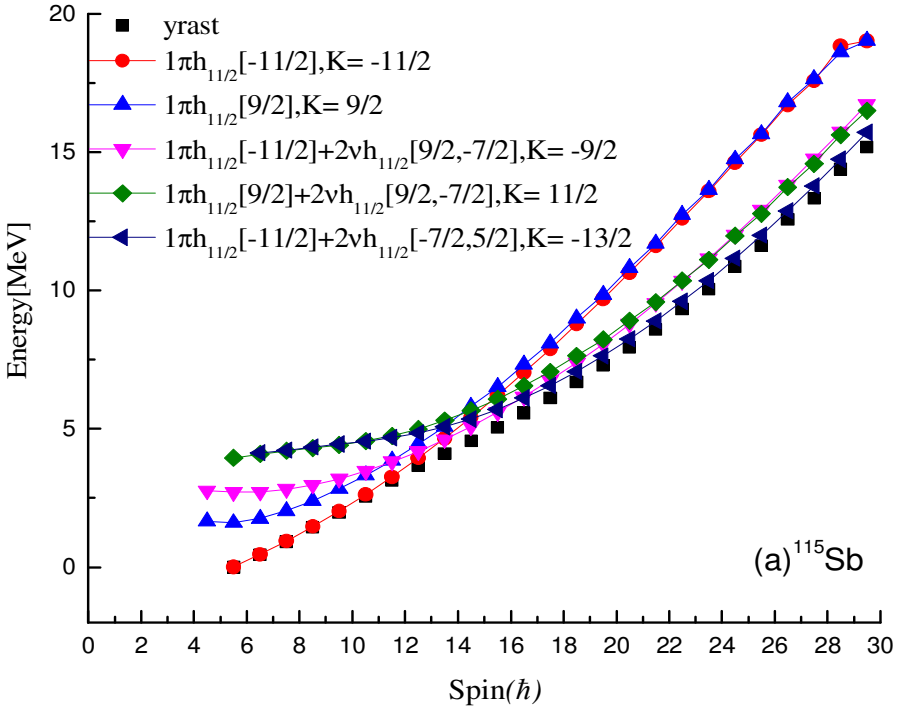

Fig. 4.3.2(a) A representative band diagram for ^{115}Sb. Here, only the important lowest lying bands in each configuration are plotted.

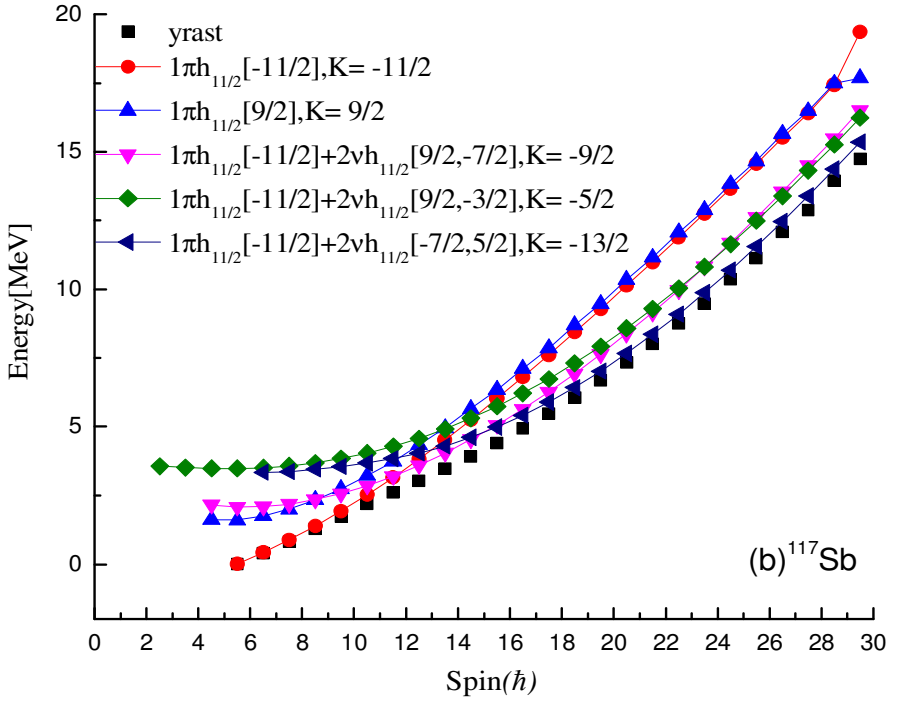

Fig. 4.3.2(b) A representative band diagram for ^{117}Sb. Here, only the important lowest lying bands in each configuration are plotted.

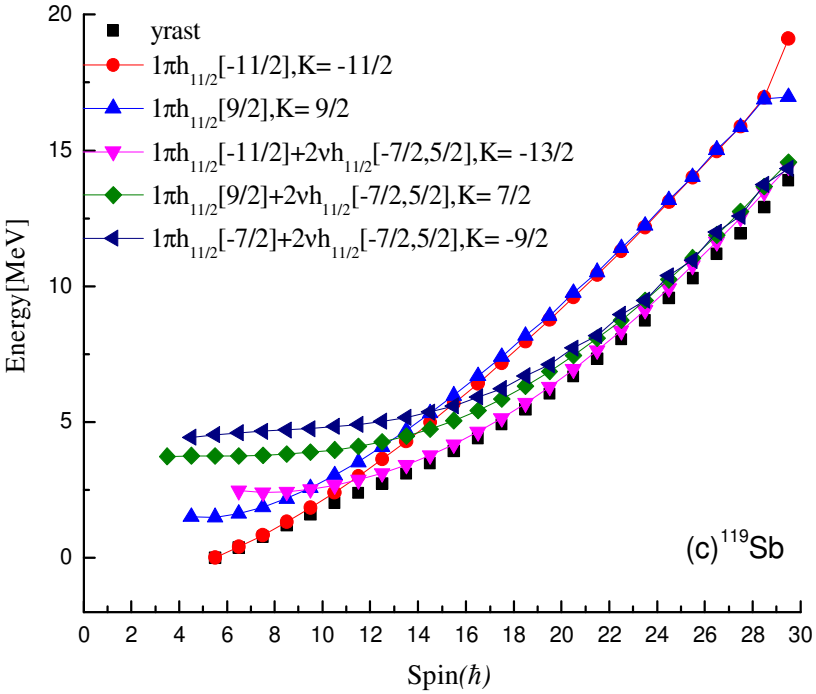

Fig. 4.3.2(c) A representative band diagram for ^{119}Sb. Here, only the important lowest lying bands in each configuration are plotted.

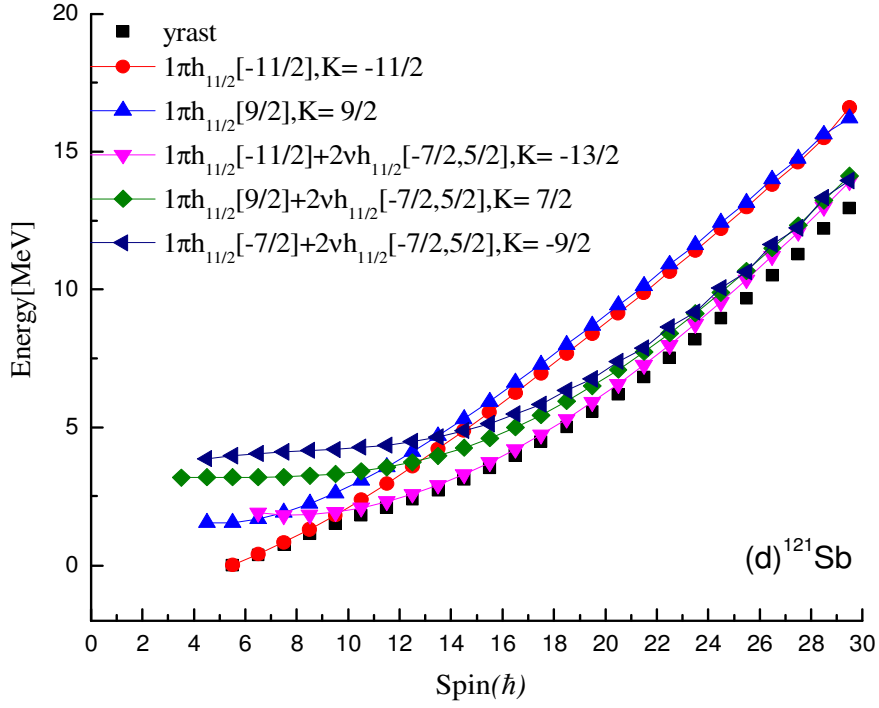

Fig. 4.3.2(d) A representative band diagram for ^{121}Sb. Here, only the important lowest lying bands in each configuration are plotted.

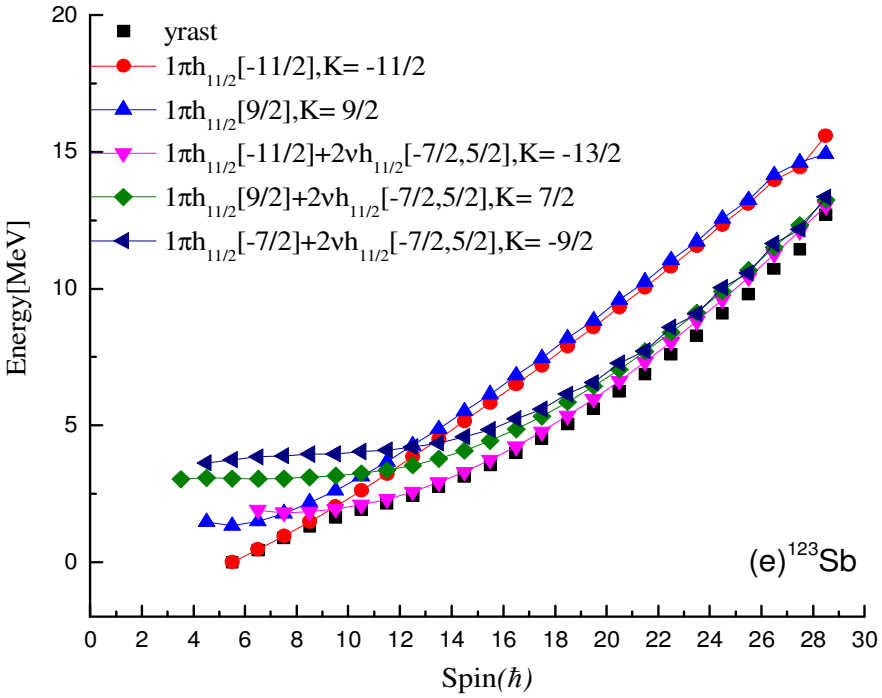

Fig. 4.3.2(e) A representative band diagram for ^{123}Sb. Here, only the important lowest lying bands in each configuration are plotted.

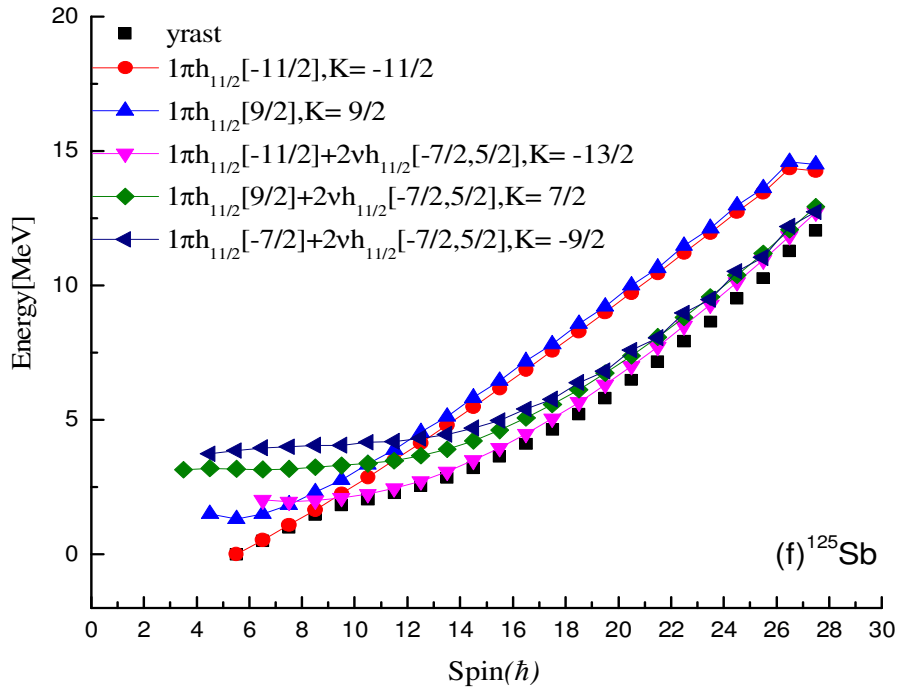

Fig. 4.3.2(f) A representative band diagram for ^{125}Sb. Here, only the important lowest lying bands in each configuration are plotted.

4.3.3 Back-bending in moment of inertia in yrast bands

Back-bending in moment of inertia is the most important quantity characterizing the nuclear rotational bands. So, the behaviour of rotational bands can be studied by the phenomenon of back-bending in moment of inertia. The mechanism of back-bending can be explained as a result of the crossing of the ground band with another rotational band having a larger moment of inertia and carries important information on the interplay between the ground band and bands with alignment of a pair of quasi-particles. In Figs. 4.3.3(a)-4.3.3(f), I have compared the PSM results with experimental data on back-bending in moment of inertia for the $^{115-125}$Sb isotopes for negative- parities. Here, the back-bending in moment of inertia has been discussed on the basis of plots between twice the kinetic moment of inertia ($2\Im^{(1)}$) and square of corresponding rotational frequency($\hbar^2\omega^2$).These quantities are calculated by using the formulae [31] as

$$2\Im^{(1)} = \frac{(2I-1)}{\omega} \tag{4.3.1}$$

$$\hbar\omega = \frac{E_\gamma}{\sqrt{(I+1)(I+2)-K^2} - \sqrt{(I-1)I-K^2}} \tag{4.3.2}$$

where the transition energy, $E_\gamma = E(I) - E(I-2)$

Figs. 4.3.3(a)-4.3.3(f), show the comparison between theoretical and experimental values of back-bending. For ^{115}Sb, the experimental back-bending is observed at spin $15/2^-$ corresponding to rotational frequency ($\hbar^2\omega^2$) of 0.19 MeV^2, while PSM predicts the back-bending at spin of $23/2^-$ with rotational frequency of 0.25 MeV^2.

For ^{117}Sb isotope, PSM predicts the back-bending at spin $19/2^-$, whereas experimental back-bending is observed at spin of $15/2^-$ with corresponding rotational frequencies of 0.14 MeV^2 and 0.13 MeV^2, respectively. For ^{119}Sb, the experimental and theoretical back

bendings have been found to occur at the spin values of $15/2^-$ and $21/2^-$, respectively at the rotational frequencies of 0.12 MeV^2 and 0.13 MeV^2.

In ^{121}Sb, back-bending is predicted theoretically at the spin $19/2^-$ with corresponding rotational frequency 0.10 MeV^2, whereas experimental back-bending is observed at the spin of $15/2^-$ with corresponding rotational frequency of 0.07 MeV^2.

For ^{123}Sb and ^{125}Sb, PSM predicts back-bendings at the same spin of $17/2^-$, which correspond to the rotational frequencies of 0.12 MeV^2 and 0.14 MeV^2, respectively, whereas experimentally, these have also been found to occur at the same spin value of $15/2^-$ for these two isotopes corresponding to the same value of rotational frequency of 0.02 MeV^2 in these isotopes.

Thus, it can be concluded from the discussion on back-bending phenomenon that PSM has predicted the back-bending in moment of inertia at almost the same value of rotational frequency at which experimental one occurs in all the odd mass $^{115-125}$Sb isotopes. Further, it has also been found from the present calculations that back-bending in moment of inertia (shown in Figs. 4.3.3(a) - 4.3.3(f)) occurs at the same spin value at which band crossing takes place in all the $^{115-125}$Sb isotopes (see Figs.4.3.2(a) - 4.3.2(f)), for negative-parity states.

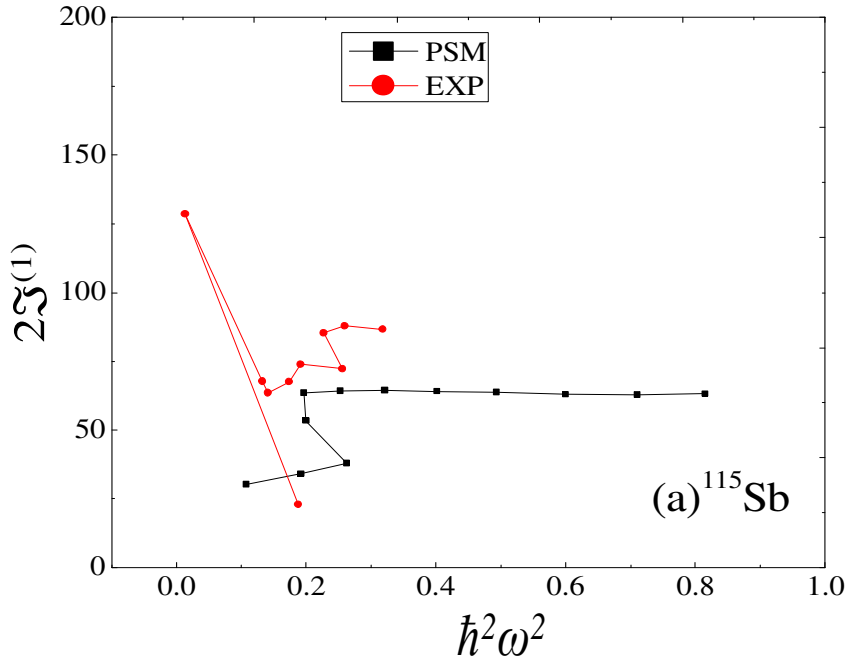

Fig. 4.3.3(a) Twice the kinetic moment of inertia ($2\Im^{(1)}$) plotted against rotational frequency squared ($\hbar^2\omega^2$) in comparison with the experimental data for ^{115}Sb.

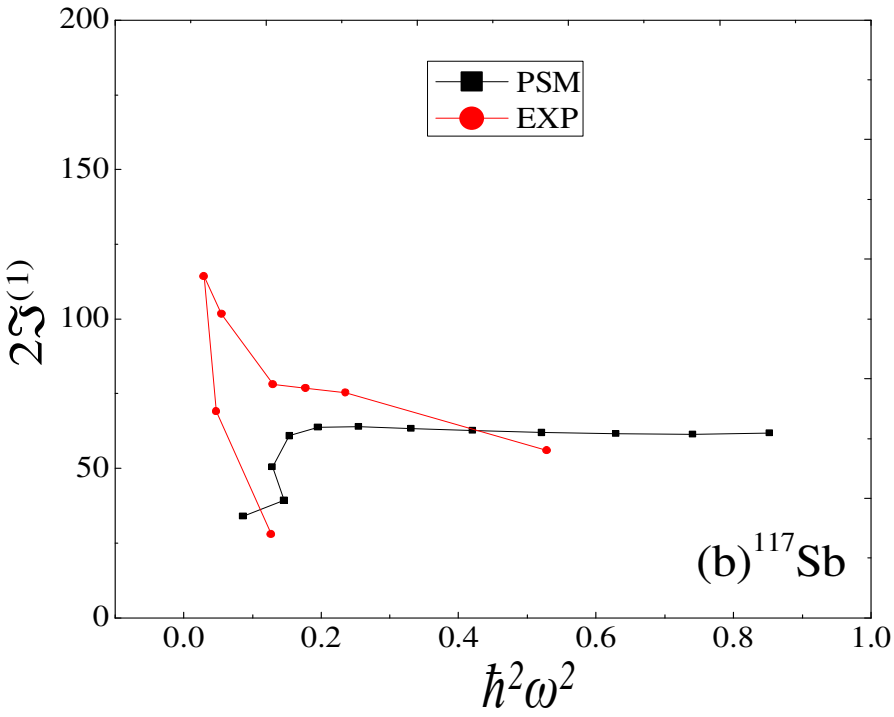

Fig. 4.3.3(b) Twice the kinetic moment of inertia ($2\Im^{(1)}$) plotted against rotational frequency squared ($\hbar^2\omega^2$) in comparison with the experimental data for ^{117}Sb.

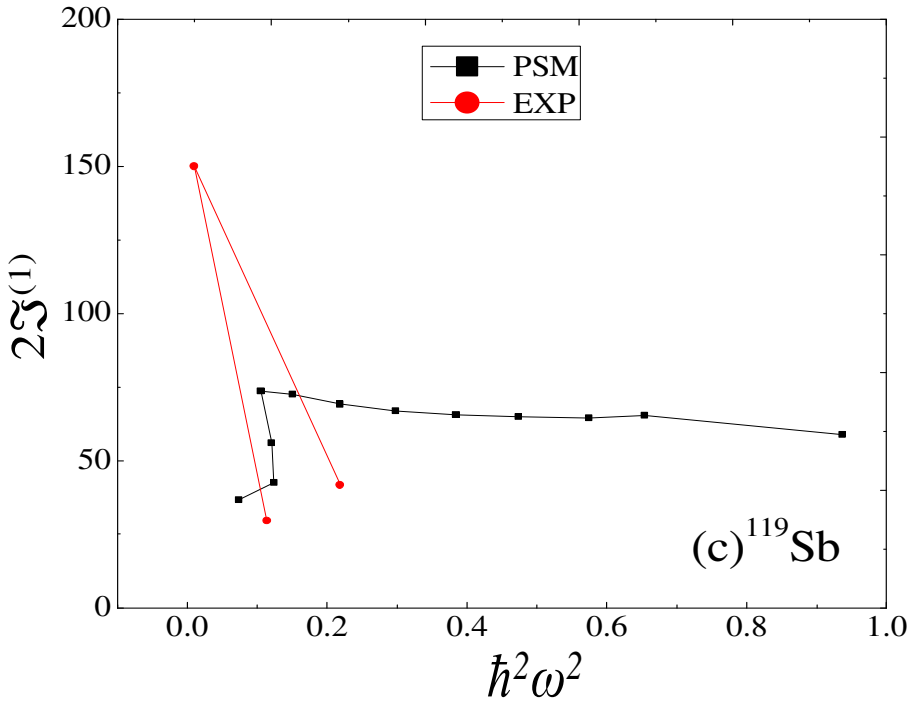

Fig. 4.3.3(c) Twice the kinetic moment of inertia ($2\Im^{(1)}$) plotted against rotational frequency squared ($\hbar^2\omega^2$) in comparison with the experimental data for ^{119}Sb.

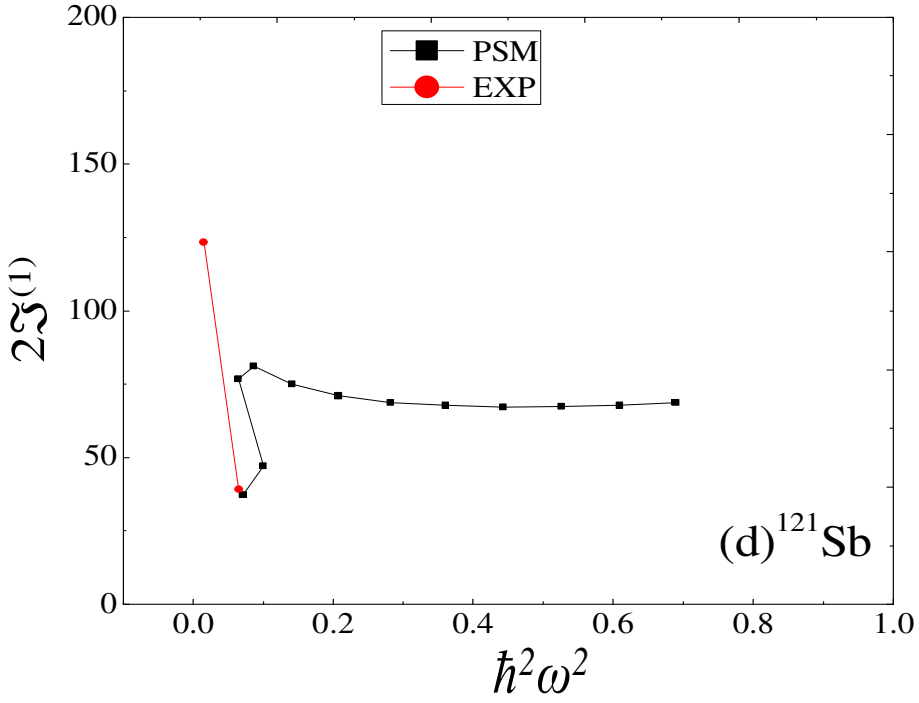

Fig. 4.3.3(d) Twice the kinetic moment of inertia ($2\Im^{(1)}$) plotted against rotational frequency squared ($\hbar^2\omega^2$) in comparison with the experimental data for ^{121}Sb.

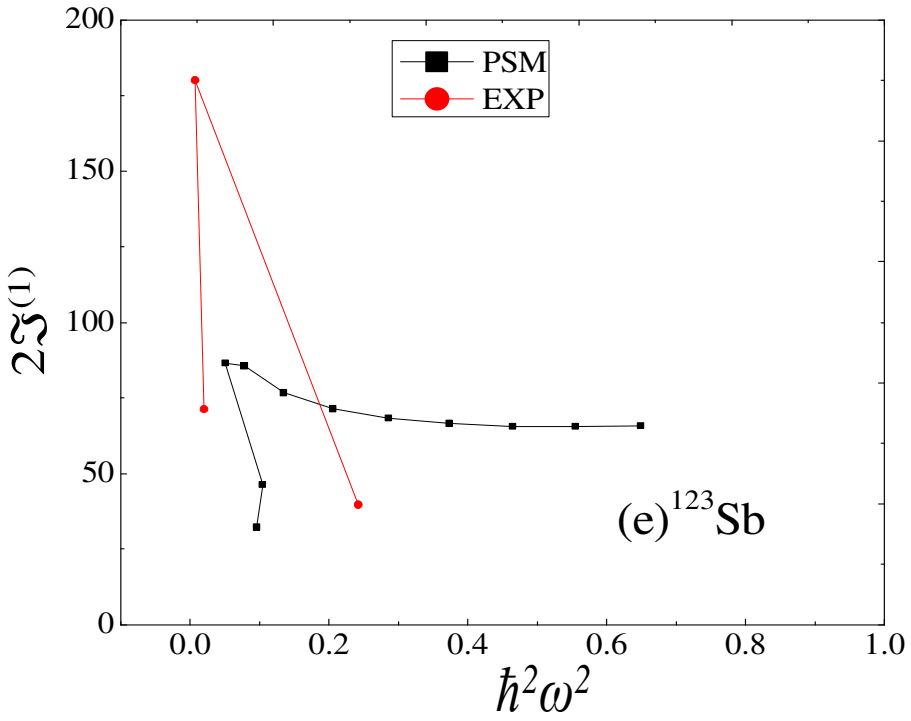

Fig. 4.3.3(e) Twice the kinetic moment of inertia ($2\Im^{(1)}$) plotted against rotational frequency squared ($\hbar^2\omega^2$) in comparison with the experimental data for ^{123}Sb.

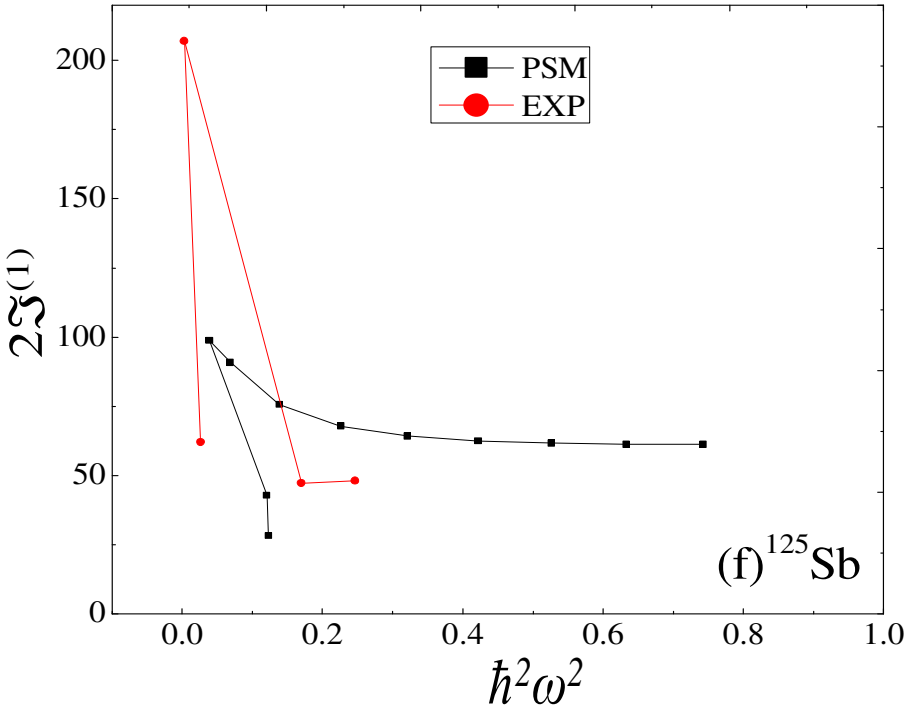

Fig. 4.3.3(f) Twice the kinetic moment of inertia ($2\Im^{(1)}$) plotted against rotational frequency squared ($\hbar^2\omega^2$) in comparison with the experimental data for ^{125}Sb.

4.3.4. Reduced transition probability

The transition probabilities, $B(E2)$ and $B(M1)$, can give important information on the nuclear structure and provide a stringent test of a particular model. Generally, these values emphasize the widespread occurrence of quadrupole deformation in nuclides and in the present work, the reduced transition probabilities $B(E2)$ have been calculated by using a quadrupole operator obtained from PSM wave functions, as given by Eq.(4.3.3).

From an initial state (I_i=I) to a final state (I_f = I - 2), the reduced electric quadrupole transition probability $B(E2)$ is represented by

$$B(E2, I_i \rightarrow I_f) = \frac{e^2}{2I_i + 1} \left| \left\langle \sigma_f, I_f \right| \left| \hat{Q}_2 \right| \left| \sigma_i, I_i \right\rangle \right|^2 \qquad (4.3.3)$$

Here, the operator $\hat{Q}_2$ is related to the quadrupole operators. In order to calculate B(E2) values, the numerical values for proton (neutron) effective charges, as e_π (e_ν), have been employed, which are defined as:

$e_\pi = 1 + e_{eff}$ and $e_\upsilon = e_{eff}$

and in the present set of calculations, I have taken e_{eff} =0.6.

In addition to this, the reduced magnetic transition probability $B(M1)$ has also been calculated using magnetic dipole operator M_1 obtained from PSM wavefunctions, as given by Eq.(4.3.4). Magnetic dipole transition strengths are sensitive to the single-particle nuclear wavefunction. The reduced magnetic dipole transition probability $B(M1)$ from initial state (I_i=I) to final state (I_f=I-1) is given by

$$B\left(M1, I_i \rightarrow I_f\right) = \frac{\mu_N^2}{2I_i + 1} \left| \left\langle \sigma_f, I_f \right| \left| \hat{\mathrm{M}}_1 \right| \left| \sigma_i, I_i \right\rangle \right|^2 \qquad (4.3.4)$$

where the magnetic dipole operator M_1 is given by the following relation

$$\hat{\mathrm{M}}_{1}^{\tau} = g_{l}^{\tau}\hat{j}^{\tau} + \left(g_{s}^{\tau} - g_{l}^{\tau}\right)\hat{s}^{\tau}$$

here τ denotes either π or ν ; g_l and g_s are the orbital and the spin gyromagnetic factors, respectively and are defined as:

$$g_{\tau}(\sigma, I) = \frac{1}{\left[I(I+1)(2I+1)\right]^{1/2}}\left(g_{l}^{\tau}\left\langle \sigma, I \middle\| J^{\tau} \middle\| \sigma, I \right\rangle + (g_{s}^{\tau} - g_{l}^{\tau})\left\langle \sigma, I \middle\| S^{\tau} \middle\| \sigma, I \right\rangle\right) \tag{4.3.5}$$

and in these calculations, one can take the free values for g_l, whereas for g_s , the free values are damped by a factor of 0.85. The standard free values of g_l and g_s for protons and neutrons are

$$g_{l}^{\pi} = 1,\ g_{l}^{\nu} = 0,\ g_{s}^{\pi} = 5.586 \times 0.85,\ g_{s}^{\nu} = -3.826 \times 0.85$$

In these calculations, the effective charges as well as damping of free values of g_s have been used to take into account the effect of core-polarization and meson-exchange current corrections.

The reduced matrix element of an operator $\hat{O}$ ($\hat{O}$ is either $\hat{Q}$ or $\hat{\mathrm{M}}$) is written by

$$\left\langle \sigma_f, I_f \middle\| \hat{O}_L \middle\| \sigma_i, I_i \right\rangle = \sum_{\kappa_i, \kappa_f} f_{I_i \kappa_i}^{\sigma_i} f_{I_f \kappa_f}^{\sigma_f} \sum_{M_i, M_f, M} (-1)^{I_f - M_f} \begin{pmatrix} \mathrm{I_f} & \mathrm{L} & \mathrm{I_i} \\ -\mathrm{M_f} & \mathrm{M} & \mathrm{M_i} \end{pmatrix}$$

$$\left\langle \phi_{\kappa_f} \middle| \hat{P}_{K_{\kappa_f} M_f}^{I_f} \hat{O}_{LM} \hat{P}_{K_{\kappa_i} M_i}^{I_i} \middle| \phi_{\kappa_i} \right\rangle \tag{4.3.6}$$

Fig.4.3.4 represents the calculated values of the reduced electric transition probabilities, {$B(E2)$} for negative-parity yrast band in $^{115-125}$Sb isotopes, whereas, the calculated data for magnetic transition probabilities {$B(M1)$} for negative-parity yrast band in these isotopes have been presented in Fig.4.3.5. Since experimental data on $B(E2)$ and $B(M1)$ values for yrast bands on these nuclei are not available, so one cannot make any comment on their degree of accuracy. However, these values have been calculated for the entire range of transitions upto which the maximum yrast levels have been obtained in the present work. Further, since the calculated data on $B(E2)$ values do not show much variation in the domain of upper-lying transitions and remain almost constant for these transitions, it therefore indicates that the deformation in the $^{115-125}$Sb isotopes is constant

for the higher-spin region of transitions. Thus, the prediction of this feature of constant deformation in the domain of higher-lying transitions in these odd-mass Sb isotopes by the present PSM calculations throws an opportunity for the experimentalists to work for this kind of data in future.

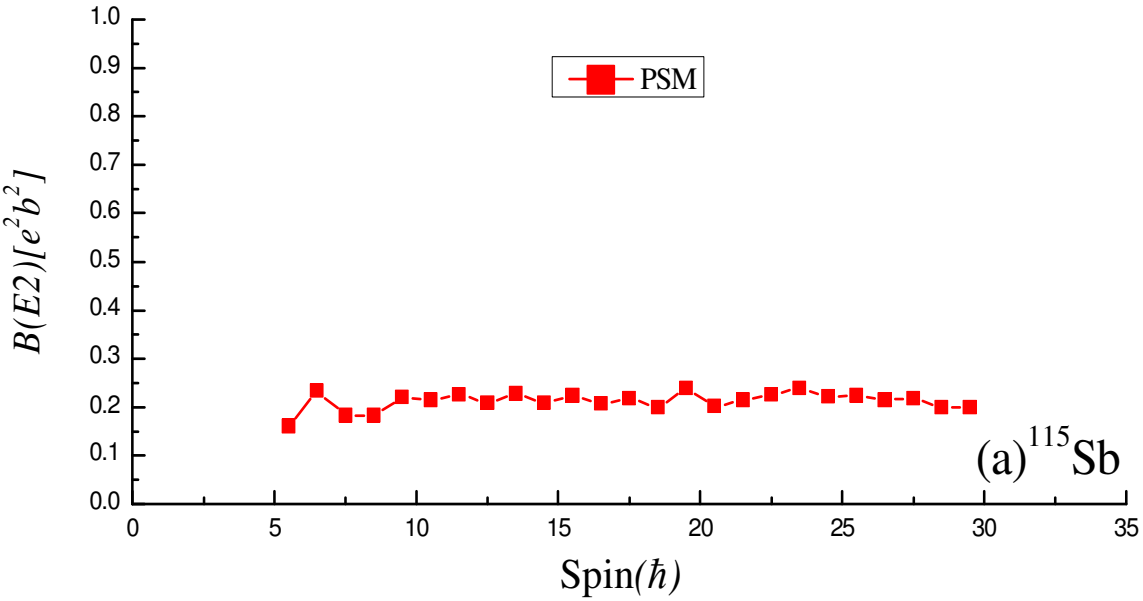

Fig. 4.3.4(a) Calculated *B(E2)* transition probabilities for yrast band in ^{115}Sb.

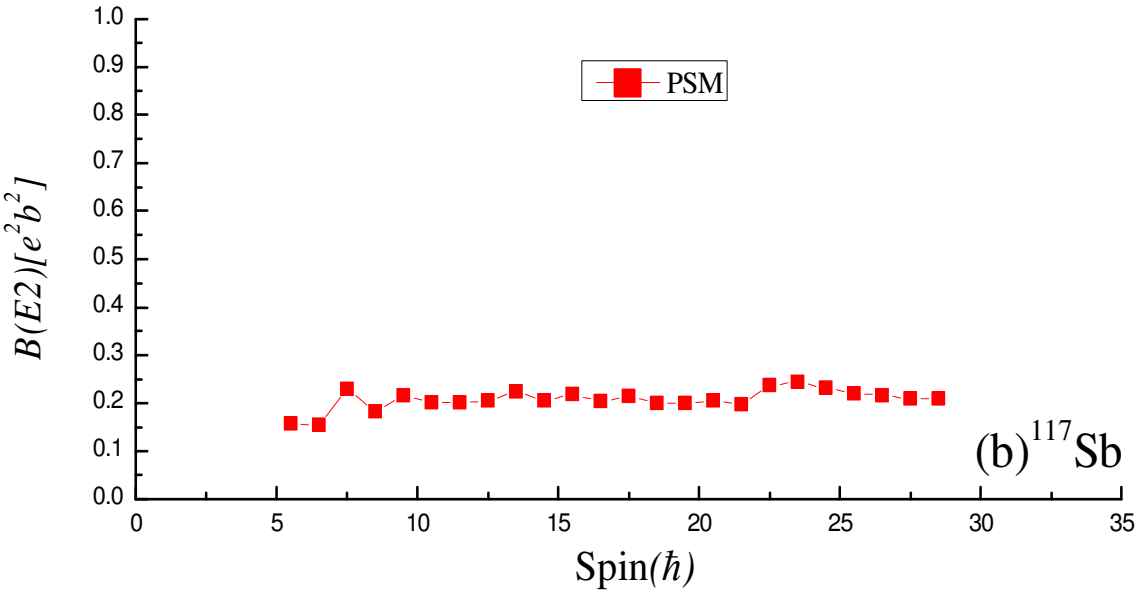

Fig. 4.3.4(b) Calculated *B(E2)* transition probabilities for yrast band in ^{117}Sb.

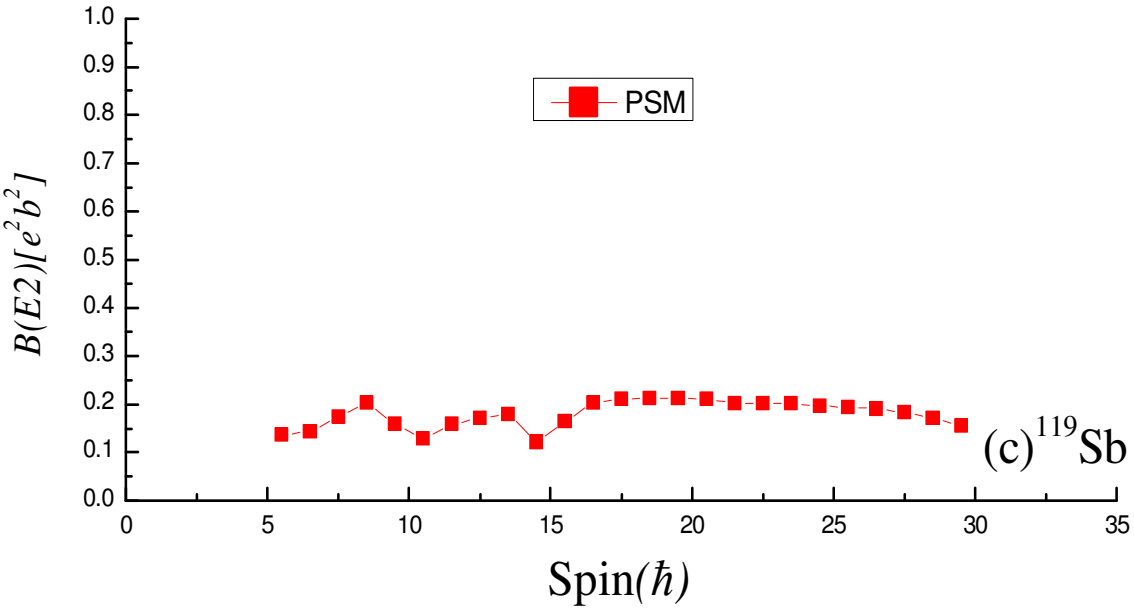

Fig. 4.3.4(c) Calculated *B(E2)* transition probabilities for yrast band in ^{119}Sb.

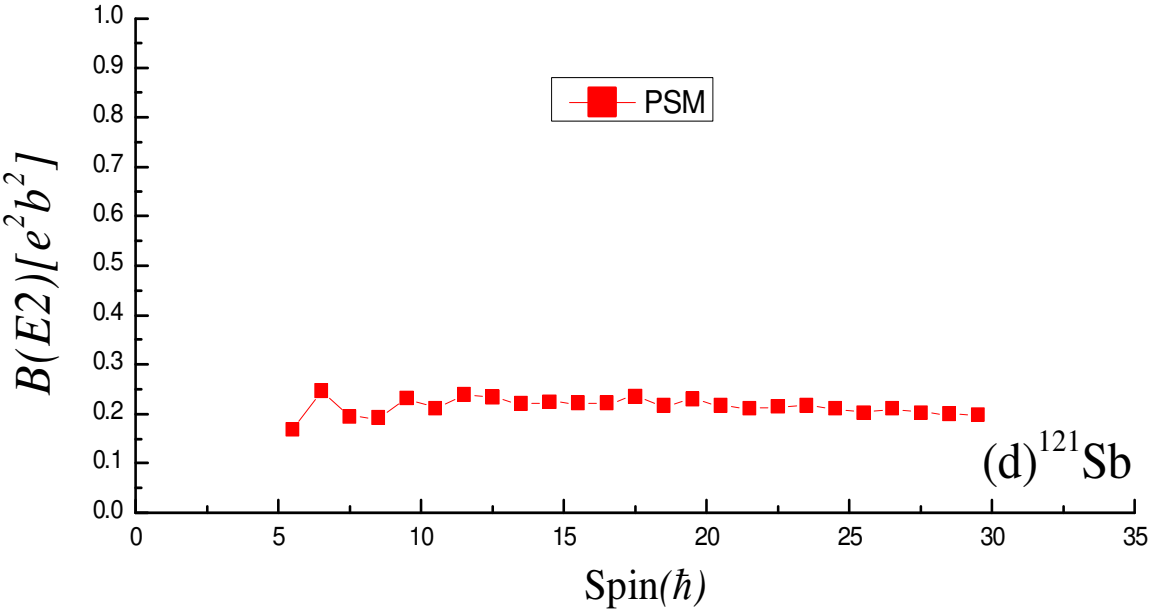

Fig. 4.3.4(d) Calculated *B(E2)* transition probabilities for yrast band in ^{121}Sb.

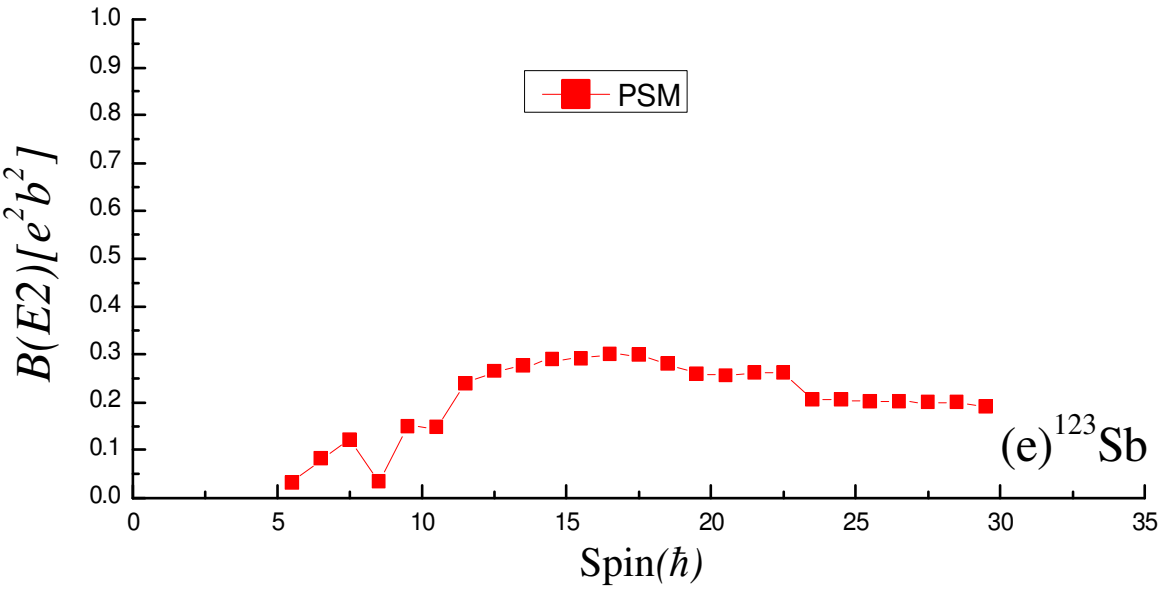

Fig. 4.3.4(e) Calculated *B(E2)* transition probabilities for yrast band in ^{123}Sb.

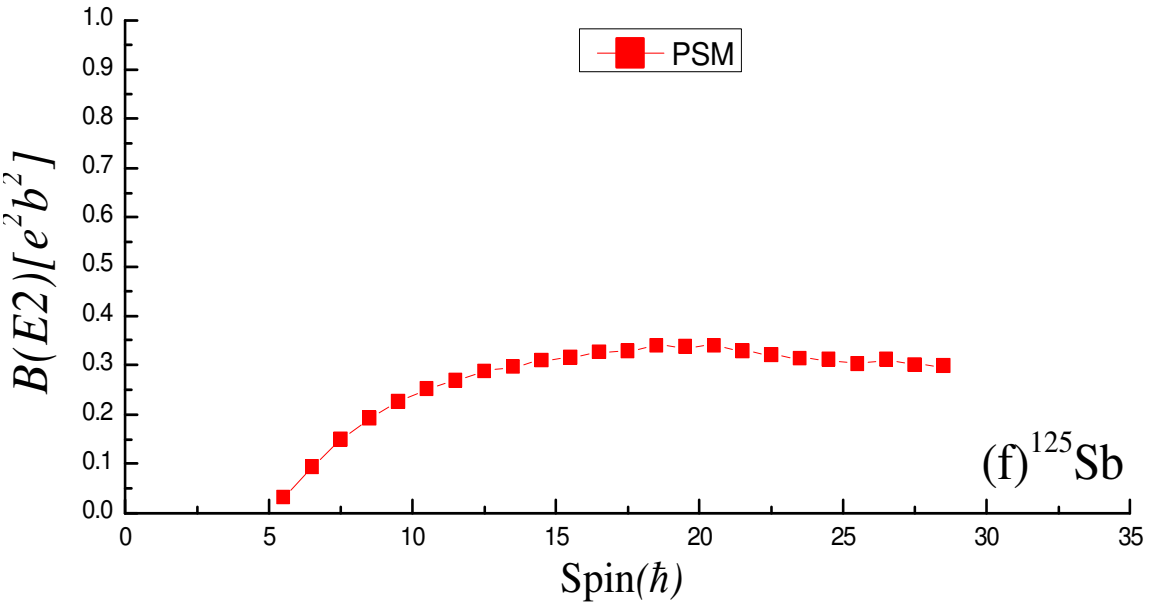

Fig. 4.3.4(f) Calculated *B(E2)* transition probabilities for yrast band in ^{125}Sb.

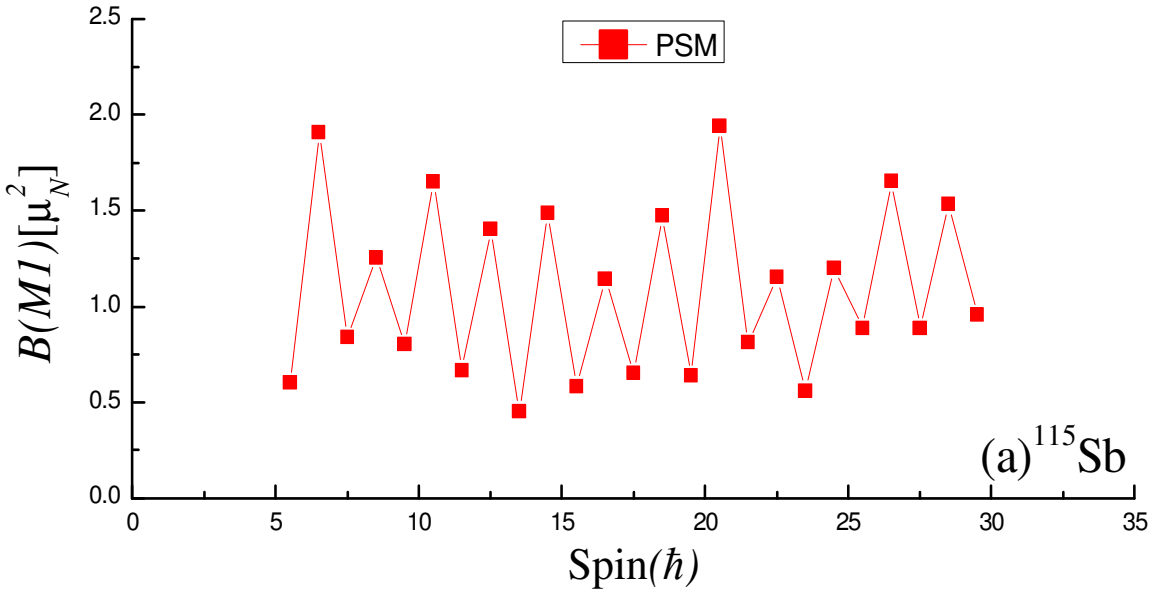

Fig. 4.3.5(a) Calculated $B(M1)$ transition probabilities for the yrast band in ^{115}Sb.

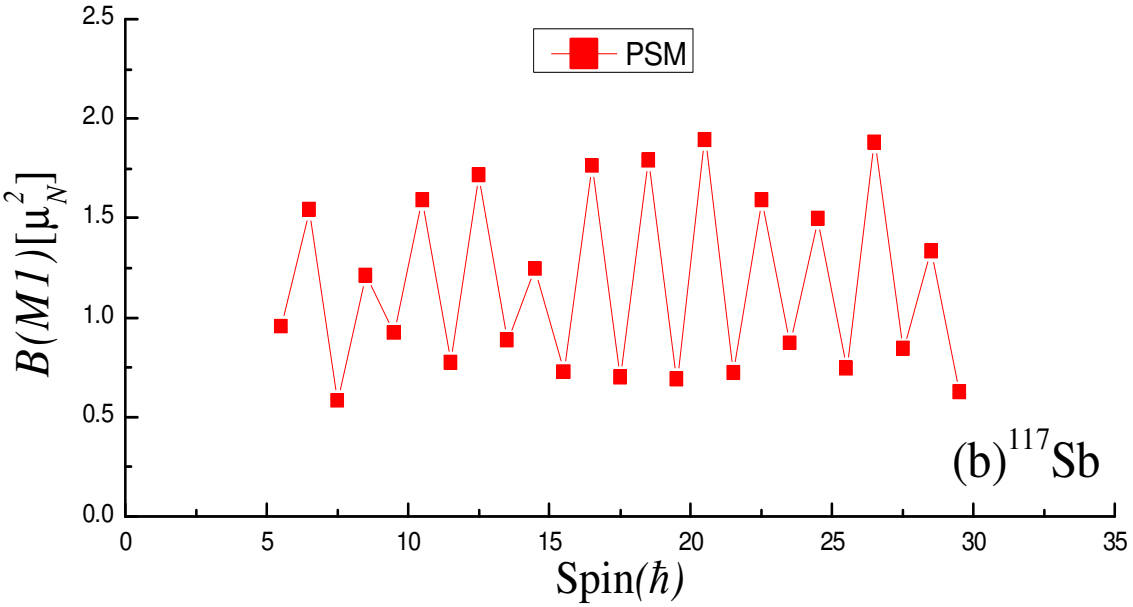

Fig. 4.3.5(b) Calculated $B(M1)$ transition probabilities for the yrast band in ^{117}Sb.

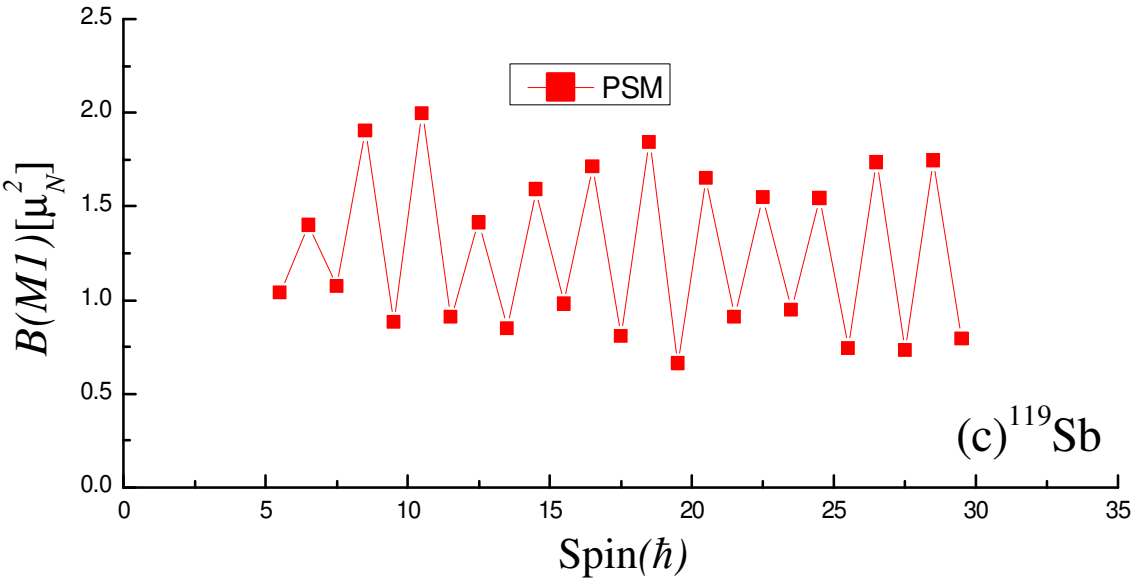

Fig. 4.3.5(c) Calculated $B(M1)$ transition probabilities for the yrast band in ^{119}Sb.

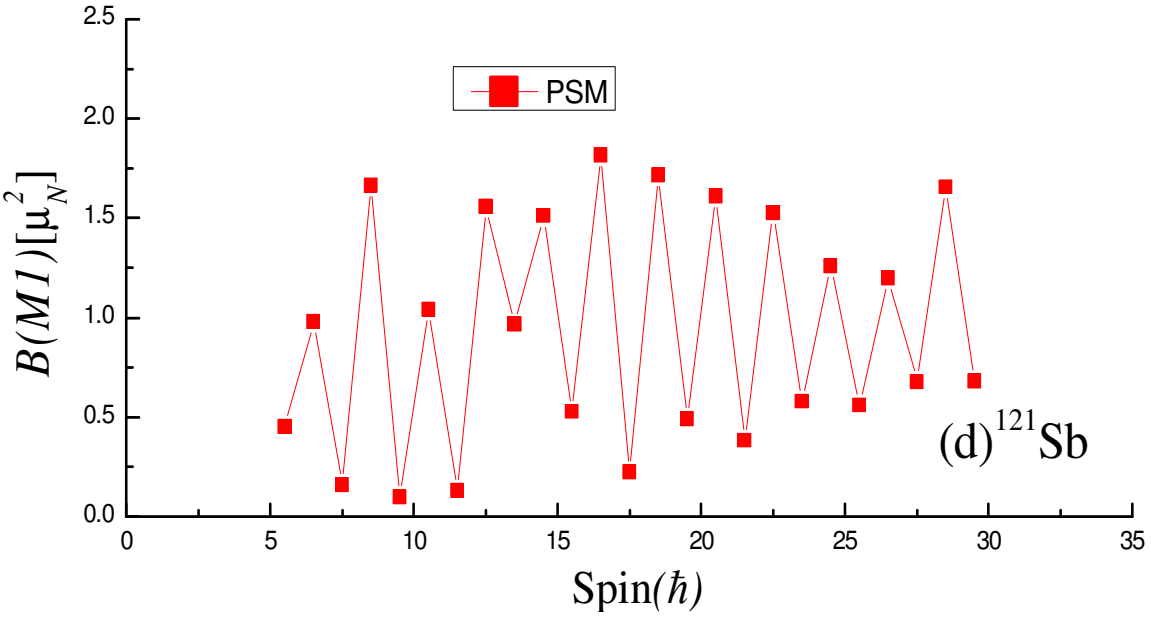

Fig. 4.3.5(d) Calculated $B(M1)$ transition probabilities for the yrast band in ^{121}Sb.

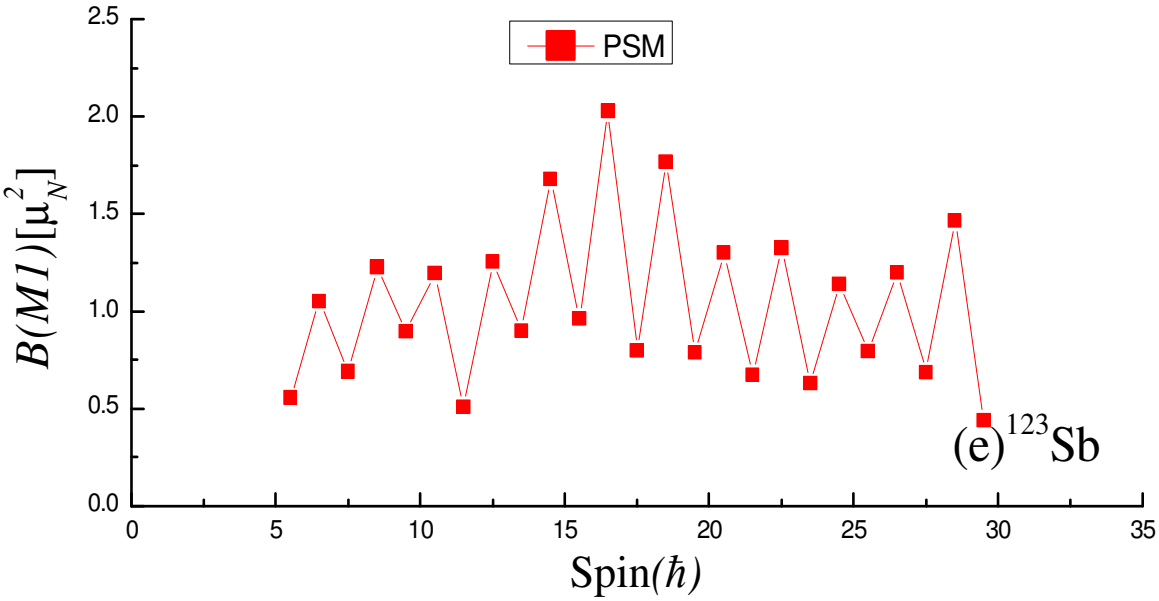

Fig. 4.3.5(e) Calculated $B(M1)$ transition probabilities for the yrast band in ^{123}Sb.

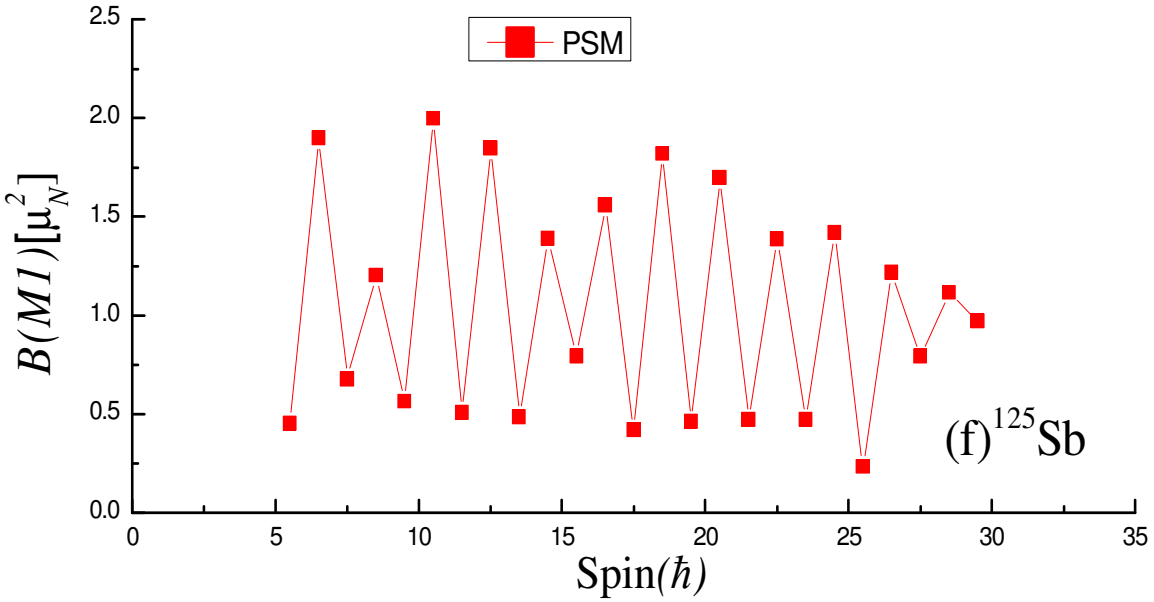

Fig. 4.3.5(f) Calculated $B(M1)$ transition probabilities for the yrast band in ^{125}Sb.

4.4 Conclusions

By using a microscopic method known as Projected Shell Model (PSM), the structure of odd-proton ^{115,117,119,121,123,125}Sb isotopes for negative parity is studied and analyzed in this chapter. PSM calculations reproduce the band head spin of all these nuclei correctly, which turns out to be $11/2^-$ for $^{115-125}$Sb. The results on the band diagrams have reported that the yrast spectra do not arise from single intrinsic (1-qp) state only but also from the multi-particle (3-qp) states. The PSM calculations have produced the back-bending in moment of inertia in these nuclei at those values of rotational frequencies which are close to the experimental ones. Nevertheless, the PSM results on back-bending have been able to reproduce this phenomenon at the same values of spins at which the phenomenon of band-crossing in band diagrams occurs. Again, the reduced electromagnetic transition probabilities, ($B(E2)$ and $B(M1)$), for yrast states are also predicted for various transitions in these Sb isotopes for which there is no experimental data available.

Further, I would like to mention here that similar PSM calculations have already been successfully performed by me on Iodine nuclei ($^{119-127}$I) lying in the same mass region around Sn core and those research results have already been published in the Ref.[32] . The present work on Sb nuclei is a continuation of the series of PSM calculations made by me on nuclei lying around Sn. So, based on the amount of qualitative research results obtained on Antimony and Iodine nuclei, PSM can be considered to be quite reliable and successful in interpreting and correlating the available data on some nuclear structure quantities of nuclei lying in the Sn core region. Hence, PSM is consistent in its application on describing nuclear structure properties of nuclei lying around Sn.

Furthermore, the results presented in this chapter-4 have been published in an international journal with the details: **International Journal of Modern Physics E, 26 (2017) 175004**

Bibliography

[1] R. E. Shroy, A. K. Gaigalas, G. Schatz, and D. B. Fossan, *Phys. Rev.* **C19** (1979) 1324.

[2] M. Conjeaud, S. Harar, and Y. Cassagnou, Nucl. Phys. **A117** (1968) 449.

[3] J. P. Schiffer *et al.,* Phys. Rev. Lett. **92** (2004) 162501.

[4] G. V. Berghe and K. Heyde, Nucl. Phys. **A163** (1971) 478.

[5] S. Sen and B. K. Sinha, Phys. Lett. **B31** (1970) 509.

[6] D. R. LaFosse, D. B. Fossan, J. R. Hughes,Y. Liang, H. Schnare, P. Vaska, M. P.Waring, and J.-y. Zhangi, Phys. Rev. **C56** (1997) 2.

[7] D. R. LaFosse, D. B. Fossan, J. R. Hughes, Y. Liang, P.Vaska, M. P. Waring, and J.-y. Zhang, Phys. Rev. Lett. **69**, (1992) 1332.

[8] V. P. Janzen, *et al.,* Phys. Rev. Lett. **70** (1993) 1065.

[9] V. P. Janzen, *et al.,* Phys. Rev. Lett. **72** (1994) 1160.

[10] H. Schnare, *et al.,* Phys. Rev. **C54** (1996) 1598.

[11] G. J. Lane, *et al.,* Phys. Rev. **C55** (1997) 2127.

[12] D. R. LaFosse, *et al.,* Phys. Rev. **C50** (1994) 1819.

[13] D. R. LaFosse, *et al.,* Phys. Rev. **C53** (1996) 2763.

[14] R. Wadsworth, *et al.,* Nucl. Phys. **A559** (1993) 461.

[15] R. Wadsworth, *et al.,* Phys. Rev. **C50** (1994) 483.

[16] J. Bron, W. H. A. Hesselink, H. Bedet, H. Verheul, and G.VandenBerghe, *Nucl. Phys.* **A279** (1977) 365.

[17] R.S. Chakrawarthy and R.G. Pillay, Phys. Rev. **C54** (1996) 5.

[18] A. K. Gaigalas, R. E. Shroy, G. Schatz, and D. B. Fossan, Phys. Rev. Lett. **35** (1975) 555.

[19] M. Ionescu-Bujor, A. Iordachescu, G. Pascovici, and C. Stan-Sion, Nucl. Phys. **A466** (1987) 317.

[20] H. Watanabe, *et al.,* Phys. Rev. **C79** (2009) 024306.

[21] G. A. Jones, *et al.,* Phys. Rev. **C77,** (2008) 034311.

[22] M.-G. Porquet, *et al.,* Eur. Phys. J. **A24**, (2005) 3949.

[23] K. Hara, Y. Sun, Int. J. Mod. Phys. **E4** (1995) 637.

[24] Jing-ye Zhang, A.J. Larabee, L.L. Riedinger, J. Phys. **G13** (1987) 75.

[25] Jean Blachot, *Nuclear Data Sheet* **113** (2012) 2391.

[26] Jean Blachot, *Nuclear Data Sheet* **84** (1998) 277.

[27] D.M. Symochko, E. Browne, J.K.Tuli, *Nuclear Data Sheet* **110** (2012) 2945-3105.

[28] S.Ohya, *Nuclear Data sheet* **111** (2010) 1619.

[29] S.Ohya, *Nuclear Data sheet* **102** (2004) 547.

[30] J.Katakura, *Nuclear Data sheet* **112** (2011) 495.

[31] A. Ibanez-Sandoval, M. E. Ortiz, V. Velazquez, A. Galindo Uribarri, P. O. Hess and Y.Sun, Phys. Rev. **C83** (2011) 034308.

[32] Dhanvir Singh, Anuradha Gupta, Amit Kumar, Chetan Sharma, Suram Singh, Arun Bharti, S.K. Khosa, G.H.Bhat, J.A.Sheikh. Nucl. Phys. **A952** (2016) 41

5 Summary of the thesis and its future perspectives

5.1 Conclusions:

The nuclear structure properties in the mass region A≈120 present a very interesting case of nuclear deformation for study. In this thesis, a theoretical investigation of the odd mass nuclei lying in the mass A≈120 has been done by using the projected shell model. The nuclei for which the theoretical investigation has been made are the Iodine ($^{119-127}$I) and Antimony ($^{115-125}$Sb). The conclusion drawn from the results presented in the thesis are summed up as follows.

In **chapter 1**, a brief introduction with special emphasis on the nuclei belonging to mass region A≈120 is presented. It starts with the general introduction of the nucleus, followed by beginning of nuclear physics, its applicability and importance. A brief account of various studies- theoretical as well as experimental, made in the past on some odd mass Iodine and Antimony isotopes nuclei using different approaches/techniques, is included in the same chapter. Since the present thesis is based on application of theoretical nuclear model, so a brief account of various theoretical models is also presented in this chapter.

In **chapter 2**, a detail explanation of the applied quantum mechanical framework, i.e. Projected Shell Model (PSM), has been presented as this model has been extensively used to describe different nuclear structure properties of neutron deficient odd mass Iodine ($^{119-127}$I) and Antimony ($^{115-125}$Sb) isotopes. This model has been chosen in the present work as it has advantages over all models. For example, this model helps in describing the finer details of high-spin spectroscopic data with simpler interpretation. Further, the numerical requirements in this model are minimal and therefore, it is possible to perform a systematic study for a group of nuclei in a reasonable time frame. This model has also been found quit successful in describing the essence of important physics from the calculated results.

In **chapter 3**, of this thesis, the results of the PSM calculation for $^{119-127}$I isotopes have been presented. For performing these calculations, the projected shell model (PSM) has been applied with the deformed single-particle states generated by the standard Nilsson potential using the same set of input parameters to study an odd mass isotopic chain of Iodine isotopes ($^{119-127}$I). Some nuclear structure properties like yrast spectra, beck-bending, band diagrams and reduced transition probabilities have been studied for both positive as well as for negative parity bands

for odd mass $^{119-127}$I isotopes and their comparison is also made with the available experimental data. By using PSM technique band head spins of all these nuclei have been successfully reproduced which is found to be $5/2^+$ for positive parity and $11/2^-$ for negative parity. Yrast spectra for $^{119-127}$I isotopes for positive as well as negative parity have been calculated for oblate and prolate deformations respectively and compared with the available experimental data. The calculated bands obtained before configuration mixing, when plotted in the form of band diagrams, predict that the low lying yrast states arise from 1-qp states. As one goes to higher angular momentum states, it is found that the intrinsic state changes and has 3-qp configurations. An occurrence of back-bendings have been found in $^{119-127}$I isotopes, for positive as well as negative-parity and these calculated back-bendings have been predicted to occur at the spins which are very close to those at which experimental ones are observed. In the same chapter, the reduced transition probabilities, B(M1) and B(E2) have also been calculated for all these Iodine ($^{119-127}$I) isotopes for which no experimental as well as other theoretical data was available.

In **chapter 4** of this thesis, the results of the calculation for $^{115-125}$Sb isotopes have been presented. Some nuclear structure properties like yrast spectra, band diagrams, beck-bending and reduced transition probabilities for negative parity has been studied for these Antimony isotopes. Results obtained are then compared with the experiment data. PSM calculations on these nuclei are able to reproduce their band head spins which turn out to be $11/2^-$ for all these $^{115-125}$Sb isotopes. Yrast spectra for all these Antimony isotopes ($^{115-125}$Sb) is found to be in good agreement with the experimental data at lower spins, while at higher spin values, PSM shows little higher energies than the experimental ones. Band diagrams have also been plotted for $^{115-125}$Sb isotopes and from these band diagrams, band structures have been understood, which reveal that yrast spectra do not arise from single intrinsic (1-qp) state only but also from the multi-particle (3-qp) states. The PSM calculations have produced the back-bending in moment of inertia in these nuclei at those values of rotational frequencies which are close to the experimental ones. The PSM results on back-bending have been able to reproduce this phenomenon at the same values of spins at which the phenomenon of band-crossing in band diagrams occurs. The reduced transition probabilities, B(M1) and B(E2), have also been calculated for these $^{115-125}$Sb isotopes. However, experimental data on B(E2) and B(M1) values for these isotopes was not available but I have calculated these values for this Antimony isotopic chain as this attempt would encourage the experimentalists to look for this data in future.

To conclude, a comprehensive analysis of the nuclear structure of $^{119\text{-}127}$I and $^{115\text{-}125}$Sb nuclei in the mass region A≈120 have been performed in the present research work. An overall satisfactory agreement between the experimental and calculated values for these odd mass Iodine and Antimony isotopes predicts the reliability of the applied model (PSM).

5.2 Future Perspectives

The Projected Shell Model (PSM) is able to explain in better way the different nuclear structure properties of nuclei around mass number A≈120, but its capability can be raised by adding more interactions, i.e. higher order terms can be included in the interaction Hamiltonian of PSM to increase the exactness of the result. Moreover, the present PSM calculations have been performed by considering axially deformed shell model basis which leads to some discrepancies in the result of Iodine and Antimony isotopes at higher spins, as these nuclei contain some degree of triaxiality. So, the addition of triaxiallity parameter could lead to better results for these isotopes. The work presented in this thesis also provides an opportunity for the experimentalists to look for the data for high spin yrast states as well as transition probabilities in future as their confirmation will further help in understanding the quasiparticle structure of these nuclei. The research work presented in this thesis is based on the PSM calculations within 1-qp and 3-qp excitations but using higher qp excitations may provide some improvement to the results and this exercise can be taken up as a future perspectives of the present work.